STRUCTURAL AND METAMORPHIC EVOLUTION OF THE ORMSBY ZONE AND RELATIVE TIMING OF GOLD MINERALIZATION: A NEWLY DEFINED ARCHEAN OROGENIC GOLD PROSPECT HOSTED ON THE DISCOVERY PROPERTY, YELLOWKNIFE GREENSTONE BELT, SLAVE PROVINCE, CANADA

by

William H.R. Whitty

B.Sc. Honours, Carleton University, Ottawa, Canada, 2004

A THESIS SUBMITTED IN PARTIAL FULFILLMENT OF
THE REQUIERMENTS FOR THE DEGREE OF

MASTER OF SCIENCE

in

THE FACULTY OF GRADUATE STUDIES

(Geological Sciences)

THE UNIVERSITY OF BRITISH COLUMBIA

December 2007

Abstract

The Yellowknife greenstone belt has produced approximately 14 million ounces of gold, 13 of which came from the well explored southern half of the belt. The northern half of the belt, where the Discovery Property (1 million ounce past producer) is located, is not as well explored, but geologically very similar to the gold producing southern half. Gold on the Discovery Property, Northwest Territories, has been historically mined from a quartz vein formed adjacent to Archean metabasaltic bodies enclosed in metasedimentary rocks. Some of the metasedimentary rocks are correlated to the Archean Banting Group, based on a U-Pb age of 2.66 Ga on zircon (SHRIMP-RG). The metabasalt is correlated to the Banting Group based on its deposition relationship with the adjacent metasedimentary rocks. The Banting Group is present in the Yellowknife greenstone belt, located near the well-known Con and Giant Mines near Yellowknife, 90 km to the south.

The two gold deposits forming the Discovery Property contains almost 2 million ounces in past production and current resources. The historical Discovery Mine was developed in quartz veins hosted in the metasedimentary rocks folded around the northern tip of one of the metabasalt bodies. In contrast, the newly defined Ormsby Zone consists of gold in silicified and sulphidized domains within metamorphosed pillowed and brecciated mafic volcanic rocks, and shares many characteristics with other Archean Orogenic gold deposits. Pyrrhotite ± arsenopyrite is directly correlated with the gold-bearing zones. Gold is also associated with pyrite and retrograde phases of chlorite, sericite and carbonate.

Through detailed outcrop mapping and petrography the history of structural and metamorphic events are sequenced and the relative time of gold mineralization placed into the geological framework.

Peak-metamorphic mineral assemblages on the property record upper greenschist to amphibolite facies conditions. Rocks on the Discovery Property have undergone at least four foliation-forming, deformational events. Three generations of folding are described, as well as a vertical lineation across the property. Gold mineralization occurred post-ductile fabric forming deformation, post-peak metamorphism, and syn-retrograde metamorphism. Although no visible evidence was observed mapping, metamorphic data present the possibility of a regional scale fault separating two metamorphic domains on the property.

Table of Contents

Abstract ……...…… ii
Table of Contents ……...……..…… iii
List of Tables ……..……..…….…..... vi
List of Figures ……...……...……..…….... vii
Acknowledgments ……...…...… ix

Chapter 1: Introduction and Setting ……..……..… 1
1.1 Thesis Introduction ……... 1
1.1.1 Methods ……..…….. 5
1.2 Archean Orogenic Gold Deposits ……...… 5
1.2.1 Geodynamic Setting …… 5
1.2.2 Host Rocks …….. 6
1.2.3 Ore-Bearing Fluids …….. 7
1.2.4 Mineralization Styles …….. 8
1.3 Regional Setting ……..… 10
1.4 Summary of Objectives ……..… 15

Chapter 2: Geology of the Discovery Property …… 17
2.1 Introduction …… 17
2.2 Previous Work …… 18
2.2.1 Previous Structural Models ……..….. 18
2.2.3 The Quartzite Unit …… 20
2.3 Rock Units ……..…….. 22
2.3.1 Burwash Formation ……..…… 22
2.3.2 Transition Unit …….. 22
2.3.3 Giauque Lake Unit …… 25
2.4 Basalt Geochemistry …….. 29
2.5 Geochronology …… 33
2.6 Pre-metamorphic Conditions 35

2.6.1 Depositional Environment 35
2.6.2 Pre-metamorphic Alteration 35
2.7 Metamorphism 36
2.7.1 Mineral Chemistry 43
2.7.2 Average P-T Estimates Using Conventional Thermobarometry 51
2.7.3 Average P-T Estimates Using THERMOCALC 53
2.8 Structures 55
2.8.1 Foliations 57
2.8.2 Lineation 60
2.8.3 Folds 62
2.8.4 Faults 69
2.9 Summary 69

Chapter 3: Gold 71
3.1 Introduction 71
3.2 Gold Paragenesis 72
3.2.1 Outcrop Observations 72
3.2.2 Drill Core Observations 73
3.2.3 Thin Section Observations 74
3.2.4 Implications 74
3.3 Summary 80

Chapter 4: Interpretations, Discussions and Conclusions 81
4.1 Introduction 81
4.2 Proposed Structural Model 82
4.3 Implications of a Post-Peak Metamorphic Fault 85
4.4 Correlation to Yellowknife Supergroup and Comparison with Previous Models 87
4.5 Comparison with Other Deposits 88
4.6 Remaining Work 90

References ……...……..….. 92

Appendix A: Mineral Chemistry ……..… **100**

List of Tables

Chapter 1: Introduction and Setting

Table 1.1: Comparison of selected Archean orogenic gold deposits …… 9

Chapter 2: Geology of the Discovery Property

Table 2.1: Rock units on the Discovery Property …… 18
Table 2.2: Incompatible element data …… 31
Table 2.3: SHRIMP-RG U-Pb isotopic data for felsic tuff in Transition Unit …… 34
Table 2.4: Representative mineral chemistry for metabasalt (WW14A) …… 45
Table 2.5: Representative mineral chemistry for metabasalt (WW05068) …… 46
Table 2.6: Representative mineral chemistry for Burwash sandstone (WW05028) …… 47
Table 2.7: Representative mineral chemistry for Transition sandstone (WW05030) …… 48
Table 2.8: Representative mineral chemistry for Transition sandstone (WW02C) …… 49
Table 2.9: Representative mineral chemistry for Burwash sandstone (WW05004) …… 50
Table 2.10: Geothermometer comparison …… 52
Table 2.11: Foliations …… 56

List of Figures

Chapter 1: Introduction and Setting

Figure 1.1: General geology of the Slave Province ……. 3
Figure 1.2: The Discovery Property and surrounding rocks, sample locations ……..….. 4
Figure 1.3: General exposure of the Yellowknife greenstone belt ……..…….. 13
Figure 1.4: Geology of the Yellowknife greenstone belt near Yellowknife ……....…. 14
Figure 1.5: Simplified stratigraphy of the Yellowknife Supergroup ……....…… 15

Chapter 2: Geology of the Discovery Property

Figure 2.1: Previously proposed structural models for the Discovery Property …… 20
Figure 2.2: Transposed layers in the Transition Unit …… 24
Figure 2.3: Transposed layers in the Transition Unit ……...……. 25
Figure 2.4: Distribution of pillows versus breccia in the Ormsby Member …….. 27
Figure 2.5: Preserved pillow structures in the metabasalt ……..… 28
Figure 2.6: Brecciated metabasalt outcrops ……...…… 29
Figure 2.7: Incompatible element plots for the metabasalt ……..….. 32
Figure 2.8: U-Pb concordia-discordia plot ……..…… 34
Figure 2.9: Two garnet textures in thin section ……...….. 39
Figure 2.10: AFM plots for metasedimentary rocks ……..…… 40
Figure 2.11: ACF plots for metabasalt ……..……. 41
Figure 2.12: Reaction topologies ……...…… 42
Figure 2.13: P-T pseudosections from pelites ……..…….. 43
Figure 2.14: P-T plots from THERMOCALC ……..…….. 54
Figure 2.15: Thin section foliation and lineation in the metabasalt ……..…….. 58
Figure 2.16: Mica defining S_2 and S_3 in metasedimentary rock thin section …… 59
Figure 2.17: S_4 crenulation in metasedimentary rock thin section ……...… 60
Figure 2.18: Hand sample (metabasalt) and thin section (metasedimentary) lineation ……. 61
Figure 2.19: Bedding/foliation relationships measure in the field ……..… 64
Figure 2.20: Interpretation of bedding trace and F_1 ……...…… 65
Figure 2.21: The past producing North Vein ……...…….. 66

Figure 2.22: Interpretation of F_2 ……...……. 67
Figure 2.23: Foliation overprinting relationships observed in thin section ……...…… 68

Chapter 3: Gold

Figure 3.1: Map showing gold mineralization relative to lithology and iron staining …….. 73
Figure 3.2: Metallic minerals aligned with foliation in thin section …….……..… 75
Figure 3.3: Sulphides overprinting metamorphic minerals in thin section …… 76
Figure 3.4: Pyrrhotite cross-cutting and infilling fractured quartz in thin section ……..…… 77
Figure 3.5: Free gold intergrown with pyrrhotite in a quartz vein …….…… 78
Figure 3.6: Overprinting relationships of oxides and sulphides in thin section …….…… 79

Chapter 4: Interpretations, Discussions and Conclusions

Figure 4.1: Proposed structural model for the Discovery Property ……..……. 83
Figure 4.2: Implication of post-peak metamorphic faulting …….……. 86

Plate 1: Detailed geological map of the Ormsby Member …….. 114

Acknowledgments

I would like to thank Dave Webb and Tyhee Development Corp. (Tyhee) for the opportunity and funding to conduct this study. Dave suggested and helped determine the scope of the study, provided unlimited access to Tyhee's property where the study took place as well as old files, reports, logs and other information in the company's records. Tyhee offered summer employment, giving me a great opportunity to learn the local geology and collect thesis data while working for them.

I would also like to thank Dick Tosdal with the Mineral Deposits Research Unit (MDRU) at the University of British Columbia (UBC) for agreeing to supervise the project and coordinating with Tyhee to get and keep the project going. Throughout the study Dick was good at providing feedback to keep the study in scope and on track. Ken Hickey, also with the MDRU, was patient and helpful in supervising and providing a lot of technical feedback throughout the study. As well, his knowledge of computer software was extremely beneficial and much appreciated.

Funding was also provided by the Natural Sciences and Engineering Research Council of Canada (NSERC) in the form of an Industrial Postgraduate Scholarship (IPS). The Society of Economic Geologists (SEG) awarded a research grant from the *Hickok-Radford Memorial Fund*.

Several other people were helpful and deserve mention as well. At UBC, I would like to thank Greg Dipple for agreeing to be on my committee and helping with the metamorphic petrology, Lori Kennedy for taking an interest in my project and helping me with micro structures, Paul Duuring for helping me identify oxides and sulphides petrographically, and Jim Mortensen, who was on my examining committee, who's constructive feedback was incorporated into the final document. Val Pratico at Tyhee was excellent to work for, supportive of my study, and willing to offer help and data throughout the study. Peter Stewart, a consulting geologist working on Tyhee's property, was always ready to have lengthy discussions and provide insight, information and data to help with my study. Hedrick Falk at the Northwest Territories Geoscience Office provided me with numerous papers, many of which were not publicly available. Alex Bath at EBA Engineering took an interest in my thesis, read over it, and offered helpful insight and discussion.

Finally I would like to thank my parents for their moral and financial support, which without, this study would not have been possible, and my fiancé Celina for all her love and support.

Chapter 1: Introduction and Setting

1.1 General Introduction

Archean orogenic gold deposits account for nearly 20% of the world gold production (Roberts, 1988), yet many features of this deposit type are poorly understood (Groves et al., 2003). In Canada over 220 orogenic gold deposits (containing >1 t Au) are known (Robert and Poulsen, 1998). These are located principally within the Archean Superior Province, and to a lesser extent in the Slave Province (Figure 1.1). The Yellowknife greenstone belt, within the Slave Province, has produced approximately 14 million ounces of gold; of these the Con (5.8 million ounces, Hauser et al., 2006) and Giant (7.1 million ounces, Canam, 2006) deposits near Yellowknife are the largest and best known. About 90 km north of the city of Yellowknife lies the Discovery Property, a small (1 million ounce; Bullen and Robb, 2006) past producer of gold and the study area of this thesis. The Discovery Property shares many geologic characteristics with the Con and Giant deposits (see Table 1.1), such as metamorphic setting, host lithologies and gold associations.

Comprehensive reviews of orogenic gold deposits can be found in: Groves et al. (1995); Groves et al. (1998); Groves et al, (2000); Hagemann and Cassidy (2000); Kerrich et al. (2000); Ridley and Diamond (2000); Goldfarb et al. (2005); Robert et al. (2005). The current consensus is that orogenic gold deposits are the result of tectonic processes wherein auriferous fluids derived from deep metamorphism or magmatism are channeled up a permeable structure provided by an evolving fault system. Gold is precipitated in, or adjacent to quartz veins at depths ranging from <5 km to 20 km. Critical to this model is the observation that gold is generally late in the deformation history.

The Discovery Property (Figure 1.2) consists of two large metabasalt bodies surrounded by predominantly metasedimentary rocks. Rocks on the property are Archean and metamorphosed at conditions ranging from greenschist to amphibolite facies. Ductile deformation including folding and shearing have deformed the rocks on the property.

The Discovery Property hosts the Discovery Mine shaft, which produced 1 million ounces of gold from 1 million tons of ore between 1950 and 1969 (data from Northwest Territories Geoscience Office). Historically, gold was mined from a quartz vein, the "North Vein," hosted in the metasedimentary rocks. In contrast, the newly defined Ormsby Zone, also located on the Discovery Property, consists of younger gold mineralization than the

North Vein (based on metamorphic fabric relationships and previous interpretations) hosted in Archean meta-mafic volcanic rocks. As of June 2007 the Ormsby Zone contains 936,000 (measured + indicated) ounces of gold with an average grade of 3.53 gpt (Tyhee Development Corp., see below – this section, NI 43-101 resource estimates).

This study defines the structural and metamorphic sequence preserved in the rocks, and places the relative timing of gold mineralization within this framework. The Ormsby Zone, one of several zones of gold on the Discovery Property, is the principal focus of this thesis. This zone is undergoing exploration and development by Tyhee NWT Corp. (a subsidiary of Tyhee Development Corp.) in the hopes of becoming a producing mine within the near future.

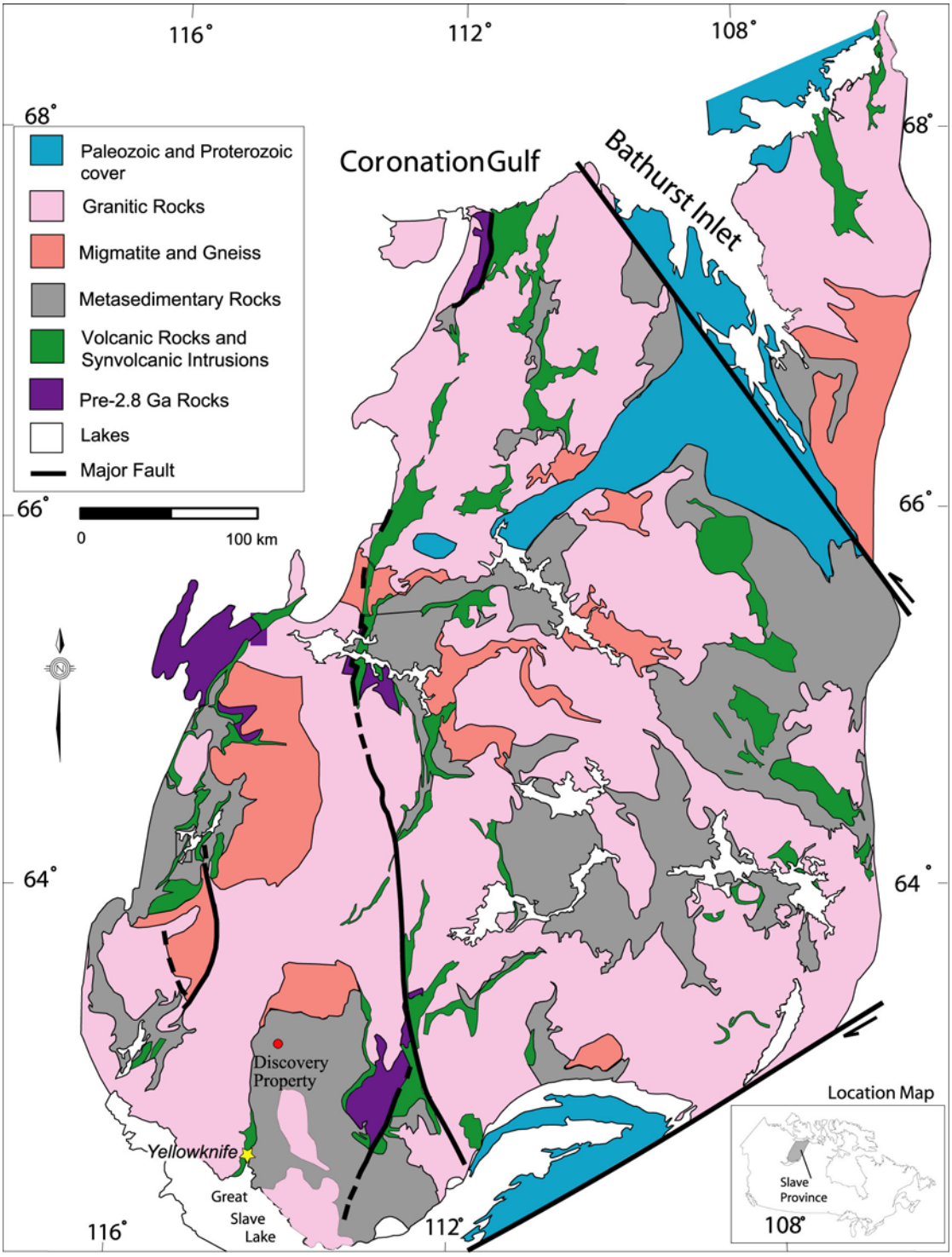

Figure 1.1: General geology of the Slave Province (Modified from Stubley, 1997).

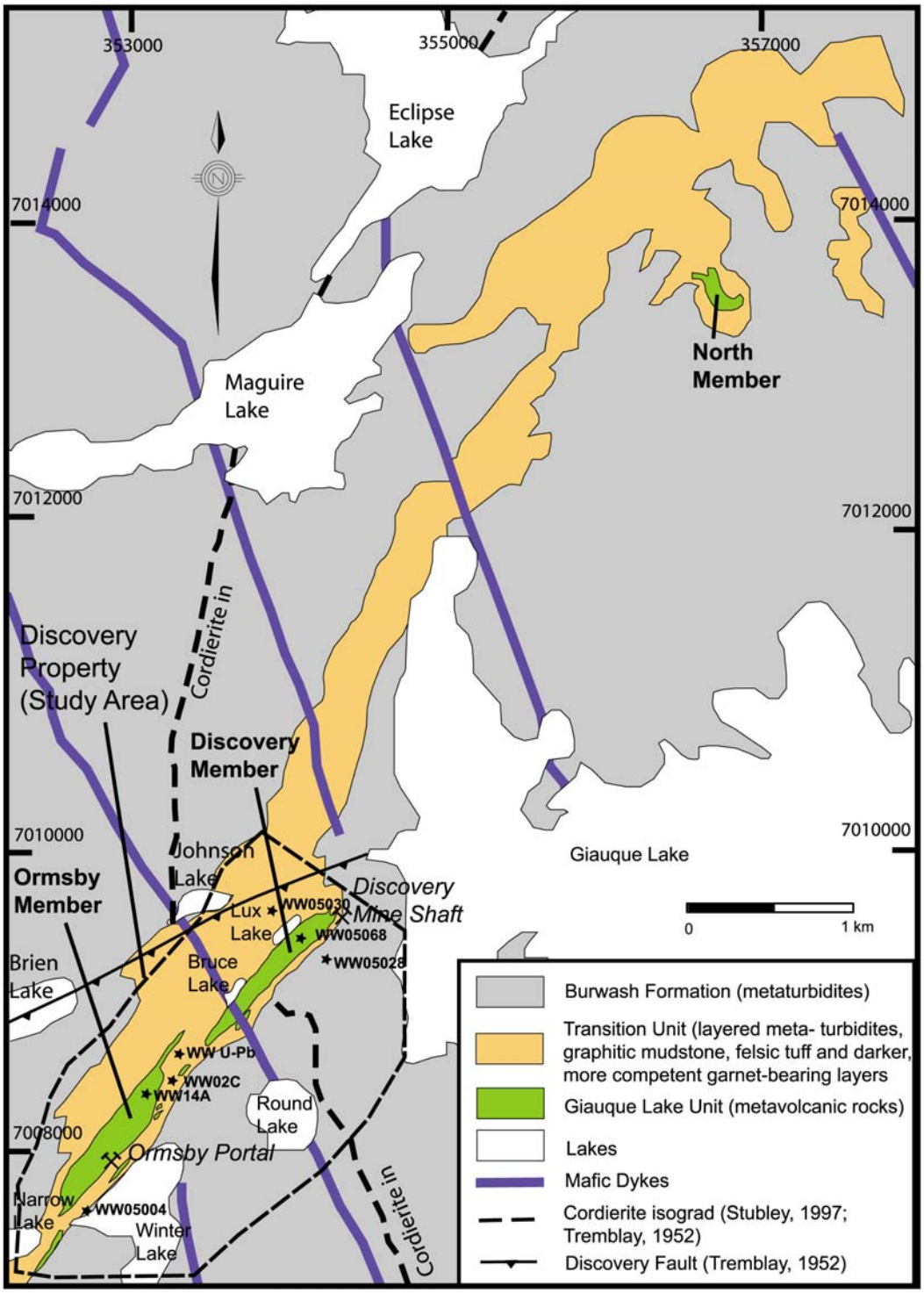

Figure 1.2: The Discovery Property (dashed outline) and surrounding rocks within the northern part of the Yellowknife greenstone belt (Tremblay, 1952; Stubley, 1997; Stewart, 2005). Note locations of sample (stars) referred to in text.

1.1.1 Methods

The sequence of geological events is defined by surface mapping supported by petrography. The geology of the Ormsby Zone is summarized on a 1:2500 scale map (Plate 1, pocket). Although there is a lot of exposure, outcrops are generally moss and lichen covered, which hinders detailed mapping. In several locations however, sections of outcrop have been washed clean by previous exploration parties providing excellent local exposure.

The first chapter of this thesis outlines the characteristics of typical Archean orogenic gold deposits and establishes the regional setting of the Discovery Property. The second chapter covers the local setting and geology of the Discovery Property, correlations to regional geology; metamorphism and structure are discussed in detail. The third chapter places gold mineralization into the geological context. The fourth and final chapter is a discussion of the results and summary of the proposed model for the Ormsby Zone and Discovery Property.

1.2 Archean Orogenic Greenstone Gold Deposits

"Orogenic" gold deposits are not precisely characterized (e.g., Groves et al., 2003), and seem to broadly include most gold deposits associated with deformation and hosted in metamorphic rocks. Besides a definitive classification scheme, currently unresolved issues for orogenic gold deposits include the following: (1) the precise tectonic setting and age of mineralization, (2) the source of ore fluids, (3) the precise architecture of the hydrothermal systems (i.e., the relationship between first and lower order structures) and (4) the specific depositional mechanism for gold (Groves et al., 2003). A general description of Archean orogenic gold deposits, with an emphasis on those hosted in greenstone belts, are summarized in this section from the following papers and reviews: Groves et al. (1995), Groves et al. (1998), Groves et al. (2000), Hagemann and Cassidy (2000), Kerrich et al. (2000), Ridley and Diamond (2000), Goldfarb et al. (2005), Robert et al. (2005).

1.2.1 Geodynamic Setting

Orogenic gold deposits are formed during compressional to transpressional deformation process in accretionary and collisional orogens where hydrated marine sedimentary and volcanic rocks are added to continental margins. These terranes are

commonly bounded by crustal scale faults and shear zones. Archean orogenic gold deposits are commonly in close proximity to crustal scale shear zones that demark the boundaries of distinct, tectonically juxtaposed, metamorphic supercrustal sequences. Archean orogenic gold deposits also are localized in proximity to the hinge of regional scale anticlines, particularly doubly plunging folds. The structural setting of the deposits is generally a function of the metamorphic grade of the rocks (Colvine, 1989; McCuaig and Kerrich, 1998). In lower greenschist facies rocks, ores are typically hosted in brittle shears zones and open folds, and in amphibolite facies and higher, ores are typically hosted in ductile shear zones and tight isoclinal folds. Although on the greenstone belt scale the deposits are spatially associated with large-scale (>100 km) transcrustal deformation zones, on a camp scale, most deposits are hosted in second or third order faults. Three structural settings are particularly favoured (Groves et al., 1990): (1) shear zones and faults developed along contacts between units of contrasting competencies; (2) competent rock units enclosed in less competent ones (such as the setting of the Ormsby Zone) and (3) fold hinges and anticlines (especially for BIF and clastic sedimentary rock hosted ores).

Other features that characterize Archean orogenic greenstone gold deposits are the presence of small rigid granitic intrusions and the presence of Timiskaming-type regional unconformities. Timiskaming-type sequences are late Archean supercrustal rock assemblages consisting of conglomerate, sandstone, and less commonly, felsic volcanic rock, and are widespread throughout the Slave and Superior provinces in Canada.

1.2.2 Host Rocks

Archean greenstone belts are predominantly volcano-plutonic terrains of oceanic back-arc felsic to mafic rocks. Although gold deposits occur in all lithologies of greenstone belts, three types are common: (1) iron-rich mafic igneous rocks, i.e. tholeiitic basalt and differentiated dolerite sills; (2) iron-rich clastic metasedimentary rocks and banded iron formation (BIF); and (3) dioritic to felsic porphyritic stocks and dykes. Iron-rich rocks are chemically the most favourable hosts (Phillips et al., 1984; Böhkle, 1989). Intermediate to felsic intrusions are favourable structural hosts because of their brittle response to regional deformation that leads to enhanced fracturing and veins (Cassidy et at., 1998). Orogenic gold

deposits found in Archean greenstone belts, such as those throughout the Canadian Shield and Western Australia, are typically hosted in greenschist to lower amphibolite facies metamorphosed tholeiitic pillowed basalts and komatiites intruded by intermediate to felsic porphyry intrusions, and sometimes swarms of albitite or lamprophyre dykes. Brittle-ductile deformation characterizes the host rocks. Deposits can be cross-cutting or parallel to shear zones, strike extensive laminated quartz veins, extensional quartz vein arrays, and/or breccias. Mineralization is epigenetic and typically post-peak metamorphism and retrograde in greenschist facies or syn-peak metamorphism in amphibolite facies.

1.2.3 Ore-Bearing Fluids

Mineralization in Archean orogenic gold deposits is interpreted to have occurred over a range of paleocrustal levels from shallow (<5 km) to deep (20 km) as a result of focused fluid flow late during active deformation and metamorphism of greenstone belts. Gold precipitation is estimated to have occured from about 1 kbar at 250ºC to 6 kbar at 700ºC (corresponding to low-pressure metamorphism at depths ranging from 3 km to 20 km) but most commonly restricted to 1-2.5 kbar at 300-350ºC. The duration of the mineralizing event has been difficult to constrain, but qualitative evidence suggests less than several million years (Ridley and Diamond, 2000).

Broadly uniform (unmodified from other sources), low to moderate salinity (1-15 wt% NaCl), mixed aqueous-carbonate fluid capable of carrying Au (as well as Ag, As and Sb) but not base metals is a crucial feature of Archean orogenic gold systems. The source of these fluids is poorly understood, but isotope tracers and mineral equilibria argue sources deeper than presently exposed greenstones. The fluid is in approximate equilibrium with the host rock sequence but not with the immediate wall rock.

Given present knowledge, two models for fluid source are allowable: either a granitoid magmatic or a metamorphic devolatization model. Alteration mineral assemblages generally show enrichment in K, CO_2 and S, and metal associations of Au, Ag ± As, B, Bi, Mo, Sb, Te, and W. Regional carbonation or chloritization associated with orogenic gold deposits can extended up to 1 km away from the deposit and are generally restricted to, or centred on first order crustal-scale fault zones. Orogenic gold fluids are unique from those of other gold types in their isotopic compositions. They generally have very limited range of

$\delta^{18}O$ most likely reflecting the lack of mixing with surface derived waters (Kerrich et al., 2000).

1.2.4 Mineralization Styles

Six different styles of gold mineralization typically occur in Archean orogenic gold deposits (Robert et al., 2005). Most deposits consist of a single style of mineralization, but many of the large deposits have two or more of these styles with systematic overprinting relationships requiring the existence of multiple gold mineralization events.

These six styles are as follows: (1) Quartz-carbonate veins are the most common style of mineralization, consisting of quartz veins with <25% carbonate, <10% sulphide, ± albite, tourmaline and scheelite. Sulphides are mainly pyrite with arsenopyrite and pyrrhotite. Veins types include laminated fault-fill and extensional veins forming complex, vertically extensive networks. The North Vein on the Discovery Property fits this style. (2) Sulphide replacement in BIF consist of strata-bound replacements of Fe-rich layers by mainly pyrite, arsenopyrite, or pyhrrotite. (3) Disseminated stockwork zones consist of 5-20% sulphides occurring as uniform dissemination or along foliation-parallel bands in highly strained rocks. This mineralization style is characterized by an absence of through-going quartz-carbonate veins. The Ormsby Zone on the Discovery Property is typical of this style. (4) Sulphide replacement and crustiform veins consist of lodes of crustiform-colloform carbonate veins and breccias with varying proportions of sulphide replacements of the wall rocks or vein carbonates themselves. (5) Sulphide-rich veins and veinlet zones contain 25-100% sulphide bearing quartz-carbonate veins. (6) Semi-massive to massive sulphide lenses are comprised of pyrite, chalcopyrite, spahalerite, and galena, and uncommonly pyhrrotite and magnetite.

Table 1.1: Comparison of selected Archean gold deposits that share similarities with Ormsby

	Deposit							
	Ormsby	**Discovery**	**Giant**	**Con**	**Hollinger-McIntyre**	**Lupin**	**Hemlo**	**Golden Mile**
Location	Yellowknife greenstone belt, Slave Province, NT, Canada	Yellowknife greenstone belt, Slave Province, NT Canada	Yellowknife greenstone belt, Slave Province, NT, Canada	Yellowknife greenstone belt, Slave Province, NT, Canada	Abitibi greenstone belt, Superior Province, ON, Canada	Contwoyto Formation, Slave Province, NU Canada	Hemlo greenstone belt, Superior Province, ON, Canada	Norseman-Wiluna greenstone belt, Yilgarn Craton, W. Australia
Host	mafic volcanic rocks (Banting Group)	greywacke tubidites (Burwash Formation)	(tholeiitic mafic volcanic rocks of the Kam Group) quartz ankerite sericite schist, and quartz-carbonate veins	(tholeiitic mafic volcanic rocks of the Kam Group) quartz ankerite sericite veins in sericite-ankerite schist, and quartz-carbonate veins	tholeiitic basalts	Banded Iron Formation (BIF)	moderately to intensely altered sedimentary, felsic volcanic and volcaniclastic rocks	mafic volcanic rocks
Metamorphic Grade	upper greenschist - amphibolite facies	upper greenschist - amphibolite facies	greenschist - amphibolite	amphibolite facies	greenschist facies	greenschist to amphibolite facies transistion (low P, mod. T)	upper amphibolite facies (580-650°C; 4-5 kb)	greenschist facies, low P, 350-400°C
Structure	localized zone of concentrated ductile deformation on the limb of a regional scale fold	fold closure	folded shear zones	north striking, west dipping planar deformation (shear) zones	NE trending, doubly plunging anticline	W-central-E limbs on the northern nose of a domical structure	moderate to high strain domains, compressional - transpressional, brittle-ductile domain, proximity to batholith margin	two NW trending folds located on the SW flank of domed anticline, Au hosted along shear zones
Relative Timing of Mineralization	post peak metamorphic, syn-retrogression, post-ductile deformation	pre - early deformation, pre peak-metamorphism	early syn-deformation	early syn-deformation	unknown	post-peak metamorphic	interpreted as pre - syn peak metamorphism	post peak metamorphism, syn deformation
Au paragenesis/alteration assemblages	disseminated free Au with po±aspy±py and chl±ser±cal	disseminated and coarse free Au in qz, no metal associations	disseminated refractory Au with aspy, and free-milling Au in qz and qz-carb veins	disseminated refractory Au with aspy in schist, and free-milling Au in veins	intrusion hosted vein and disseminated Cu±Au±Ag, and qz-carb vein and altered wall-rock hosted Au	qz, hbl (grnsh-amph facies) & qz, di, ab, hed, sch, wo, gt, spn (amph facies)	disseminated, fracture controlled, qz-carb veins mc-ms-bi-qz±bar; ab-qz-carb-phl &/or tr/act; minor porphyry Cu-Ag-Au-Mo	disseminated Au in py in wallrock, ms, qz, sid, ab & chl, cal, ank, ab, qz

Au-gold, *aspy*-arsenopyrite, *Cu*-copper, *Ag*-silver, *qz*-quartz, *carb*-carbonate, *hbl*-hornblende, *grnsh*-greenschist, *di*-diopside, *ab*-albite, *hed*-hedenburgite, *sch*-scheelite, *wo*-wollastonite, *gt*-garnet, *spn*-sphene, *amph*-amphibolite, *mc*-microcline, *ms*-muscovite, *bi*-biotite, *bar*-barite, *al*-albite, *phl*-phlogopite, *tr*-tremolite, *act*-actinolite, *py*-pyrite, *ser*-sericite, *As*-arsenic, *Sb*-antimony, *Mo*-molybdenum, *sd*-siderite, *chl*-chlorite, *cal*-calcite, *ank*-ankerite (McDonald et al., 1993; Kerrich et al., 2000; Poulsen et al., 2000; Siddorn et al., 2006; Muir, 2002; Muir, 2003; Geusebroek and Duke, 2004; Shelton et al., 2004; Hauser et al., 2006)

1.3 Regional Setting

The Slave Province is a small Archean craton that makes up a major part of the northwestern Canadian Shield (Figure 1.1). It consists mainly of granitic and metasedimentary rocks ranging in age from 4.0 Ga to 2.6 Ga (Bowring et al., 1989; Isachsen et al., 1991; van Breeman et al., 1992; Stern and Bleeker, 1998; Bethune et al., 1999; Bleeker, 2002) and is bound by Paleoproterozoic orogenic belts on the east and west. The tectonic evolution of northern Canada involved a series of accretionary events alternating with periods of continental extension. Proposed settings for the evolution of the Slave Province and greenstone belts within it range from intercontinental rift models (e.g. Henderson, 1985) to collisional models (e.g., Kusky, 1989, 1990; Yamashita et al., 2000, van der Veldon and Cook, 2002) involving subduction and accretion of island arcs. Back-arc basin models proposing lithospheric extension followed by collapse and collision (e.g., Helmstaedt and Padgham, 1986; Helmstaedt et al., 1986) are basically hybrids of the above end-members. Currently these models are still debated. Seismic reflection data along a single line (LITHOPROBE's SNORCLE transect) in the southwestern Slave Province still do not resolve the issue. LITHOPROBE observations permit two distinct models for the formation of the Yellowknife greenstone belt (Snyder et al., 2006). These are (1) collapsed ensialic rift basins and (2) accreted oceanic crust. Based on observations acquired as part of LITHOPROBE's SNORCLE transect, Snyder et al. (2006) argue in favour of the structural basin model (1). In this model the Burwash Formation metaturbidites (see below – this section) fill a structural basin bordered by metamafic volcanic rocks of greenstone belts, such as the Yellowknife greenstone belt. The second model proposes crust in the Yellowknife area thickened by a series of thrust wedges with the greenstone belt representing one wedge boundary and the metaturbidites forming the top most flake or wedge. Geochemical studies of Cousens et al. (2006; see below – this section) support the rift model (1).

The south central Slave Province is underlain by a Mesoarchean crystalline basement block, consisting of granodioritic to tonalitic gneiss, known as the Central Slave Basement Complex (Bleeker et al., 1999). The Central Slave Basement Complex is overlain by the Central Slave Cover Group (Bleeker et al., 1999), a highly deformed and locally imbricated autochthonous sequence consisting of ultramafic, mafic and minor felsic volcanic rocks, conglomerate, chromite-bearing quartzite, and banded iron formation.

The Yellowknife greenstone belt is the southernmost of numerous greenstone belts, and is exposed in the southwestern part of the Slave Province. This belt strikes north-northeast from Yellowknife Bay for approximately 100 km (Figure 1.3). The southern half (Figure 1.4) is continuously exposed, and well documented and mapped. The northern half is poorly studied and consists of discontinuous exposures of metavolcanic rocks. The rocks within the belt dip steeply to the east. Sequences of greenschist to amphibolite facies metamorphosed mafic to felsic volcanic rocks subdivided into the 2.73-2.70 Ga Kam Group and the 2.69-2.66 Ga Banting Group (Isachsen, 1992; Snyder et al., 2006) compose the belt. The Kam and Banting groups form the basal strata of the Yellowknife Supergroup (Figure 1.5; Henderson, 1970), which is a supercrustal sequence of metamorphosed volcanic and sedimentary rocks throughout the Slave Province. Younger strata of the Duncan Lake Group consist of metamorphosed sedimentary rocks of predominantly sandstone. Long-term (lasting 25-30 millions years) regional metamorphism of the belt, punctuated by multiple short-term contact metamorphic events, occurred approximately 2.62-2.60 Ga ago (Thompson, 2006). Chlorite-carbonate retrograde zones overprint peak-metamorphism within or adjacent to intense deformation zones (Thompson, 2006).

Metamorphosed mafic pillow lavas and massive flows interbedded with thin chert-rich volcaniclastic to quartz feldspathic sandstone compose the Kam Group. In contrast, the younger Banting Group is composed mainly of metamorphosed, intermediate to felsic pyroclastic rocks with less common mafic volcanic and sedimentary rocks. The contact between the Kam and Banting groups is unconformable, and the depositional relationship between the two groups is unresolved (Cousens et at., 2006, Martel and Lin, 2006). In most places however, it appears faulted with rocks of the younger Jackson Lake Formation (see below – this section), separating the two groups (Martel, 2003; Martel and Lin, 2006). Mafic to intermediate volcanic rocks of the Banting Group are chemically very similar to those of the Kam Group (Cousens et al., 2002). They are tholeiitic melts derived from Archean depleted upper mantle. Cousens et al. (2006) show that the Kam Group was emplaced within a rift environment. They also show that mafic rocks of the Banting Group are consistent with an extensional setting. Cousens et al. (2006) argue that felsic rocks of the Banting Group are the product of crustal melting from a widespread tectonothermal event in that part of the Slave Province.

Banting Group rocks grade up into the metasedimentary Walsh and Burwash formations of the Duncan Lake Group. The Walsh Formation is composed of metamorphosed thinly bedded graphitic argillite and siltstone, whereas the Burwash Formation is composed of metamorphosed more thickly bedded greywacke, siltstone and mudstone. The youngest formation of the Yellowknife Supergroup is the Jackson Lake Formation consisting of a basal breccia overlain by conglomerate, parallel and cross-bedded sandstone, and argillite.

Regional deformation and associated structures within the southwestern Slave Province have been documented and interpreted by Ramsey (1973), Drudy (1977), Fyson (1978, 1982), Bleeker and Beaumont-Smith (1995), Bleeker (1996), and Davis and Bleeker (1999), and the structural evolution of the Yellowknife greenstone belt has most recently been interpreted by Martel (2003). The dominant deformational events are briefly outlined here and correlated to deformation on the Discovery Property in the concluding chapter. Workers contend that two main phases of deformation (D_1 and D_2) resulted from tectonism in the southwestern Slave Province. D_1 produced large-scale folding (F_1) and associated S_1 foliation. Although the original orientation of these structures is unknown, it is assumed to be either east-west (Henderson, 1985) or northeast-southwest (Bleeker and Beaumonth-Smith, 1995). D_2 is widely documented and recognized as a regionally significant, approximately east-west, compressive event producing regional scale folds (F_2) and associated axial planar parallel foliation (S_1).

Gold deposition near Yellowknife is estimated to be ca. 2.60 Ga based on relative timing of associated structures and host rock formations (Ootes et al., 2007). Gold was possibly introduced during early intrusions, prior to the formation of gold hosting shear zones, and later shearing of these intrusions and interactions with metamorphic fluids may have contributed gold to the shear zone hosted gold deposits in the belt (Ootes et al., 2007). Timing of gold mineralization at Con-Giant is interpreted as syn-D_1 (for refractory gold) and syn-D_2 (for free-milling gold; Siddorn et at., 2006).

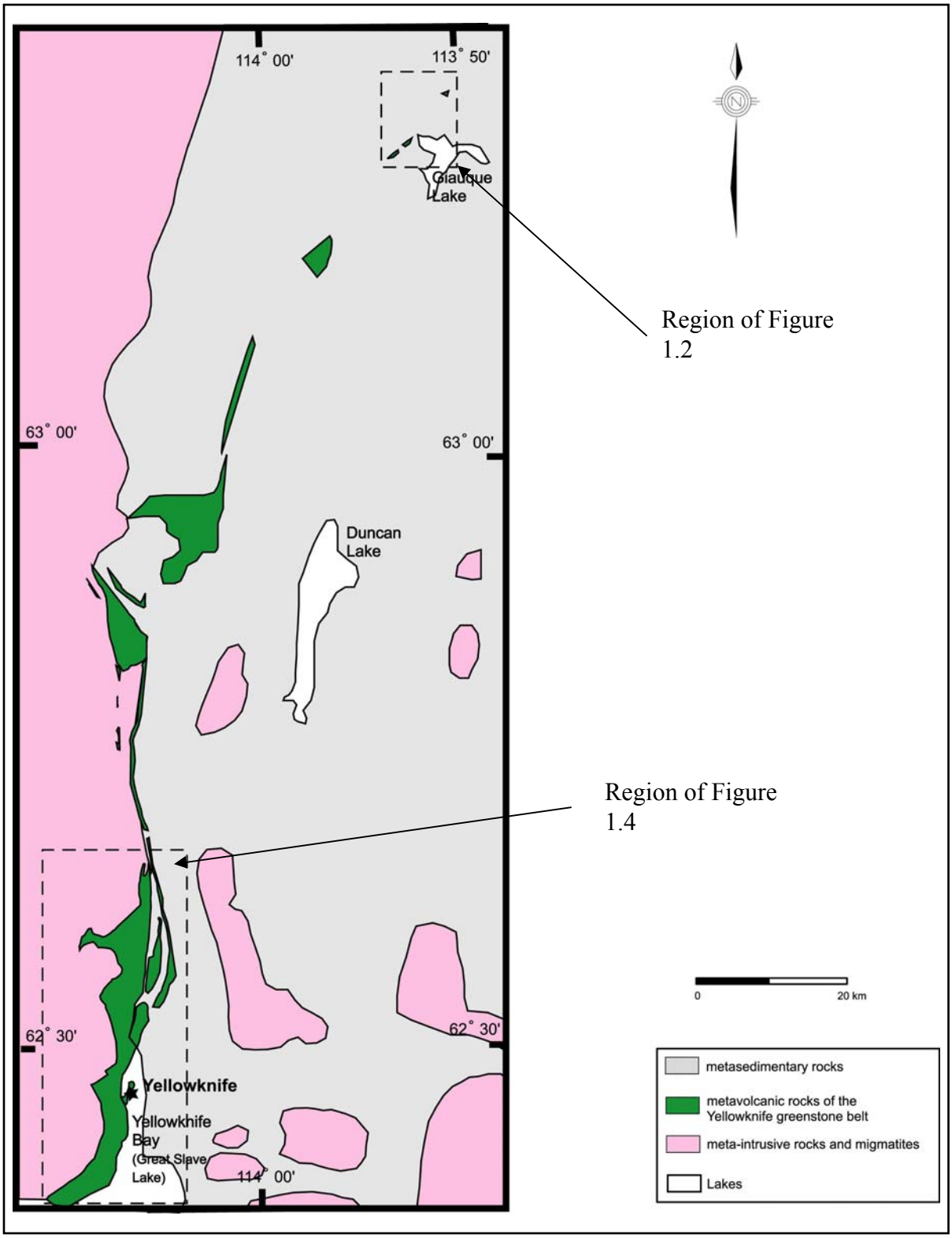

Figure 1.3: General exposure of the Yellowknife greenstone belt (Tremblay, 1952; Martel, 2003; Jackson et al., 2006).

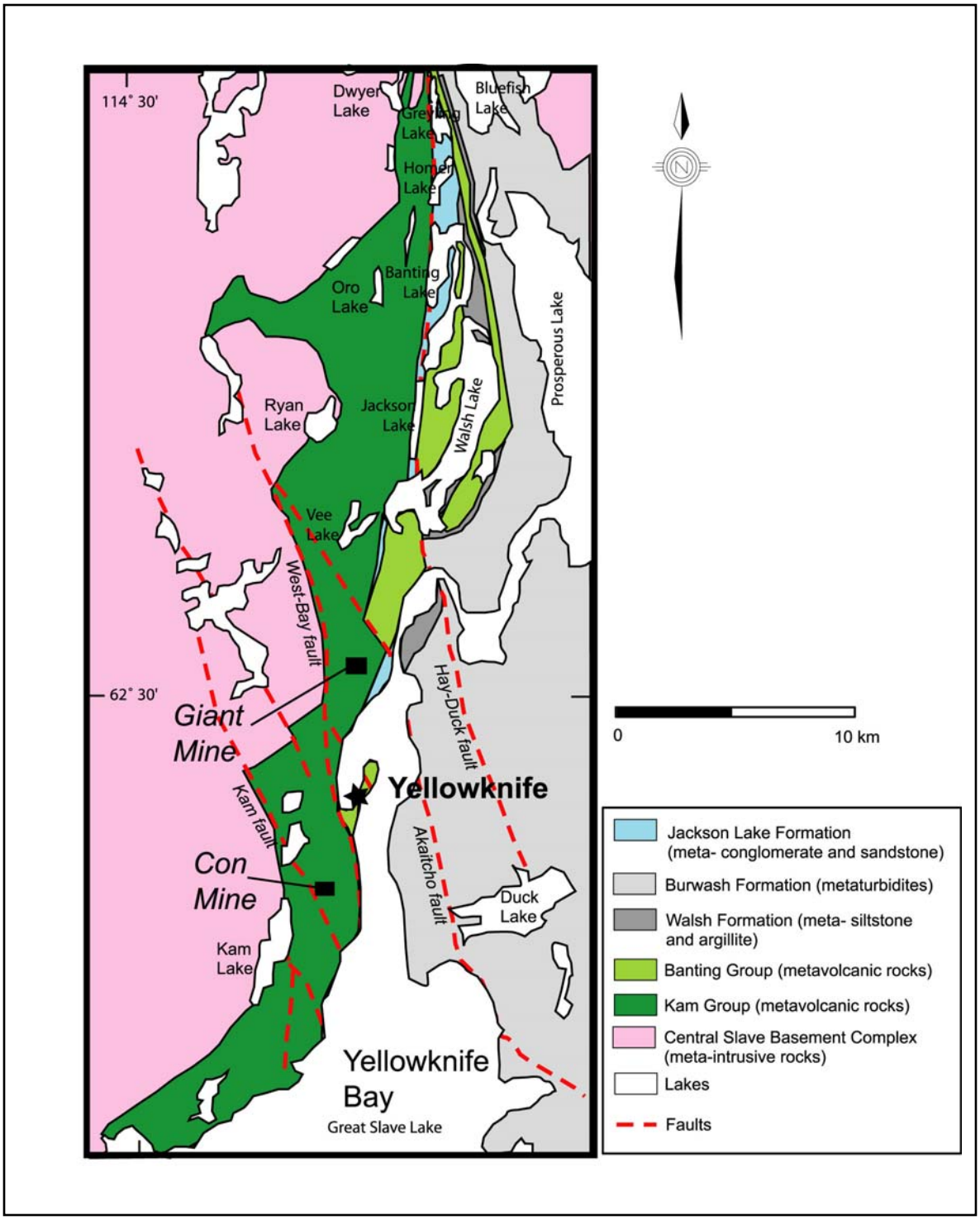

Figure 1.4: Simplified geology of the Yellowknife greenstone belt near the city of Yellowknife (modified from Martel, 2003).

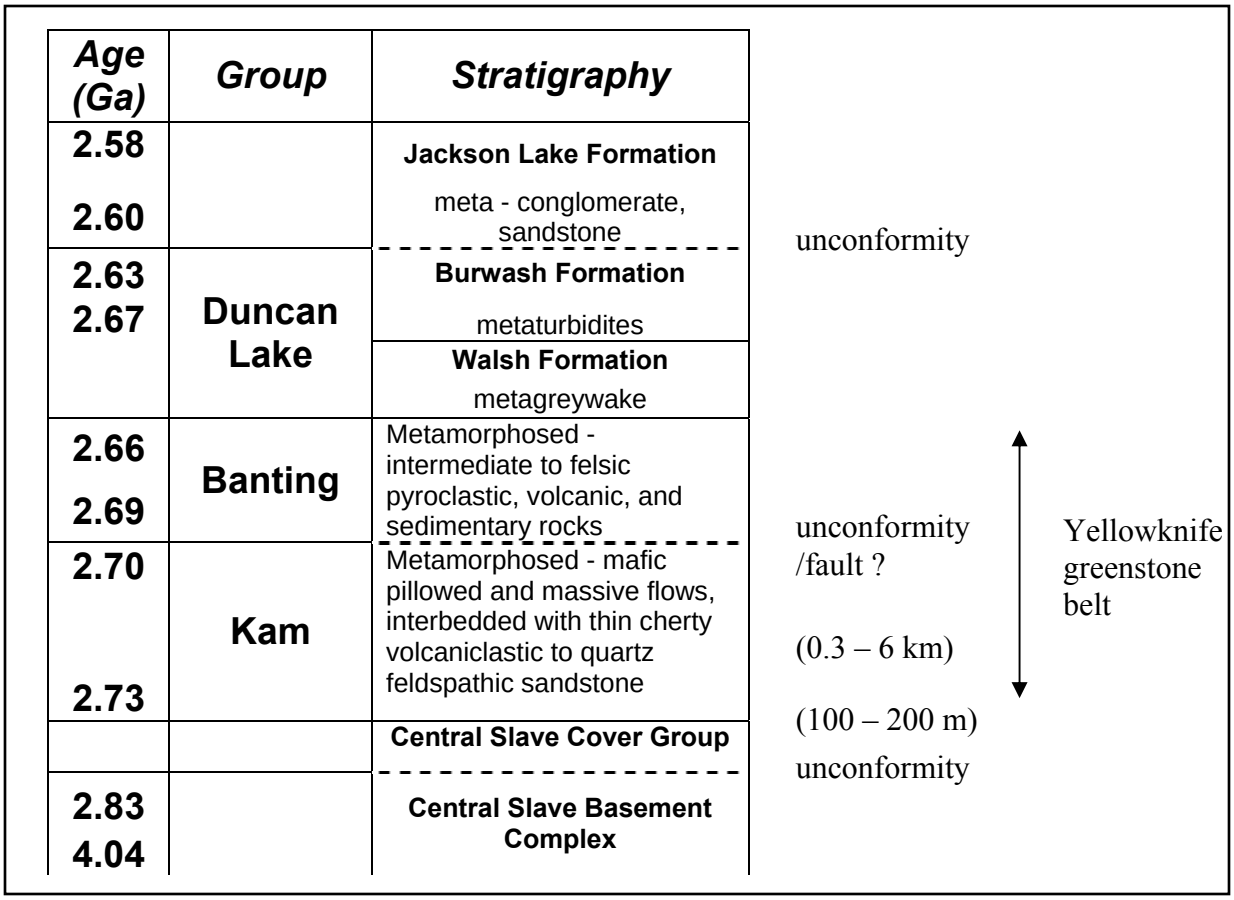

Figure 1.5: Simplified stratigraphy of the Yellowknife Supergroup emphasizing rock units important to the Discovery Property (Henderson, 1970; Helmstaedt and Padgham, 1986; Isachsen, 1992; Isachsen and Bowring, 1994; Isachsen and Bowring, 1997; Bleeker, 2002; Martel, 2003; Synder et al., 2006).

1.4 Summary of Objectives

The main objective of this thesis is to place the gold mineralization into a geological context. Detailed surface mapping, structural analysis and petrography are the principle tools used to reach the objective. The map (Plate 1) is used to identify patterns of alteration and lithology and correlate those patterns to identified areas of gold mineralization. A detailed geological map of the Ormsby Member and its contacts with the surrounding rocks (Plate 1) is a by-product of the thesis. Using structural data and samples collected while mapping, deformational structures preserved in the rocks are delineated, defined and sequenced. Relative timing of metamorphism is placed into the sequence of deformational events by

determining peak-metamorphic assemblages and retrograde phases and their overprinting relationships. Where data are available, peak temperature and pressure are estimated to help quantify metamorphism. Gold paragenesis is described and sequenced into the established deformational and metamorphic history. Other objectives of the thesis are to (1) correlate the rocks mapped to previously described rocks in the Yellowknife greenstone belt, and (2) to compare the Ormsby Zone with deposits of similar characteristics. The first will mainly be done using lithology observation obtained from mapping and petrography combined with a U-Pb geochronology sample. Understanding the geological history of the rocks is a prerequisite to establishing the relative timing of gold mineralization. As well, better understanding the geology and being able to compare the Ormsby Zone to documented gold deposits helps to further the understanding and nature Archean orogenic gold deposits and their occurrences.

As well as a tool to reach the above academic objectives, the accompanying geological map is of practical use for identifying exploration drill sites and targets for surface sampling. Understanding the basic geology and having a detailed map of the rocks sets the ground for further studies. Over 1000 hours were spent mapping and compiling the data into a GIS database to produce a finished professional geological map of the Ormsby Member. Surface mapping was carried out at 1:500 (but printed for this thesis at 1:2500) with emphasis on lithology, alteration and ductile fabrics. Outcrop patterns and key features were all surveyed by professional surveyors using a differential GPS system providing centimetre accuracy. Approximately 1000 survey points were used to ensure the accuracy of the map.

Chapter 2: Geology of the Discovery Property

2.1 Introduction

Rocks of the Yellowknife Supergroup (Figure 1.5) underlie the Discovery Property. Three distinct stratigraphic units are recognized on the property (Figure 1.2; Plate 1): (1) the Burwash Formation, (2) the Transition Unit, correlated to the Banting Group, and (3) the Giauque Lake Unit, also correlated to the Banting Group. The latter units have been assigned local informal names as their stratigraphic positions within the Yellowknife Supergroup were uncertain prior to this study. Herein, the Giauque Lake and Transition units are interpreted as occurring collectively within the Banting Group based on rock associations and U-Pb age (see below – section 2.5). For the purpose of this thesis, the author has retained the local names for the rock units, and will discuss the basis for the correlations in the following sections.

All the rocks are deformed and metamorphosed at greenschist to amphibolite facies conditions. Nonetheless, their protoliths are recognizable based on preserved textures. As a result they are referred to herein using their protoliths, but metamorphic rock names are shown in Table 2.1. Ductile fabrics (foliations and folds) preserved in the rocks are described and placed in sequence from both field and petrographic observations of cross-cutting relationships.

Table 2.1: Brief description of mapped rock units on the Discovery Property

Unit	Lithology	Peak-Metamorphic Assemblage	Metamorphic Rock Name	Rock Name Used in Text
Burwash Formation	metamorphosed turbidites made up of varying proportions of medium to thickly bedded light to medium brown/grey sandstone and siltstone	qz+pl+bi+ms±chl+cd; qz+pl+bi±ms±chl	biotite muscovite phyllite, and cordierite biotite muscovite phyllite	metasedimentary rocks
Transition Unit (Banting Group)	metamorphosed bedded alternations of sandstone, siltstone, mudstone, felsic tuff and more competent reworked mafic volcanic layers	qz+pl+bi+ms+chl+st; qz+pl+bi+ms+chl+and; qz+pl±bi±ms±gra; qz+pl+bi±chl±ep±hbl±gt	biotite muscovite phyllite, (commonly graphitic) Slate, and garnet hornblende biotite schist,	metasedimentary rocks
Giauque Lake Unit (Banting Group)	dark-green to black, medium-grained, variably strained, brecciated, pillowed metamorphosed basaltic rocks; white weathered fragments	hbl±act±cumm+qz+pl±gt±ep±bi	garnet hornblende amphibolite schist	metabasalt

and = andalusite, act = actinolite, bi = biotite, ms = muscovite, chl = chlorite, cd = cordierite, ep = epidote, gt = garnet, hbl = hornblende, pl = plagioclase, qz = quartz, st = staurolite, gra = graphite, cumm = cummingtonite

2.2 Previous Work

The region surrounding and including the Discovery Property was mapped by L.P. Tremblay (1952) at a scale of 1:24,000, and the western part of this area was remapped at 1:10,000 by P.W. Stewart in 2004 (unpublished; 2005). The Discovery Property was mapped at 1:2400 by M.P. Stubley in 1997 (unpublished). A B.Sc. thesis (Prince, 1998) was undertaken to help classify some of the metasedimentary rocks on the property.

2.2.1 Previous Structural Models

Stubley (1997) proposes that the Discovery Property straddles a major northeast-striking crustal scale fault system (Ormsby Break) with a prolonged and complex history of reactivation and associated alteration. Two main episodes of faulting are proposed. The oldest is a décollement separating the Giauque Lake and Transition units from the Burwash Formation. A steep northwesterly dip is inferred from cleavage orientations. Younger brittle deformation reactivated the décollement forming the Ormsby Fault Zone. Drill-hole

intersections and displacement along some of the splay faults were used to propose an overall geometry of the Ormsby Fault Zone as a series of ca. 035º-striking oblique-slip anastomosing subvertical faults. Stubley (1997) envisioned the Ormsby Fault Zone as a "positive flower structure" (Figure 2.1a) dominated by sinistral displacement, with both east- and west-side-up components of movement. Refraction of the master Ormsby Fault into a "releasing bend" between the Ormsby and Discovery members (Figure 2.1b) is proposed to have developed an extensional duplex structure.

In contrast, Stewart (2005); working from the model of Stubley (1997), proposes that rocks of the Giauque Lake and Transition units across the Ormsby Fault Zone form part of a regional-scale tight anticline. This model, as well as that of Stubley's (1997) assumes that the metabasaltic rocks of the Giauque Lake Unit are stratigraphically lower than the Transition Unit. Figure 2.1 illustrates how the fold model is compatible with the fault zone model. Shearing is interpreted as limb-parallel slip in the hinge zone.

Mapping presented herein conclude that these models require significant modification. Interpretations of this study are presented below. In brief, the Ormsby Fault Zone is recognized as a zone of more concentrated ductile deformation resulting from contrasting competencies of more rigid metabasalt bodies being rotated in more ductile metasedimentary rocks. Metamorphic data collected and analyzed are suggestive (but not conclusive) of a large scale ductile fault running along the southwest contact with the Burwash Formation and the Giauque Lake and Transition units. No brittle evidence of this inferred fault was observed, and it interpreted to have a slightly different trace from the "Omsby Fault" of Stubley (1997).

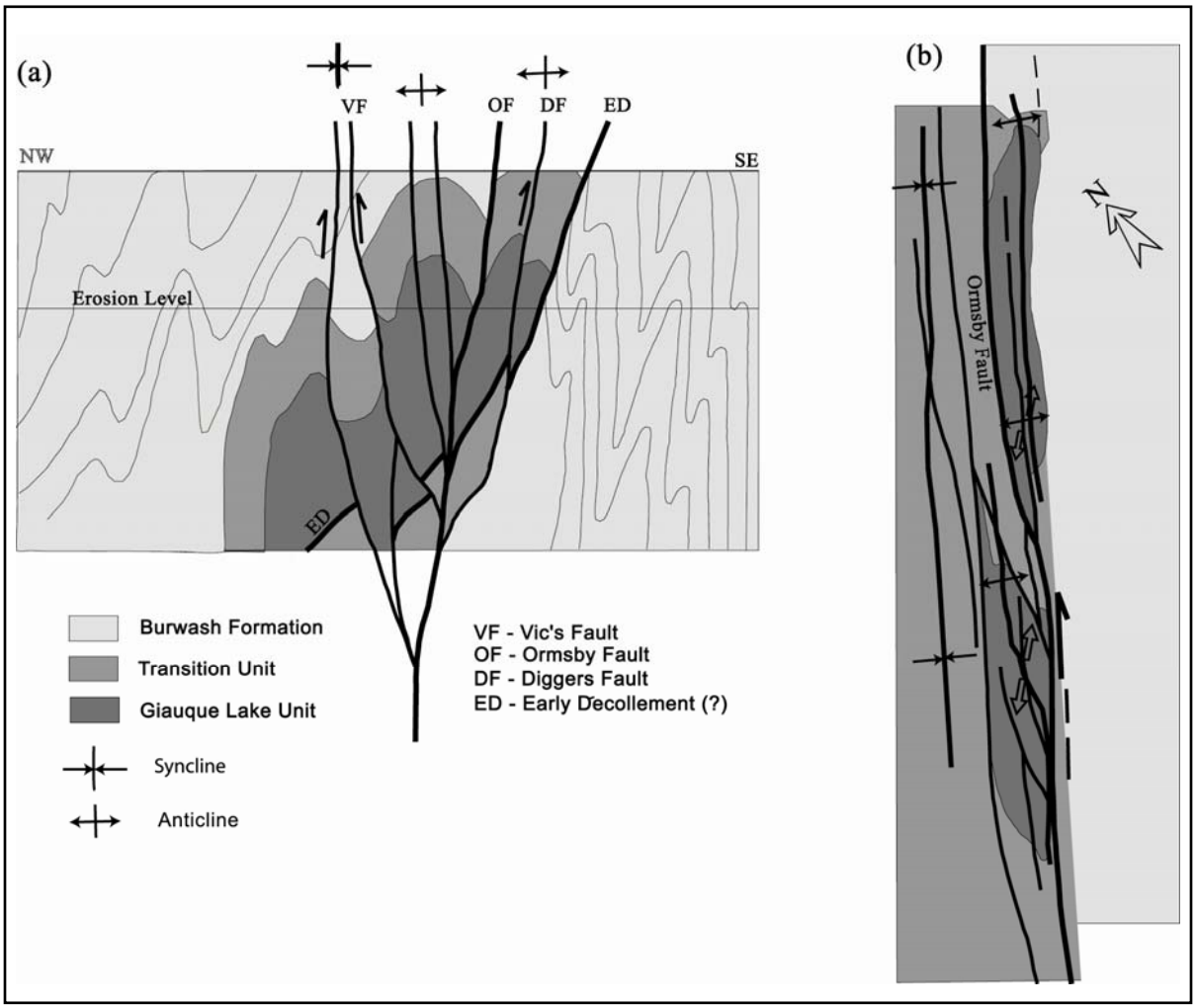

Fig 2.1: Hybrid of the two previously proposed models for the Ormsby and Discovery members: the folding proposed by Stewart (2005) superimposed on the extensional duplex proposed by Stubley (1997). The faults and décollement comprise the Ormsby Fault Zone. (a) cross-section across the Ormsby Fault Zone, and (b) plan view of the Ormsby Fault Zone across the property. (Stewart, 2005, modified from Stubley (1997) to illustrate compatibility of both models).

2.2.3 The Quartzite Unit

Rocks assigned to the Transition Unit (described below - section 2.3.2) in this study have been assigned other names in previous studies. A summary of previous work is provided here to help correlate more detailed descriptions of previous studies to the rocks described in this study.

The Quartzite Unit of Tremblay (1952) comprises two components: "quartzite" and

"granulite". The "quartzite" is fine-grained with a glassy white to grey, polished weathered surface. The "granulites" are weathered dark to rusty brown, fine to coarse grained generally with conspicuous garnets protruding above the weathered surfaces, and a narrow, apparently bleached white zone commonly surrounding bodies of this rock. They are composed of mostly hornblende and biotite with garnet, calcic andesine, quartz and minor epidote. Tremblay (1952) describes another group of "granulites" that is more variable in texture and mineralogy. He reports observing one type from this group between the Ormsby and Discovery members as "thick beds mixed with greywacke and presenting a sandy, coarsely streaked to banded appearance". This second group of "granulites" is composed of hornblende, andesine, quartz and garnet, with minor epidote and tourmaline. Tremblay (1952) proposes a sedimentary origin to the "granulites" since they are interbedded with sedimentary rocks.

Stubley (1997) subdivides the Quartzite Unit of Tremblay (1952) into two units: one still called the Quartzite Unit, and the second termed the Transition Unit. It is not clear how the two are differentiated. He describes the Quartzite Unit as comprising "well bedded alternations of wacke, siliceous wacke, hornblende-biotite-quartz-plagiclase±garnet layer, and white-weathering siliceous sediments". The Transition Unit is described as simply lacking the more siliceous layers. Hornblende-bearing layers are described as "mafic layers," but he suggests they could be of either continentally-derived sedimentary origin, or mafic tuffs. Prince (1998; see below – this section) proposes they are of the former. These "mafic" layers correspond to the "granulite" of Tremblay (1952).

Prince (1998) conducted a geochemical study on the Quartzite Unit (of Stubley, 1997) to determine its origin. Her study classifies each component of the Quartzite Unit as the Si-rich (corresponding to the quartzite), and Fe-rich (corresponding to the granulite/mafic layers) sub-units. She proposed terrigenous sediments as the origin for both sub-units based on trace element analysis and field observations. She reports that the mineral assemblages for both sub-units is consistent along strike with the Si-rich sub-unit typically consisting of quartz + biotite ± muscovite ± hornblende ± chlorite ± staurolite ± garnet ± feldspar, and the Fe-rich sub-unit consisting of biotite + quartz + chlorite ± plagioclase ± garnet ± staurolite ± hornblende ± grunerite ± sericite. The apparent difference between the two sub-units is that the Si-rich sub-unit contains more muscovite, whereas the Fe-rich sub-unit contains more

biotite. Geochemical analyses show that the Si-rich sub-unit contains higher Al_2O_3 reflecting higher abundances of muscovite and staurolite, whereas the Fe-rich sub-unit contains more Fe_2O_3 reflecting higher abundances of biotite, garnet and grunerite. Prince (1998) also concludes from geochemical analyses that there is little variation in the composition of metamorphic garnet, amphibole and staurolite throughout the unit, and between the two sub-units implying isochemical metamorphism. This indicates similar original bulk compositions for both sub-units (Prince, 1998).

2.3 Rock Units

2.3.1 Burwash Formation (Map Unit 3)

The most abundant unit on the property is made up entirely of metamorphosed sandstone and siltstone composing a sequence of turbiditic sedimentary rocks. These metaturbidites are correlated based on lithology (Stubley, 1997) to the Burwash Formation of the Yellowknife Supergroup (Figure 1.5). On the Discovery Property, the Burwash Formation is medium to thickly bedded (from several cm's to about 30 cm thick) and weathers light grey to pale brown, whereas fresh surfaces are darker grey.

Petrographically, the rocks are composed of porphyroclasts of quartz and minor twinned feldspar in a fine-grained matrix of quartz, biotite, muscovite, peak-metamorphic chlorite, untwinned feldspar and trace opaque minerals. Retrograde chlorite is intergrown with or replaces biotite. Very coarse (0.5-1 cm) cordierite porphyroblasts characterize the rocks in the northeast part of the study area (Figure 1.2). In thin section, cordierite is included with matrix minerals. Biotite porphyroblasts are present throughout much of the unit.

2.3.2 Transition Unit (Map Unit 2)

The Transition Unit rocks are more abundant northwest of the metabasalt of the Giauque Lake Unit (described below) on the Discovery Property. The Transition Unit is composed of metamorphosed beds of sandstone, siltstone, mudstone (commonly graphitic) ranging from millimetres to about 50 cm in thickness. At outcrop scale, the presence of dark brown to green typically garnet bearing (Fe-rich sub-unit described below), and mudstone layers distinguish the Transition Unit from the stratigraphically younger Burwash Formation.

Since Prince (1998) shows that there is no true quartzite present (see above – section

2.2.3), the term "quartzite" is dropped, and the rocks previously assigned to the quartzite unit are now assigned to the Transition Unit. The current study correlates the Transition Unit to the Banting Group of the Yellowknife Supergroup (Figure 1.5) based on a U-Pb age of 2661 ±5 Ma (see below – section 2.5) from a felsic tuffaceous layer.

Light to medium grey weathered sandstone and siltstone layers of the Si-rich sub-unit (described above) are indistinguishable in outcrop from those of the Burwash Formation. They differ in thin section from the Burwash Formation by the presence of staurolite and andalusite and absence of cordierite. Darker layers of rock containing epidote ± amphibole ± garnet are not found in the Burwash Formation.

Dark brown to green garnet bearing layers (Fe-rich layers of Prince, 1998) are the most distinctive distinguishing feature of the Transition Unit relative to the Burwash Formation. Although Prince (1998) shows these horizons to be mineralogically and chemically similar to the more siliceous layers (Si-rich layers), they respond to strain quite differently. The darker Fe-rich layers are conspicuously more competent, commonly boudinaged, transposed and rotated into S_3 (Figure 2.2 and 2.3; described below).

Characteristically graphite-rich metamorphosed mudstone is common along or near contacts with the metabasalt unit (Giauque Lake Unit, described below). It is very fine-grained, black, commonly has rusty weathering, and with laminations and bedding from mm's to cm's thick that are commonly folded at outcrop scale. Biotite, muscovite, quartz, minor sulphides, and typically graphite compose the rocks.

The Transition Unit appears anomalous in the Yellowknife greenstone belt region (Stubley, 1997), and is not consistent with the bulk of the Banting Group that occur farther south near Yellowknife. Although metabasalts and metasedimentary rocks occur in the Banting Group, they are much less common than metafelsic rocks (Helmstaedt and Padgham, 1986; Isachsen, 1992; Cousens et al., 2002; Martel, 2003). Since the proportions of rock types on the Discovery Property are atypical of the Banting Group, it will be described and referred to as the "Transition Unit" rather than the "Banting Group" to avoid confusion.

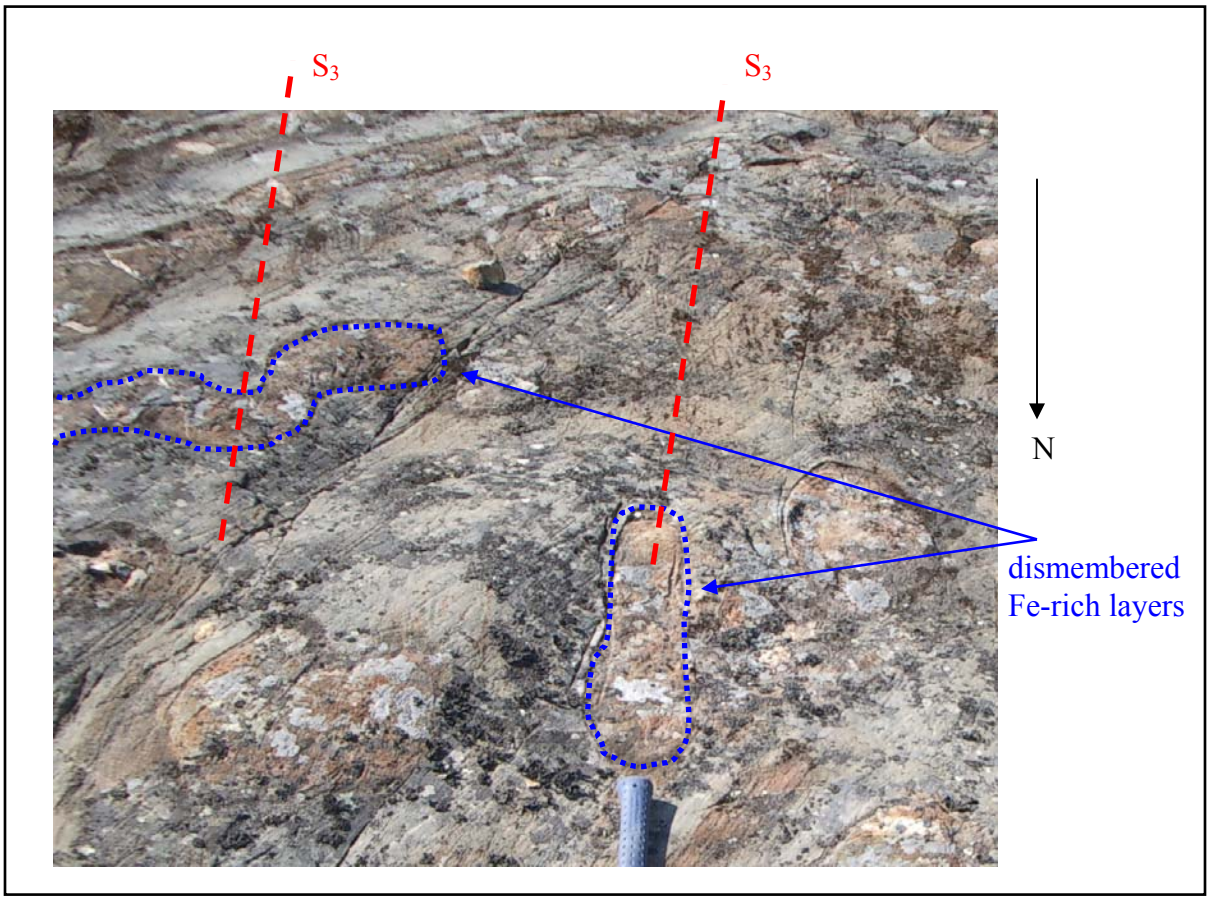

Figure 2.2: More competent layers in the Transition Unit dismembered and transposed into S_3 – note similar geometry as the Ormsby and Discovery members. (Note: north is down the page.)

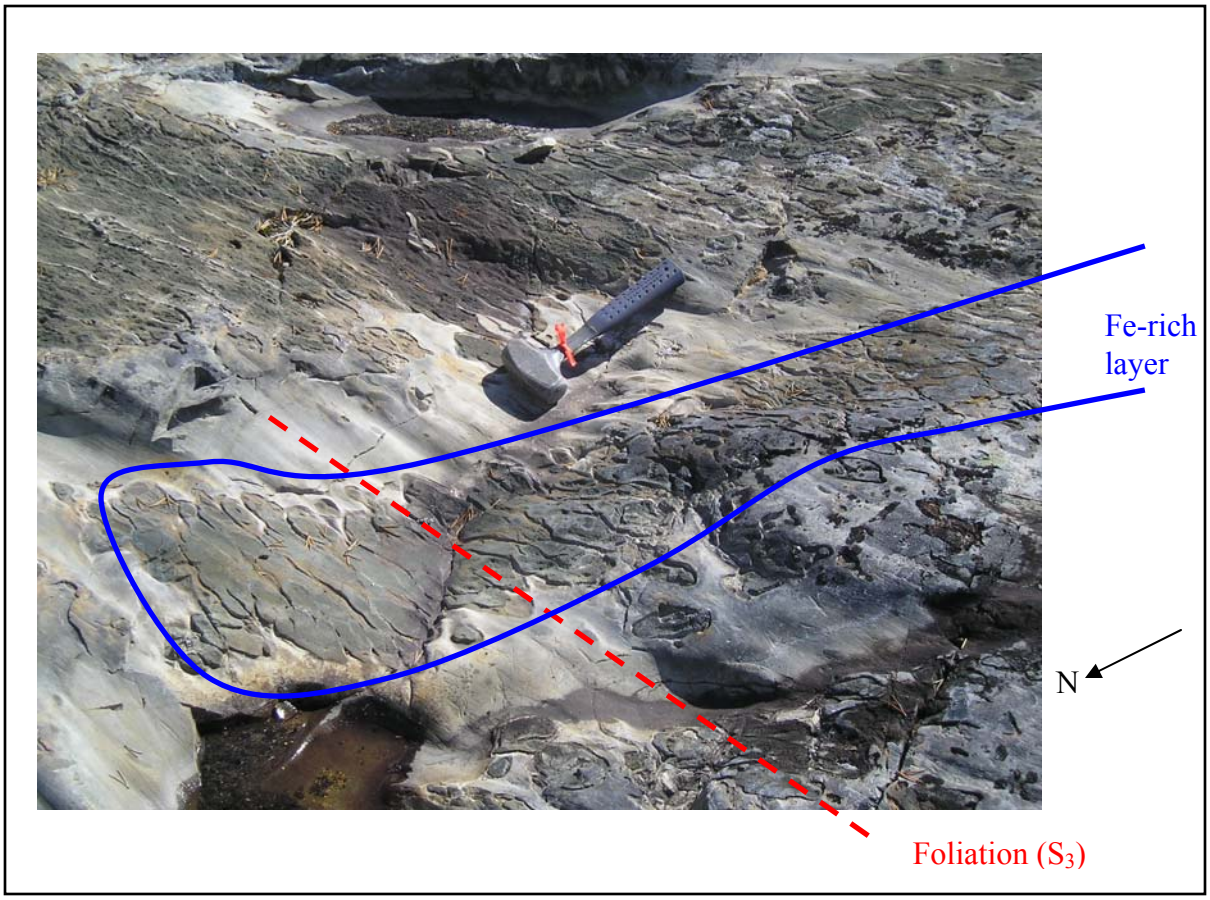

Figure 2.3: More competent Fe-rich layers in the Transition Unit transposed by foliation; S_3. (Hammer head points to north)

2.3.3 The Giauque Lake Unit (Map Unit 1)

Stewart (2005) proposes the informal name "Giauque Lake Unit" to include all the metavolcanic rocks on the Discovery Property (Figure 1.2). Chemical data are not available to confirm whether or not these rocks are true basalts in composition, but for brevity will be referred to as metabasalt herein. The Giauque Lake Unit consists of three main bodies of metabasalt (Figure 1.2). The two largest bodies on the property are known as the Ormsby and Discovery members. The Ormsby Member is the southernmost of the two, and the focus of this study. It measures approximately 1 km long by 200 m wide in surface outcrop. Exploration drilling indicate the Ormsby Member tapers with depth from being approximately 200 m wide at surface to approximately 120 m wide at a depth of 550 m below surface. The Discovery Member also measures approximately 1 km long but is narrower at only 120 m wide. The Discovery Member tapers with depth similarly to the

Ormsby Member (Tremblay, 1952). Farther to the north and outside of the study area is the smaller North Member (Figure 1.2).

Foliated and variably deformed metamorphosed volcanic rocks compose the Giauque Lake Unit. Protoliths range from pillow lavas with preserved selvages, to breccia, to massive coherent rocks.

The Ormsby Member is predominantly meta-breccia with breccia fragments occurring in all parts of the Ormsby Member. Intact pillowed lava however is restricted to the southeast side, where they occur mainly over the Ormsby Portal (Plate 1, Figure 2.4). Fractured to dismembered pillows (Plate 1) are present within the breccia. Contacts observed in drill core between the Ormsby Member metabasalt and surrounding metasedimentary rocks are steeply dipping. There is no evidence of brittle faulting at the contacts in conflict with the model of Stubley (1997). The metasedimentary rocks are tightly folded around the northern tip of the Ormsby Member (see below – section 2.8.3).

Coherent pillows are characterized by anastomosing white seams, <1 cm thick (Figure 2.5) that are aligned with the foliation (S_1; see below – section 2.8.1) parallel to the length of the Ormsby Member. These seams are interpreted as altered pillow selvages termed palagonite (Figure 2.5b-c; – 2.6.2). Atypically larger and more rounded clasts than the breccia fragments (described below) are present in close proximity to the continuous palagonite seams, and are also aligned with the foliation (S_1; Figure 2.5d). These atypical clasts are interpreted as dismembered relict pillows rather than larger breccia fragments. They are distinguished from breccia fragments by being rimmed, or partially rimmed with palagonite seams, their larger and more rounded shape, and because they weather slightly paler. Because these seams weather white, they are easily recognized on weathered outcrops against the green wall rock.

On fresh surfaces, the palagonite seams are almost black, like the wall rock, and distinguished by their finer-grained texture. Under the microscope, the palagonite seams are light brown and distinctly finer-grained than the wall rock. Their mineralogy consists of amphibole, biotite, quartz, tourmaline and lesser amounts of sphene and prehnite set in a talc groundmass.

Breccia fragments are vertically elongated, but in horizontal section, range from less commonly equidimentional (from several mm's to about 15 cm in diameter) to most

commonly elongate and banded in places (Figure 2.6). Breccia fragments weather light grey to white and stand out from the green wall rock on weathered surfaces. Locally (Plate 1) breccia fragments contain abundant biotite imparting a brownish colour. On fresh surfaces however, the fragments are hard to distinguish and were recognized by a faint stripe-like appearance to the rock; the stripes are the edges of the fragments. On fresh surfaces, the rocks are very dark green to almost black. The breccia fragments are composed of quartz + plagioclase ± biotite ± apatite. Wall rock mineralogy comprises quartz + hornblende ± actinolite ± cummingtonite, untwined oligoclase ± biotite ± apatite ± epidote ± chlorite ± calcite ± sericite and garnet porphyroblasts and opaque minerals (pyrrhotite, pyrite, arsenopyrite, ilmenite and minor sphalerite, chalcopyrite and magnetite).

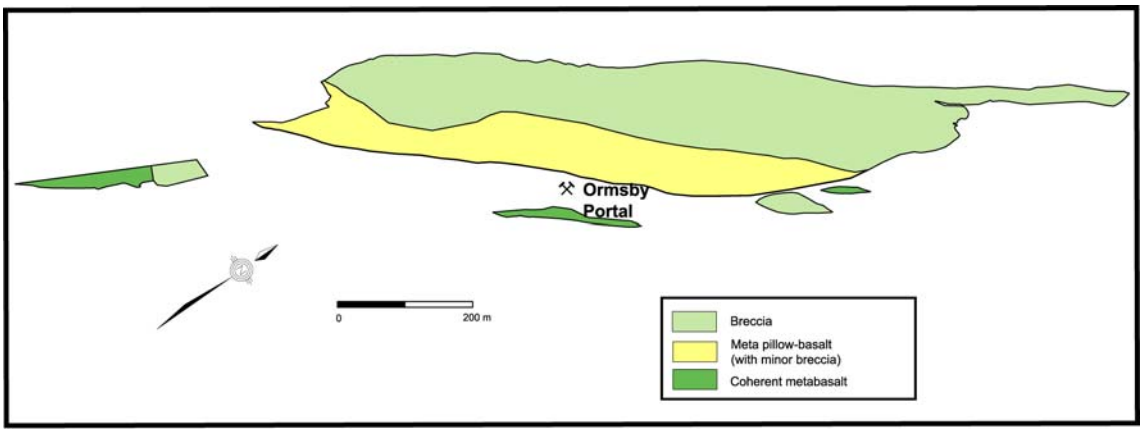

Figure 2.4: Simplified map of the Ormsby Member of the Giauque Lake Unit showing distribution of pillows, breccia and coherent, non-pillowed non-brecciated rocks throughout the Ormsby Member and surrounding metabasalt.

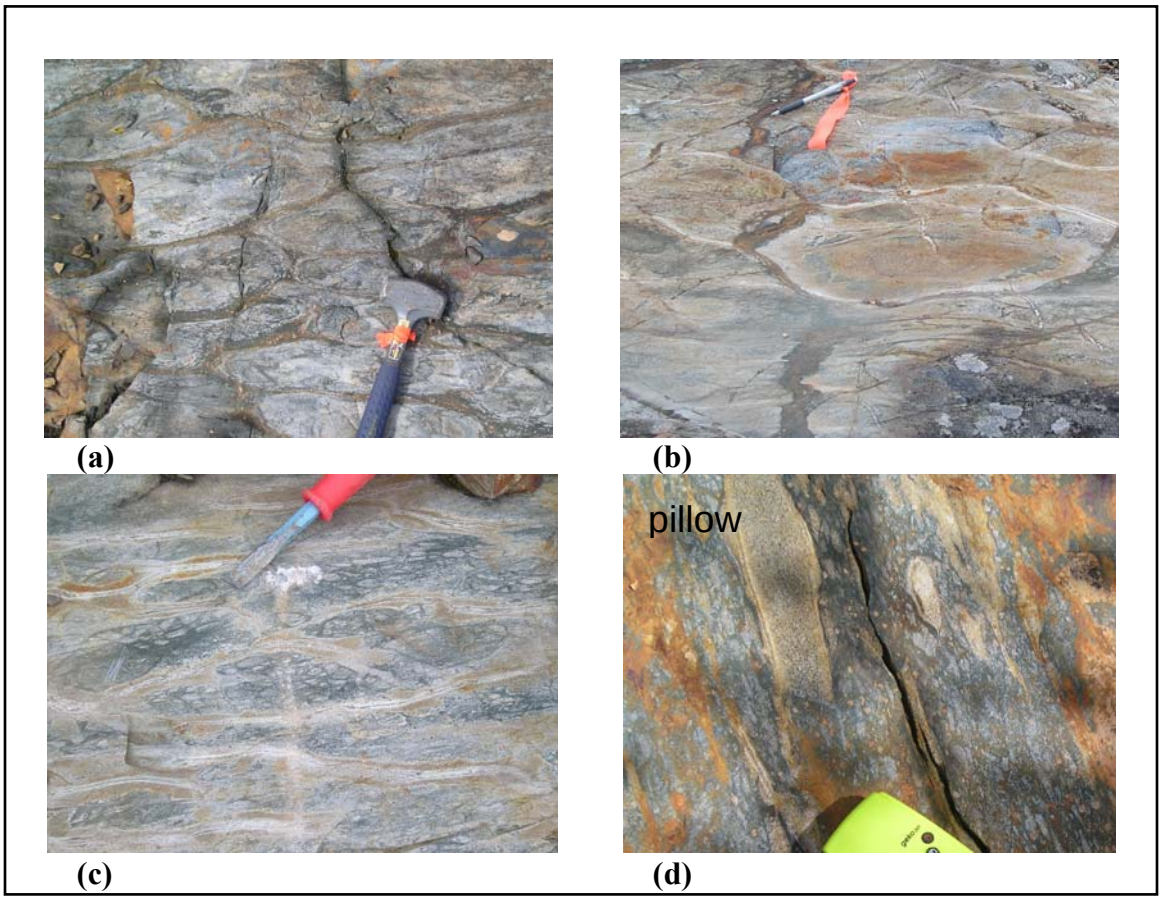

Figure 2.5: Metabasaltic pillowed rocks; all rocks contain upper greenschist – amphibolite facies mineral assemblages. (The following rock descriptions refer to protoliths.) **(a)** well formed pillows in the Discovery Member **(b)** Pillows in the Ormsby Member with thick green pillow selvage still recognizable, as well as white alteration seams of palagonite define shape. **(c)** Flattened pillows in the Ormsby Member recognizable by vague pillow shape and palagonite seams. **(d)** Flattened and dismembered pillow in the Ormsby Member recognized by the palagonite rim.

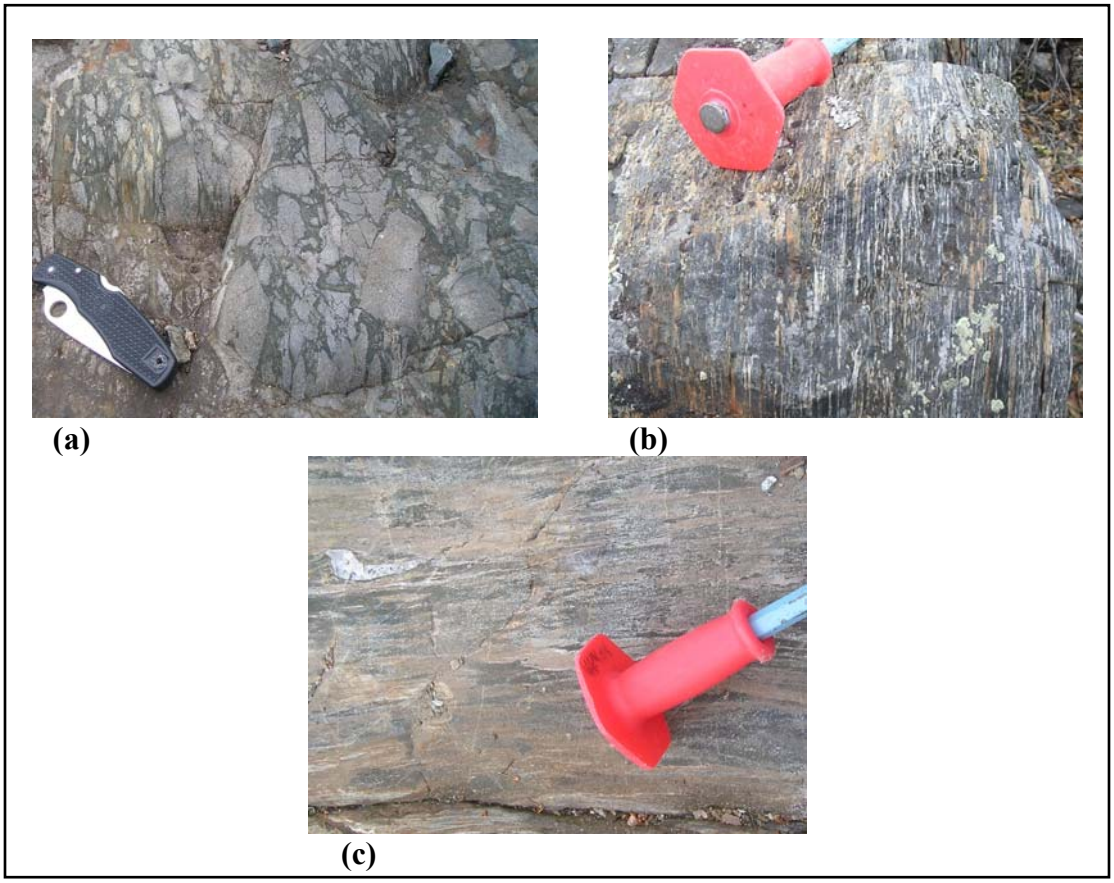

Figure 2.6: Metamorphosed brecciated basalt in outcrop displaying a range of superimposed deformation. **(a)** Equidimentional in horizontal section representing relatively undeformed rocks. **(b)** Banded, representing more highly strained rocks. **(c)** Example of brownish breccia fragments containing biotite.

2.4 Basalt Geochemistry

Basaltic flows from both Kam and Banting Group have flat to slightly light rare earth element- (REE) enriched patterns that commonly lack negative Nb anomolies (Cousens et al., 2002). Andesitic to dacitic pillow lavas from the Banting Group are moderately light REE-enriched with large Nb depletions and enrichments in Th and have a concave-up pattern from Gd through Lu (Cousens et al., 2002). Mafic rocks of the Kam and Banting groups are indistinguishable from the REE patterns. The felsic rocks from each group however have distinct patterns (Cousens et al., 2006). Banting Group felsic rocks are strongly light REE-enriched, heavy REE-depleted, have negative Nb anomalies and lack Eu anomalies. Felsic

rocks from the Kam Group are moderately light REE-enriched, have flat heavy REE patterns, negative Nb anomalies and Eu anomalies.

Six samples from the Giauque Lake Unit were selected by Tyhee NWT Corp. (current property owners) for incompatible element geochemistry (Table 2.2). Data are plotted (Figure 2.7) to help correlate the rocks with those farther south near Yellowknife. Elements are plotted in the same order as Cousens (2002) for easy comparison. The rocks sampled are slightly light REE enriched and slightly heavy REE depleted with minor depletions in Nb and Eu in two of the samples. On the basis of this data the Giauque Lake Unit metabasalt are indistinguishable in terms of incompatible element patterns from mafic rocks of the Kam and Banting group rocks farther south near Yellowknife. Distinguishing between the two groups using REE geochemistry can only be done when felsic rocks are present with the mafic rocks. The Giauque Lake Unit is correlated to the Banting Group based on its depositional relationships with the Transition Unit (which is correlated to Banting Group in age) described below (sections 2.6.1 and 4.4).

Table 2.2a: Incompatible element data in ppm

	Primitive Mantle(PM)	67351 (Ormsby Member)	65001 (Discovery Member)	65003 (Discovery Member)	65091 (Discovery Member)	65094 (Discovery Member)	1000356 (Ormsby Member)
Th	0.085	1.3	0.8	1.1	1.8	1.4	1.7
Nb	0.713	7.8	9.4	9.9	21.9	21.2	8.7
La	0.687	8.9	10.4	9.7	18.7	17.7	11.1
Ce	1.775	23.6	25.8	24.7	45.8	44.7	29.1
Pr	0.276	3.6	3.78	3.69	6.83	6.49	4.38
Nd	1.354	18.1	17.8	17.8	31	30.2	20.9
Sm	0.444	5.14	4.52	4.41	8.04	7.46	6.01
Zr	11.200	160.7	126	124	205.2	194.8	165.8
Hf	0.309	4.4	3.5	3.6	6	5.9	4.9
Eu	0.168	1.59	1.56	1.51	2.56	2.58	1.65
Gd	0.596	6.11	5.13	5.03	8.51	8.08	7.23
Tb	0.108	1.17	0.99	0.94	1.51	1.46	1.43
Dy	0.737	6.84	5.25	5.27	8.38	7.75	8.28
Y	4.550	40.5	30.5	29.3	47.2	45.1	49.9
Ho	0.164	1.39	1.09	1.07	1.7	1.59	1.69
Er	0.480	4.18	2.99	2.99	4.72	4.49	5.07
Tm	0.074	0.6	0.46	0.46	0.71	0.69	0.76
Yb	0.493	3.75	2.61	2.66	4.27	4.22	4.73
Lu	0.074	0.59	0.43	0.43	0.67	0.64	0.75

(PM values from Sun and McDonough, 1989)

Table 2.2b: Primitive Mantle (PM) normalized (Sun and McDonough, 1989) incompatible element data in PPM

	67351 (Ormsby Member)	65001 (Discovery Member)	65003 (Discovery Member)	65091 (Discovery Member)	65094 (Discovery Member)	1000356 (Ormsby Member)
Th	15.29	9.41	12.94	21.18	16.47	20.00
Nb	10.94	13.18	13.88	30.72	29.73	12.20
La	12.95	15.14	14.12	27.22	25.76	16.16
Ce	13.30	14.54	13.92	25.80	25.18	16.39
Pr	13.04	13.70	13.37	24.75	23.51	15.87
Nd	13.37	13.15	13.15	22.90	22.30	15.44
Sm	11.58	10.18	9.93	18.11	16.80	13.54
Zr	14.35	11.25	11.07	18.32	17.39	14.80
Hf	14.24	11.33	11.65	19.42	19.09	15.86
Eu	9.46	9.29	8.99	15.24	15.36	9.82
Gd	10.25	8.61	8.44	14.28	13.56	12.13
Tb	10.83	9.17	8.70	13.98	13.52	13.24
Dy	9.28	7.12	7.15	11.37	10.52	11.23
Y	8.90	6.70	6.44	10.37	9.91	10.97
Ho	8.48	6.65	6.52	10.37	9.70	10.30
Er	8.71	6.23	6.23	9.83	9.35	10.56
Tm	8.11	6.22	6.22	9.59	9.32	10.27
Yb	7.61	5.29	5.40	8.66	8.56	9.59
Lu	7.97	5.81	5.81	9.05	8.65	10.14

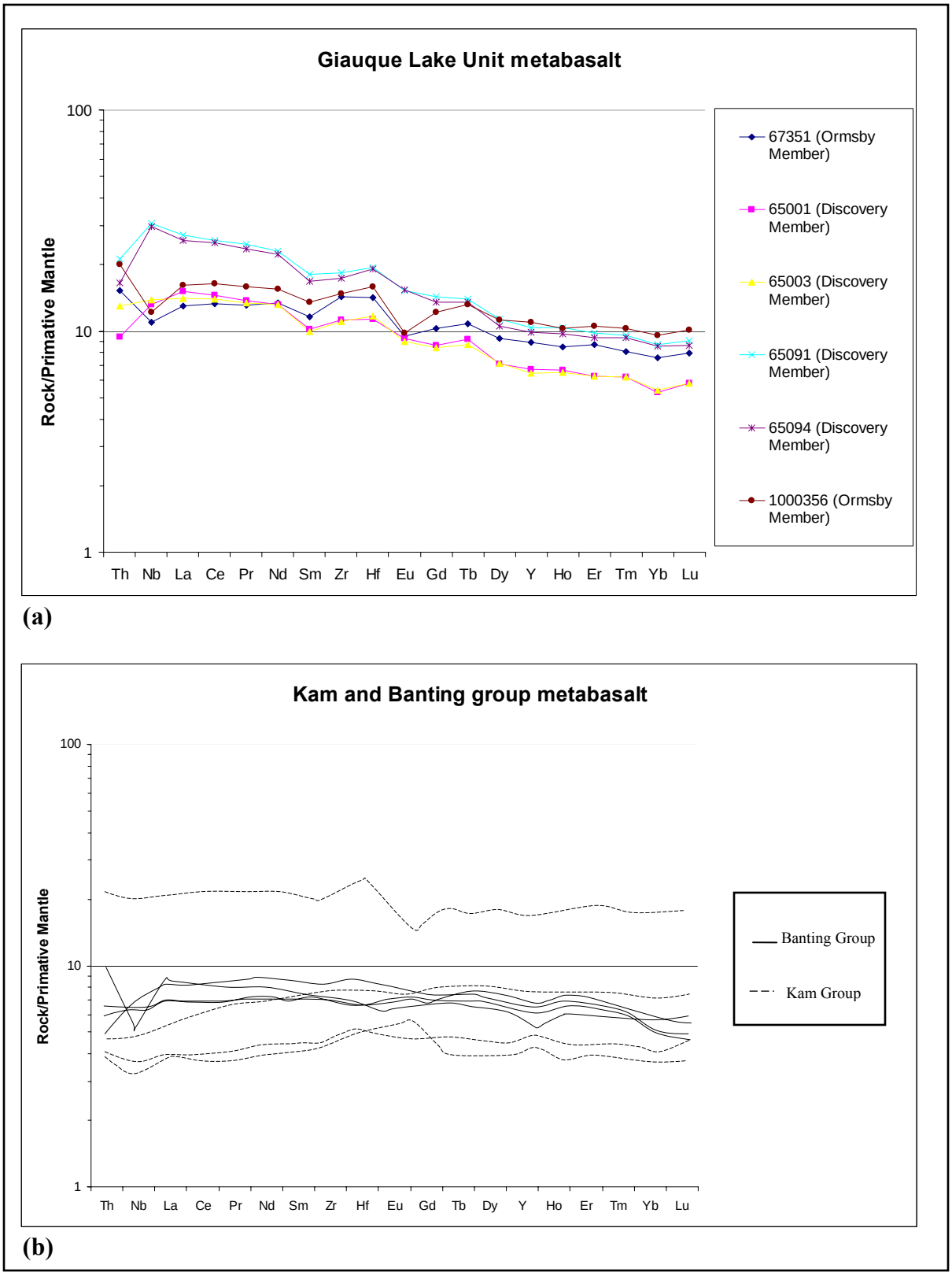

Figure 2.7: Primitive Mantle Normalized (Sun and McDonough, 1989) incompatible element plots for **a)** metabasaltic rocks from the Giauque Lake Unit and **b)** metabasalts from the Kam and Bantinig groups (Cousens et al., 2002).

2.5 Geochronology

A sample from a layer with a felsic tuffaceous component in the Transition Unit (Figure 1.2; see above – section 2.3.2), was collected for U-Pb geochronology. This layer is common within the Transition Unit, and possibly the "Quartzite" component, or part of it, described by Tremblay (1952). These layers are about 30-40 cm thick and weather light grey. They contain eye-shaped quartz crystals 1-2 mm long that are interpreted as blastophenocrysts. In thin section, primary textures are obliterated by deformation, and the rock contains blastophenocrysts of quartz appearing similar to quartz porphyroclasts observed in sandstone layers across the property. The sample dated is interpreted as a reworked tuff based on outcrop and thin section observations and on zircon ages (described below) implying zircons came from largely a single source.

The sample was crushed using a Rhino jaw crusher, and ground with a Bico disk grinder equipped with ceramic grinding plates. The grind was then processed on a Wilfley wet shaking table equipped with a machined Plexiglass top, followed by conventional heavy liquids and magnetic separation using a Frantz magnetic separator. A representative suite of zircons (of at least 50 crystals) were hand picked under a binocular microscope and 12 were selected for Sensitive High-Resolution Ion Micro-Probe – Reverse Geometry (SHRIMP-RG) analysis (Table 2.3).

The zircons were generally euhedral, very dark purple, and turbid with obvious cracks. Cathodoluminesence and backscatter electron imaging showed generally smooth to oscillatory zoning, and no distinctive differences in zoning with respect to elongate or stubby crystals.

Spots on the twelve zircons give discordant U-Pb isotopic systematics. Nine of the 12 form a discordia array with an upper concordia intercept of 2661 ±5 Ma (Figure 2.8). This age is interpreted to be the crystallization age of the protolith. Three grains gave older U-Pb ages, and are interpreted to be xenocrysts incorporated into the tuff during eruption or deposition. Based on this age, the Transition Unit rocks are correlated to the Archean Banting Group (Figure 1.5).

Table 2.3: SHRIMP-RG U-Pb isotopic data for WWU-Pb

Grain	% comm 206Pb	ppm U	ppm Th	232Th /238U	ppm Rad 206Pb	204corr 206Pb /238U Age (Ma)	1σ err (Ma)	204corr 207Pb /206Pb Age (Ma)	1 σ err (Ma)	207Pbr /235U	% err	206Pbr /238U	% err	err corr
1	0.00	292	233	0.82	128.8	2673.4	37.5	2662	6	12.82	1.8	.5139	1.7	.977
2	0.00	139	75	0.56	63.7	2753.6	39.3	2657	9	13.26	1.8	.5329	1.8	.956
3	0.01	227	73	0.33	103.7	2747.4	38.9	2719	7	13.73	1.8	.5314	1.7	.971
4	0.03	232	244	1.09	108.2	2796.0	39.2	2655	7	13.49	1.8	.5430	1.7	.970
5	-0.01	217	158	0.75	94.0	2632.2	37.3	2670	7	12.65	1.8	.5043	1.7	.970
6	0.04	144	133	0.96	63.6	2674.3	38.8	2653	10	12.76	1.9	.5141	1.8	.945
7	0.06	231	276	1.24	98.0	2587.3	38.0	2655	8	12.27	1.9	.4938	1.8	.963
8	0.05	242	211	0.90	109.0	2715.8	38.2	2655	7	13.02	1.8	.5239	1.7	.969
9	0.03	273	193	0.73	115.1	2574.2	36.4	2674	7	12.34	1.8	.4908	1.7	.973
0	-0.01	237	142	0.62	103.5	2646.5	37.4	2660	7	12.65	1.8	.5076	1.7	.971
11	0.10	234	104	0.46	107.3	2751.5	39.0	2819	7	14.61	1.8	.5324	1.7	.969
12	0.04	644	155	0.25	290.0	2715.8	37.6	2734	4	13.66	1.7	.5239	1.7	.988

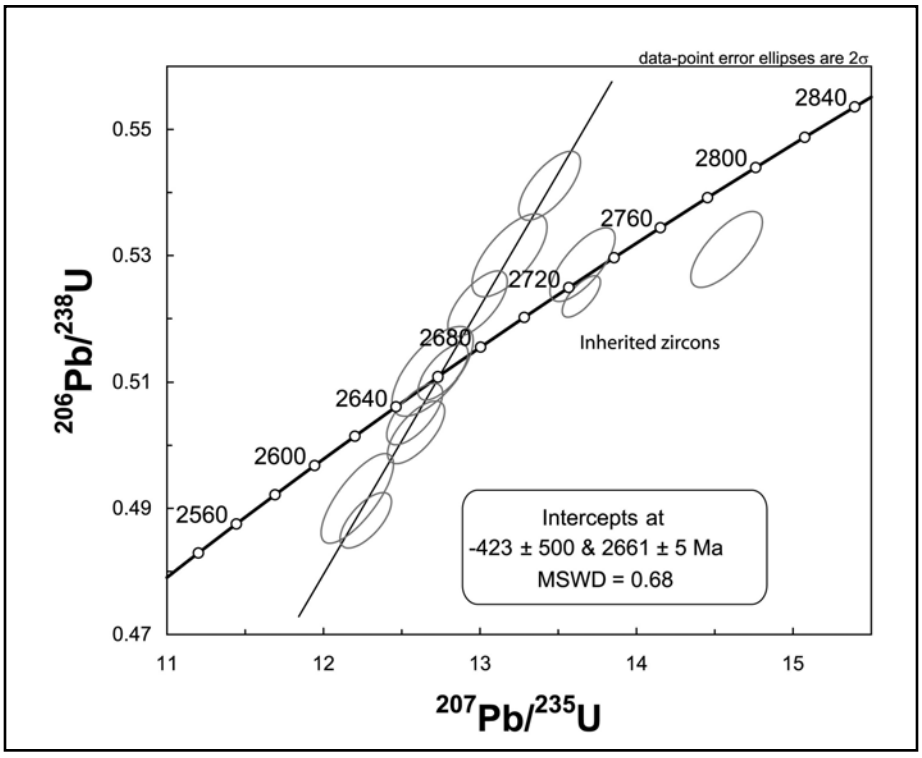

Figure 2.8: U-Pb Concordia diagram of zircons from tuffaceous layer within the Transition Unit. Anaytical data from sample WWU-Pb. SHRIMP-RG (Table 2.3); sample location (7,008,921 mN, 353,338 mE) shown on Figure 1.2 and Plate 1.

2.6 Pre-metamorphic Conditions

2.6.1 Depositional Environment

A brief interpretation of the depositional environment is presented here and will be drawn upon in the concluding chapter to help reinforce the argument that the Giauque Lake and Transition units are part of the same sequence. The following descriptions of depositional environments for basaltic lavas are from McPhie et al. (1993) and references therein.

Rocks of the Giauque Lake Unit were emplaced subaqueously as indicated by the presence of pillows. The abundance of breccia forming much of the Ormsbsy Member is also characteristic of magma erupted into a subaqueous setting. The breccia may be a result of either autobrecciation or quench fragmentation or both. Metamorphism and deformation hinder interpretations of exact emplacement and fragmentation processes. Autobrecciation involves the non-explosive fragmentation of flowing lava where cooler more viscouse lava (commonly outer surfaces), or parts of the flow that are subject to locally higher strain, respond to stress in a brittle fashion. Quench fragmentation, commonly forming hyaloclastite, occurs in response to thermal stress built up during rapid cooling, as well as stress imposed on chilled outer parts of lava flows by continued movement of the molten interior. Textural differences between autobreccia and hyaloclastite are subtle; autobreccia lacks evidence of quenching, and typically contain very minor amounts of fine clasts. Breccia ranges from in situ closer to the pillows, to resedimented farther from the pillows. Resedimented and reworked volcanic and pyroclastic material is commonly interlayered with surrounding sedimentary rock, much like the Transition Unit on the Discovery Property. Breccia is most common along the front and top of lava flows. As lava flows up and forward some of the breccia on top or in front of the flow gets resedimented.

2.6.2 Pre-metamorphic Alteration

The degree of seafloor metasomatism that occurred during the formation of the Yellowknife greenstone belt remains debated. Baragar et al. (1979) argue that seafloor metasomatism was probably minor. Duke et al. (1990) and McDonald et al. (1993) in contrast, suggest that seafloor metasomatism played a more significant role completely transforming the rocks in the belt. Thompson (2006), agreeing with Baragar et al. (1979),

contends that seafloor metasomatism was not pervasive, although the absence of sub-greenschist facies rocks in the belt limit interpretation of early metamorphism and alteration.

Basaltic protoliths of the Yellowknife greenstone belt are tholeiitic in composition, based on trace-element analyses (Cousens, 2002). Tholeiitic basalts are characterized by low concentrations of Na and K. Although no chemical data are available to confirm it, the basaltic rocks in the Ormsby Member are interpreted to have experienced significant alkalic metasomatism, as shown by the abundant metamorphic sodic plagioclase and biotite. Sodium-bearing plagioclase (oligoclase, identified using electron microprobe) is common throughout the Ormsby Member, whereas biotite is localized (Plate 1). The presence of these Na- and K-bearing phases in rocks of basaltic composition can be explained by pre-metamorphic seafloor alteration, which involves the addition of K and Na from sea water as the rocks were erupted onto the seafloor and cooled.

There are two process responsible for K-Na metasomatism of basalt (Bloch et al., 1979) on the seafloor. The first is palagonitization, which is the low temperature alteration of glassy rims of pillow basalts by circulating seawater. Palagonite (reviewed by: Stroncik and Scmincke, 2002; Gifkins et al., 2005 *pp. 99-100*), is a heterogeneous composition of smectite and may contain zeolites in vesicles or fractures. The second process by which K is added to submarine basalts is through fracture filling by seawater. This fracture-controlled alteration results in the formation of K-rich phases, such as biotite, in vesicles and fracture zones. Such a process could explain the heterogeneous distribution of biotite within the metabasalt of the Ormsby Member.

Ion exchange reactions with the sea water replaces Ca from plagioclase with Na. This metasomatic process (reviewed by Gifkins et al., 2005 *p. 114*) results in a more sodic rich plagioclase composition upon metamorphism. Albitization commonly progresses preferentially along plagioclase grain fractures and cleavage traces. Typically albite is included with sericite, calcite and clay that formed as by-products consuming Ca and Al released during albitization.

2.7 Metamorphism

The mineral assemblages in all rocks on the property indicate metamorphism at greenschist to amphibolite facies conditions. The peak-metamorphic assemblages observed in

the Burwash Formation are quartz + plagioclase (oligoclase) + biotite + muscovite ± chlorite + cordierite and quartz + plagioclase (oligoclase) + biotite ± muscovite ± chlorite. The presence of cordierite porphyroblasts marks a cordierite-in isograd (Figure 1.2) southeast of the Discovery Member. The peak-metamorphic assemblages observed in the Transition Unit include: quartz + plagioclase ± biotite ± muscovite ± graphite; quartz + plagioclase (andesine) + biotite + muscovite + chlorite + staurolite; quartz + plagioclase (oligoclase) + biotite + muscovite + chlorite + andalusite; and quartz + plagioclase + biotite ± chlorite ± epidote ± hornblende ± garnet. Evidence of two textures of garnet, possibly indicating continued garnet growth as deformation progressed, is preserved by older cores with inclusions and younger less inclusion-rich rims (Figure 2.9). Chloritized biotite is evidence of retrograde metamorphism in the metasedimentary rocks. Finer-grained chlorite grains aligned with the foliation and texturally similar to muscovite and biotite are interpreted as growing peak metamorphism. In contrast, larger grains of chlorite cutting the foliation, or biotite grains partially replaced by chlorite, are interpreted as retrograde metamorphic chlorite growth.

The peak-metamorphic assemblage in the Giauque Lake Unit of hornblende ± actinolite ± cummingtonite + quartz + oligoclase ± garnet ± epidote ± biotite record upper greenschist to amphibolite transition facies conditions. Hornblende, which dominates the assemblage, generally grows at higher temperatures than actinolite. As actinolite co-exists with hornblende locally, the rocks are interpreted to have been metamorphosed at conditions spanning the transition between greenschist and amphibolite facies. As these rocks have likely been altered on the seafloor and Na added (see above – section 2.6.2), it is uncertain whether the abundance of Na over Ca in the plagioclase has any metamorphic significance. Garnet porphyroblasts (1-10 mm in diameter) are generally present and distributed throughout the Ormsby Member (Plate 1). Garnet is indicative of medium to high pressure (amphibolite facies) and high temperature greenschist facies. Chlorite, calcite and sericite overprinting metamorphic mineral assemblages in the metabasalt are evidence of retrograde metamorphism.

Six thin sections were selected for microprobe analysis in order to determine mineral chemistry to help constrain bulk composition and help quantify peak-metamorphic conditions. The most representative mineral compositions for each sample are presented in

Tables 2.4 to 2.9, and all data are presented in Tables A1 to A10 (Appendix A). Poor analyses with incorrect molar ratios were omitted from the data tables in Appendix A. Peak pressure and temperature (P-T) estimates are calculated using conventional geothermobarometry (calibrated reactions) and THERMOCALC (computer software consisting of a thermodynamic dataset). Samples that were selected from each of the rock units on the property (Figure 1.2) contain most representative peak-metamorphic mineral assemblages. Thin sections were examined using a petrographic microscope and grains were selected for analysis based on their textural relationship. Grains selected are in close proximity (within 1-2 mm) and appear to have grown in equilibrium. Texturally, the peak-metamorphic assemblages from each sample appear to have formed at the same time relative to deformation (see below – this section). Since all the metasedimentary rocks analyzed contain quartz and muscovite in equilibrium with the rest of the peak-metamorphic assemblage, their assemblages are projected onto an AFM diagram (Figure 2.10) to show the range of possible bulk compositions for each sample. The metabasalt rock compositions are shown on an ACF diagram (Figure 2.11).

Figure 2.12 shows the relative topologies of the reactions for the four metasedimentary samples probed. P-T pseudosections (taken from Wei et al., 2004; Dymoke and Sandiford 1992) for rocks of similar assemblages (but different bulk compositions; Figure 2.13) show the effect of bulk composition on these topologies. As X_{Fe} increases, the cordierite-chlorite field approaches the staurolite-chlorite field. At $X_{Fe} = 0.4$ these two fields are approximately 2.5 kbar apart (Figure 2.13a) and at $X_{Fe} = 0.7$ the two fields are in contact (Figure 2.13b). Figure 2.10 shows that X_{Fe} for the Transition Unit ranges from 0.69 to 0.94 and 0.5 to 0.54, and for the Burwash Formation from 0.36 to 0.51. Using these X_{Fe} values and the published pseudosections in Figure 2.13 as a general indicator of where rocks of those bulk compositions might plot in P-T space, it appears that rocks of the Transition Unit experienced peak metamorphism around 3-4 kbar, and 550-600ºC. In contrast, rocks of the Burwash Formation possibly experienced peak metamorphism as low as 1-2 kbar and 450-500ºC. This would imply that two metamorphically different domains have been juxtaposed post-peak metamorphism. This is the basis for the interpretation of a possible ductile fault cutting the property (see below – this section).

Microprobe data show that the bulk composition of the Burwash Formation and andalusite bearing layers of the Transition Unit are similar. Although calculated uncertainties on P-T estimates for the Transition Unit (see below – this section) overlap with estimated P-T ranges for the Burwash Formation, based on reaction topologies for the given range of potential bulk compositions, assuming assemblage formed at the same time, and a closed KFMASH system, the Burwash Formation was metamorphosed at a shallower depth than the Transition Unit. Since the samples analyzed were only several hundred metres apart on surface (Figure 1.2), there is the possibility of a post-peak metamorphic fault separating rocks of the Burwash Formation from rocks of the Giauque Lake and Transition units on the property. Nevertheless, conclusive evidence of a through-going fault remains elusive. Evidence of through-going faulting was not observed mapping or in drill core, so if a fault is present, it is likely a ductile fault overprinted by retrograde metamorphism.

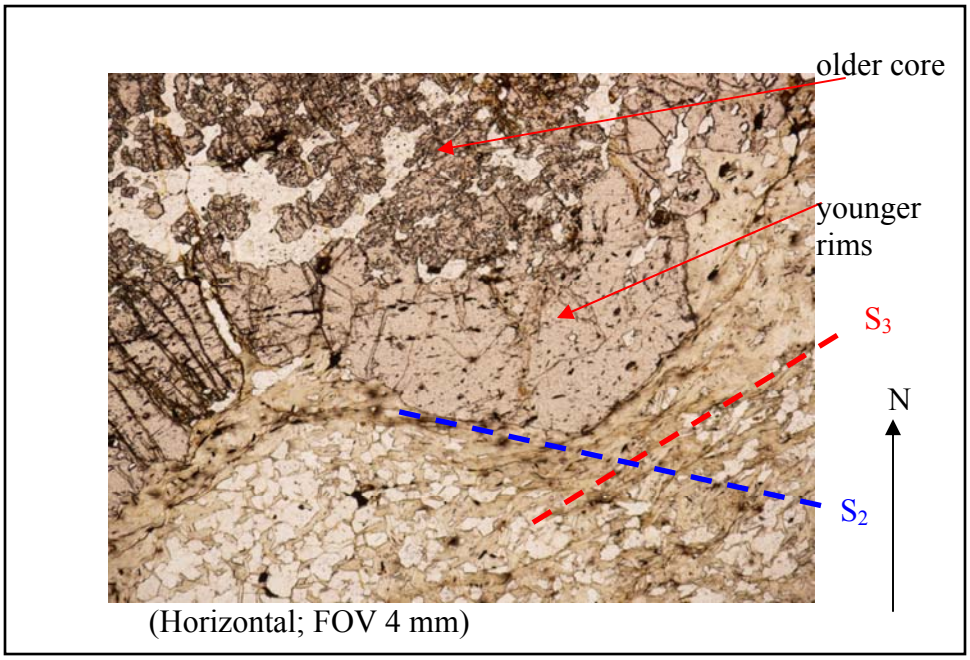

Figure 2.9: Two garnet textures, older core is sieve textured whereas younger rims are not. Chlorite defines the foliation in the groundmass

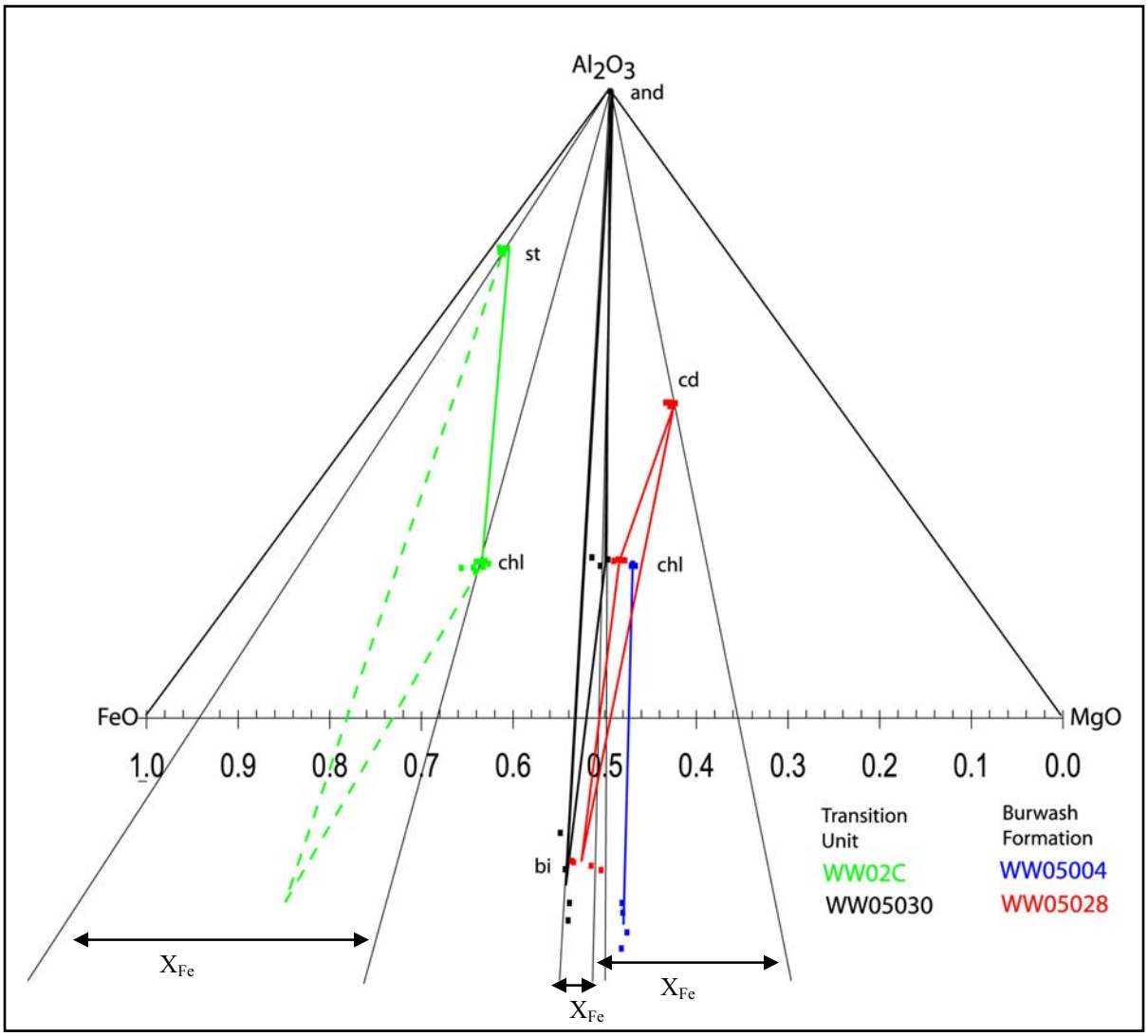

Figure 2.10: AFM diagram for metasedimentary rocks, arrows indicate range of possible X_{Fe}. Samples include:

- WW02C (Transition Unit): bi + ms + chl + st + q + ads
  The biotite analyzed was partially chloritized and the analyses were not considered. The dashed lines are an interpretation of where the biotite present in the rock might plot.

- WW05030 (Transition Unit): bi + and + chl + ms + q + olg

- WW05004 (Burwash Formation): bi + ch + ms + q + olg

- WW05028 (Burwash Formation): bi + chl + cd + ms + q + olg

(and = andalusite, st = staurolite, cd = cordierite, chl = chlorite, bi = biotite, q = quartz, ads = andesine, olg = oligoclase)

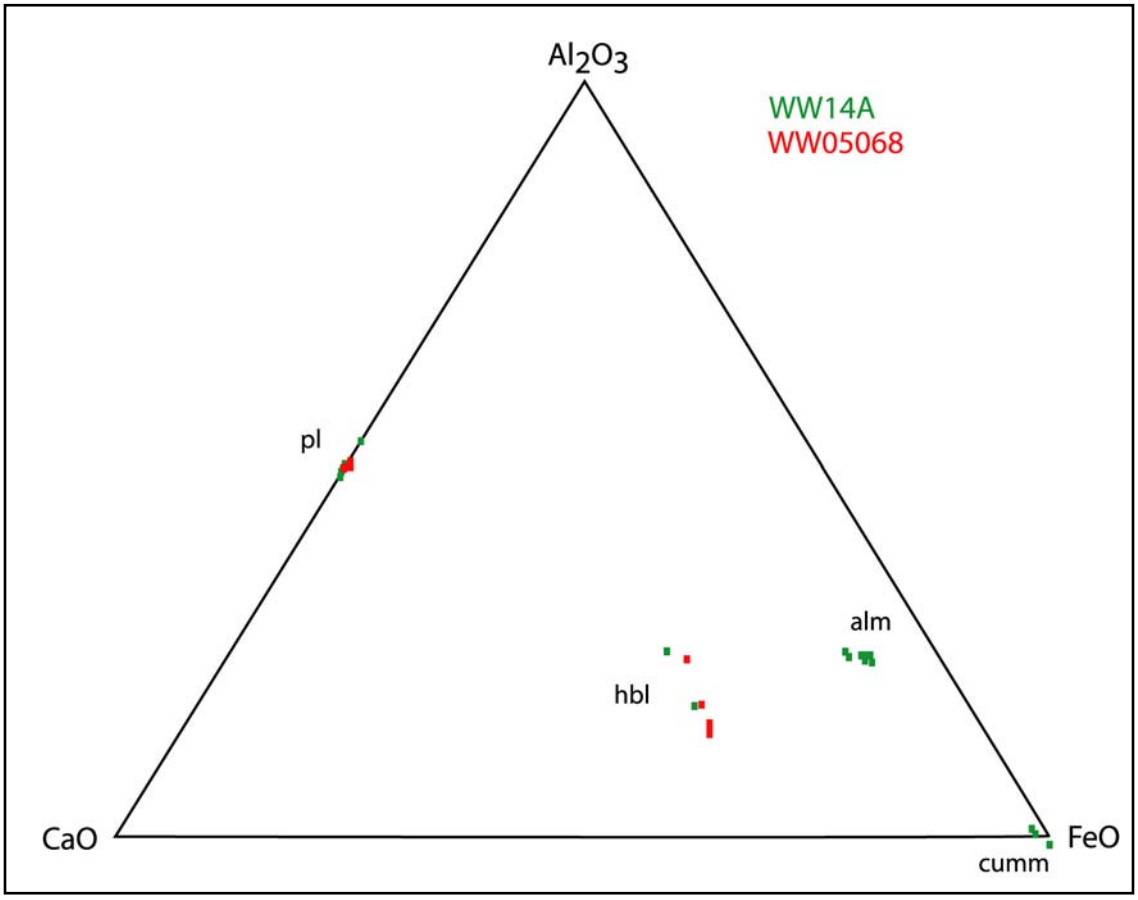

Figure 2.11: ACF diagram for metabasalt. Samples include:

- WW14A (Ormsby Member): q + olg + bi + hbl + alm + cumm
- WW05068 (Discovery Member): q + olg + bi + hbl

(q = quartz, pl = plagioclase, hbl = hornblende, alm = almandine, cumm = cummingtonite)

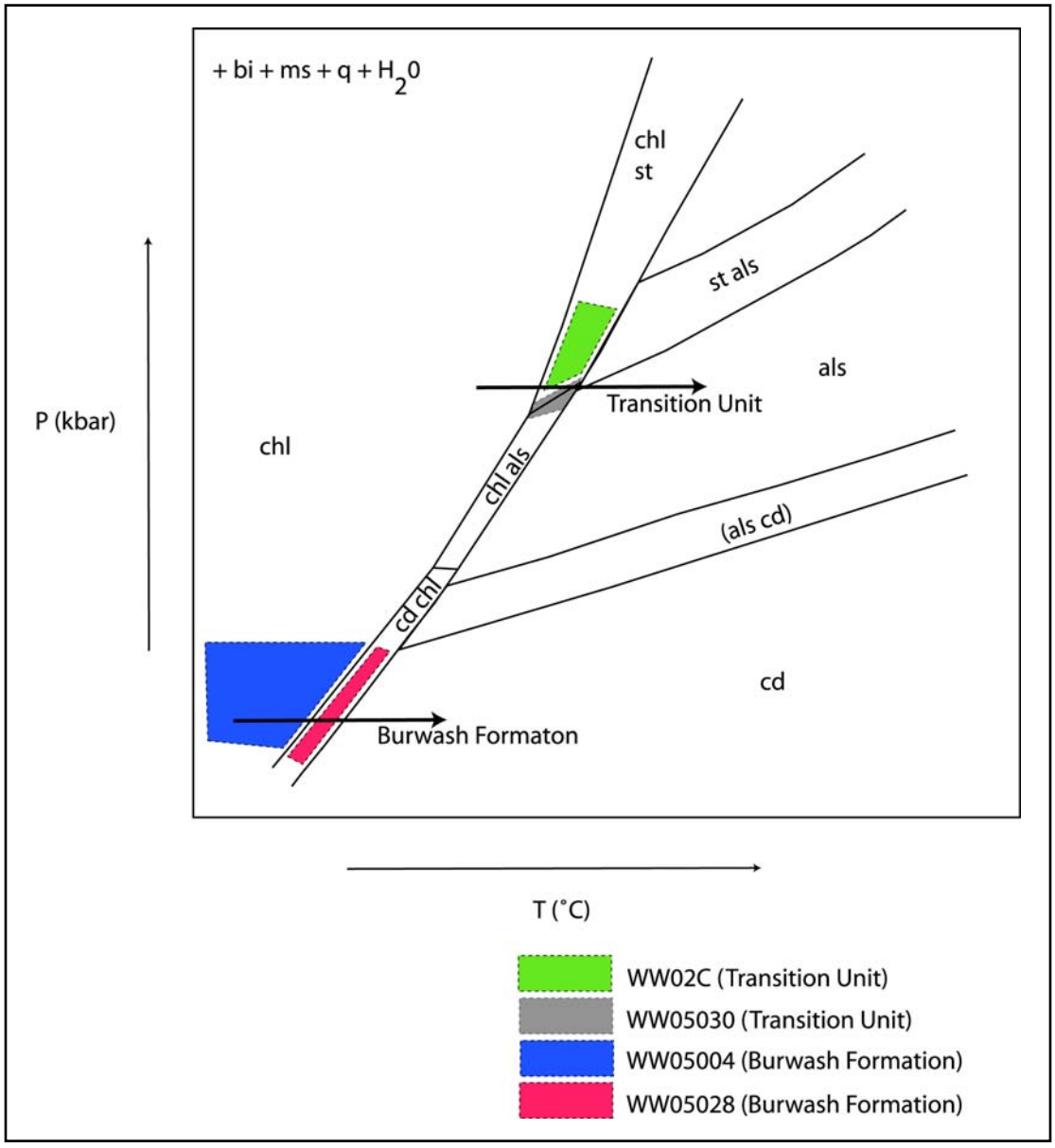

Figure 2.12: Relative reaction topologies for the four metasedimentary rock samples analyzed.
The fields where each sample is generally expected to plot in P-T space are shaded in colour. The arrows indicate the direction in which the metamorphic reactions for each unit are interpreted to progress.
(bi = biotite, ms = muscovite, q = quartz, chl = chlorite, st = staurolite, als = alumina-silicate, cd = cordierite)

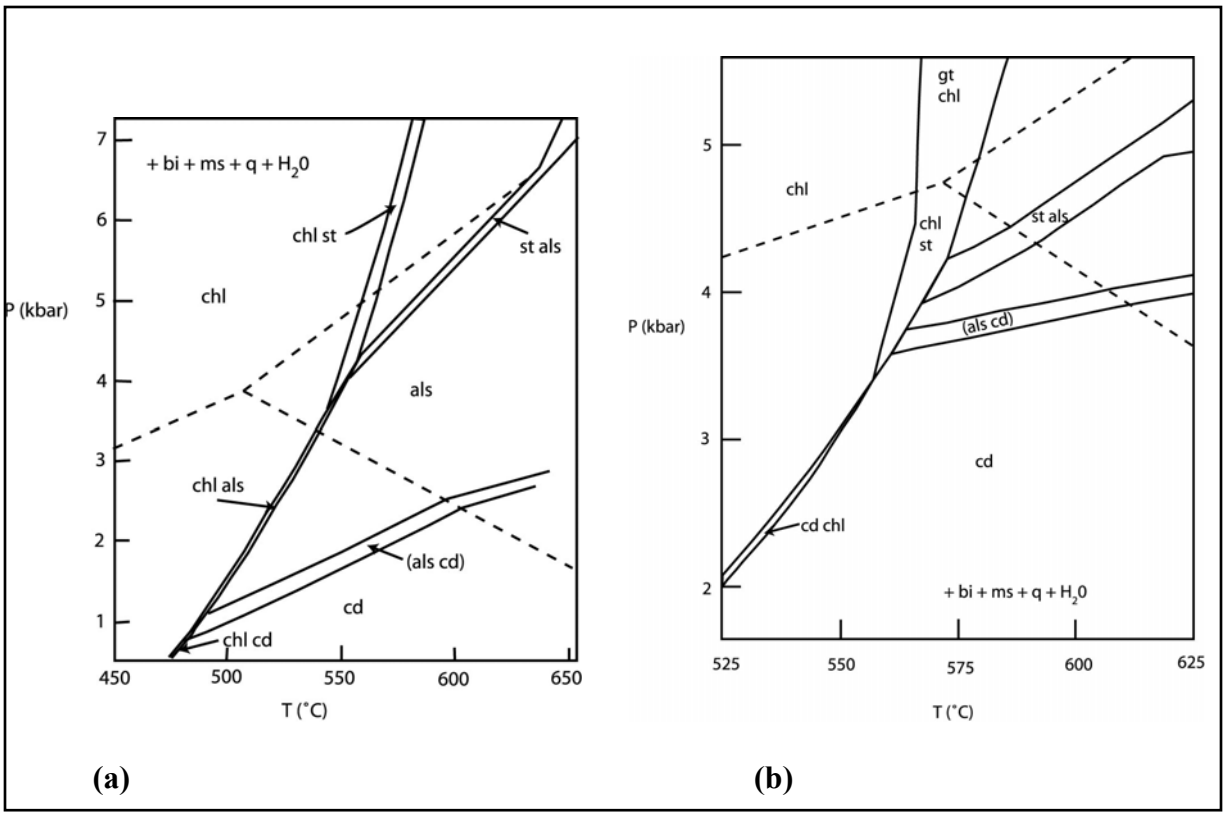

Figure 2.13: P-T grids showing similar mineral assemblages and reactions, but different bulk composition to illustrate the effect of X_{Fe} on reaction topologies. As X_{Fe} increases, the cordierite-chlorite field approaches the staurolite-chlorite field, and the chlorite-alumina-silicate field gets smaller and eventually disappears. **(a)** from Wei et al. (2004); part of a pseudosection for a typical pelite used by Mahar et al. (1997): $X_{Fe} = 0.4$. **(b)** from Dymoke and Sandiford (1992); pseudosection for pelite with $X_{Fe} = 0.7$
(bi = biotite, ms = muscovite, q = quartz, chl = chlorite, st = staurolite, als = alumina-silicate, cd = cordierite, gt = garnet)

2.7.1. Mineral Chemistry

Garnet analyzed from the metabasalt is almandine-rich, and the hornblende is mostly ferro-tschermakite. Cummingtonite was identified based on chemistry from the microprobe, and distinguished from anthophyllite optically. Actinolite was not probed or considered part of the mineral assemblage garnet + hornblende + cummingtonite + biotite + quartz + plagioclase, but does occur locally in equilibrium with hornblende in some layers within the same sample. It was distinguished from cummingtonite by optic properties. Plagioclase in the metabasalt is oligoclase. Biotite in the metabasalt has Fe/Fe+Mg ~ 0.73.

Plagioclase in the metasedimentary rocks is oligoclase, except in sample WW02C where it is andesine. Biotite in the metasedimentary rocks has Fe/Fe+Mg ~ 0.5. The micas and chlorite in the Transition Unit are more iron-rich than those of the Burwash Formation (Fe/Fe+Mg ~ 0.55-0.7 vs. 0.45).

A problem was encountered discriminating between peak-metamorphic and retrograde chlorite in the metasedimentary rocks. Both peak-metamorphic and retrograde chlorite is present in the samples, and distinguishing between the two was difficult with BSE imaging on the microprobe. Peak-metamorphic chlorite grains were identified in thin section (see above – this section) to be analyzed with the microprobe. The rocks are so fine-grained that probing the actual grains identified under the petrographic microscope was not possible in many cases. Nonetheless, chlorite grains analyzed have the same composition (within each sample). If some retrograde grains were accidentally analyzed, they have similar composition to the peak-metamorphic grains so it does not affect the AFM plots. The AFM plots assume that all grains analyzed are peak-metamorphic and in equilibrium with the rest of the peak-metamorphic mineral assemblage.

Table 2.4: Representative mineral chemistry for WW14A (Giauque Lake Unit metabasalt) (No refers to analysis presented in Appendix A)

	hornblende	cummingtonite		biotite		plagioclase		garnet
No	19	17	**No**	62	**No**	18	**No**	9
	wt%	**wt%**		**wt%**		**wt%**		**wt%**
SiO_2	38.96	51.23	SiO_2	33.71	SiO_2	63.75	SiO_2	35.91
TiO_2	0.32	0.02	TiO_2	2.29	Al_2O_3	22.61	TiO_2	0.10
Al_2O_3	16.15	0.29	Al_2O_3	15.96	FeO	0.39	Al_2O_3	20.94
Cr_2O_3	0.00	0.00	FeO	28.26	CaO	4.10	FeO	31.54
FeO	25.14	35.59	MnO	0.15	Na_2O	9.38	MnO	4.78
MnO	0.26	1.11	MgO	5.85	K_2O	0.04	MgO	1.07
MgO	3.38	9.23	CaO	0.01	MgO	0.00	CaO	4.66
CaO	10.70	0.59	Na_2O	0.06	MnO	0.09	Na_2O	0.01
Na_2O	1.59	0.10	K_2O	8.43			Cr_2O_3	0.00
K_2O	0.50	0.02	Cr_2O_3	0.03				
F	0.09	0.00	F	0.08				
Total	**96.99**	**98.20**	**Total**	**94.77**	**Total**	**100.36**	**Total**	**99.02**
no. of O	23	23	**no. of O**	11	**no. of O**	8	**no. of O**	12
	moles	**moles**		**moles**		**moles**		**moles**
Si	5.994	7.947	Si	2.706	Si	2.816	Si	2.930
Al	2.006	0.053	Al	1.294	Al	1.177	Al	0.070
ΣT	**8.000**	**8.000**	**ΣT**	**4.000**	**Σ**	**3.993**	**ΣT**	**3.000**
Al	0.921	0.000	Al	0.216	Ca	0.194	Al	1.963
Ti	0.037	0.003	Ti	0.138	Na	0.803	Ti	0.007
Cr	0.000	0.000	Fe(ii)	1.897	K	0.002	Fe	0.029
Fe(iii)	0.912	0.013	Mn	0.010	**ΣX**	**0.999**	**ΣY**	**2.000**
Fe(ii)	2.321	4.604	Mg	0.700	Fe(iii)	0.005	Fe	2.099
Mn	0.034	0.146	**ΣR**	**2.962**			Mn	0.352
Mg	0.774	2.136	Ca	0.001			Mg	0.107
ΣC	**5.000**	**6.901**	Na	0.010			Ca	0.488
Ca	1.763	0.099	K	0.864			**ΣX**	**3.046**
Na	0.474	0.030	**ΣA**	**0.875**				
K	0.098	0.004	F	0.020				
ΣA	**2.336**	**0.134**						
Total	**15.336**	**15.035**	**Total**	**7.837**	**Total**	**4.998**	**Total**	**8.046**
Fe/Fe+Mg	**0.750**	**0.683**	**Fe/Fe+Mg**	**0.730**			**Fe/Fe+Mg**	**0.952**
Species	**Ferro-tschermakite**				**An**	**19**	**Py**	**3**
					Ab	**80**	**Alm**	**69**
					Or	**0**	**Gro**	**16**
							Sp	**11**

Hornblende normalized based on 13 cations excluding K, Na, Ca
Cummingtonite normalized based on 15 cations excluding Na, K
Fe(iii) estimates using equations (6) & (5) of Droop (1987)

Table 2.5: Representative mineral chemistry for WW05068 (Giauque Lake Unit metabasalt)
(No refers to analysis presented in Appendix A)

	hornblende		**plagioclase**
No	33	**No**	21
	wt%		**wt%**
SiO_2	42.64	SiO_2	63.67
TiO_2	0.68	Al_2O_3	23.03
Al_2O_3	10.58	FeO	0.12
Cr_2O_3	0.02	CaO	4.35
FeO	23.74	Na_2O	8.97
MnO	0.64	K_2O	0.14
MgO	5.78	MgO	0.00
CaO	11.62	MnO	0.00
Na_2O	1.18		
K_2O	0.76		
F	0.06		
Total	**97.65**	**Total**	**100.28**
no. of O	23	**no. of O**	8
	moles		**moles**
Si	6.549	Si	2.806
Al	1.451	Al	1.196
ΣT	**8.000**	**Σ**	**4.002**
Al	0.464	Ca	0.205
Ti	0.079	Na	0.767
Cr	0.002	K	0.008
Fe(iii)	0.502	**ΣX**	**0.9800**
Fe(ii)	2.547	Fe(iii)	0.002
Mn	0.083		
Mg	1.323		
ΣC	**5.000**		
Ca	1.913		
Na	0.351		
K	0.149		
ΣA	**2.413**		
Total	**15.413**	**Total**	**4.983**
Fe/Fe+Mg	**0.658**		
Species	**Ferro-hornblende**	**An**	**21**
		Ab	**78**
		Or	**1**

Hornblende normalized based on 13 cations excluding K, Na, Ca
Fe(iii) estimates using equations (6) & (5) of Droop (1987)

Table 2.6: Representative mineral chemistry for WW05028 (Burwash Formation metasedimentary rock)
(No refers to analysis presented in Appendix A)

	biotite	muscovite		chlorite		cordierite		plagioclase
No	46	56	**No**	52	**No**	8	**No**	16
	wt%	**wt%**		**wt%**		**wt%**		**wt%**
SiO_2	35.81	46.07	SiO_2	24.49	SiO_2	47.62	SiO_2	62.27
TiO_2	1.46	0.34	TiO_2	0.04	TiO_2	0.00	Al_2O_3	23.84
Al_2O_3	19.92	36.30	Al_2O_3	23.74	Al_2O_3	32.28	Fe_2O_3	0.06
FeO	19.07	0.70	FeO	24.30	FeO	8.25	CaO	5.27
MnO	0.07	0.03	MnO	0.16	MnO	0.33	Na_2O	8.66
MgO	9.84	0.40	MgO	14.37	MgO	8.20	K_2O	0.06
CaO	0.01	0.00	CaO	0.00	CaO	0.02	MgO	0.00
Na_2O	0.35	1.45	Na_2O	0.07	Na_2O	0.27	MnO	0.00
K_2O	9.16	9.14	K_2O	0.02	K_2O	0.02		
Cr_2O_3	0.23	0.03	Cr_2O_3	0.03	Cr_2O_3	0.00		
F	0.20	0.10	F	0.00	F	0.10		
Total	**95.92**	**94.45**	**Total**	**87.23**	**Total**	**97.00**	**Total**	**100.16**
no. of O	11	11	**no. of O**	14	**no. of O**	18	**no. of O**	8
	moles	**moles**		**moles**		**moles**		**moles**
Si	2.700	3.067	Si	2.578	Si	4.984	Si	2.756
Al	1.300	0.933	Al	1.422	Ti	0.000	Al	1.243
ΣT	**4.000**	**4.000**	**ΣT**	**4.000**	Al	3.981	**Σ**	**3.999**
Al	0.470	1.914	Al	1.524	Fe(ii)	0.722	Ca	0.250
Ti	0.083	0.017	Ti	0.003	Mn	0.029	Na	0.743
Fe(ii)	1.202	0.039	Fe(ii)	2.139	Mg	1.279	K	0.004
Mn	0.005	0.002	Mn	0.014	Ca	0.002	**ΣX**	**0.9962**
Mg	1.106	0.039	Mg	2.256	Na	0.056	Fe(iii)	0.001
ΣR	**2.866**	**2.011**	**ΣR**	**5.936**	K	0.003		
Ca	0.001	0.000	Ca	0.000				
Na	0.051	0.187	Na	0.014				
K	0.881	0.776	K	0.003				
ΣA	**0.933**	**0.963**	F	0.000				
F	0.047	0.022						
Total	**7.799**	**6.974**	**Total**	**9.954**	**Total**	**11.055**	**Total**	**4.996**
Fe/Fe+Mg	**0.521**	**0.499**	**Fe/Fe+Mg**	**0.487**	**Fe/Fe+Mg**	**0.361**		
							An	**25**
							Ab	**75**
							Or	**0**

Table 2.7: Representative mineral chemistry for WW05030 (Transition Unit metasedimentary rock)
(No refers to analysis presented in Appendix A)

	biotite	muscovite		chlorite		plagioclase
No	15	19	**No**	22	**No**	7
	wt%	**wt%**		**wt%**		**wt%**
SiO_2	35.76	45.89	SiO_2	27.45	SiO_2	63.86
TiO_2	1.37	0.16	TiO_2	0.22	Al_2O_3	22.90
Al_2O_3	20.64	36.08	Al_2O_3	23.78	Fe_2O_3	0.17
FeO	18.43	1.22	FeO	23.97	CaO	3.75
MnO	0.13	0.01	MnO	0.12	Na_2O	9.28
MgO	9.25	0.59	MgO	12.63	K_2O	0.06
CaO	0.04	0.00	CaO	0.02	MgO	0.00
Na_2O	0.16	1.23	Na_2O	0.07	MnO	0.00
K_2O	9.33	9.78	K_2O	0.81		
Cr_2O_3	0.16	0.11	Cr_2O_3	0.06		
F	0.63	0.03	F	0.17		
Total	**95.26**	**95.07**	**Total**	**89.14**	**Total**	**100.02**
no. of O	11	11	**no. of O**	14	**no. of O**	8
	moles	**moles**		**moles**		**moles**
Si	2.703	3.057	Si	2.808	Si	2.818
Al	1.297	0.943	Al	1.192	Al	1.191
ΣT	**4.000**	**4.000**	**ΣT**	**4.000**	***Σ***	**4.009**
Al	0.542	1.889	Al	1.675	Ca	0.177
Ti	0.078	0.008	Ti	0.017	Na	0.794
Fe(ii)	1.165	0.068	Fe(ii)	2.050	K	0.003
Mn	0.008	0.000	Mn	0.010	***ΣX***	**0.9748**
Mg	1.042	0.058	Mg	1.926	Fe(iii)	0.002
ΣR	**2.835**	**2.024**	**ΣR**	**5.679**		
Ca	0.003	0.000	Ca	0.002		
Na	0.024	0.159	Na	0.014		
K	0.899	0.831	K	0.106		
ΣA	**0.927**	0.991	F	0.055		
F	0.151	0.006				
Total	**7.761**	**7.014**	**Total**	**9.802**	**Total**	**4.986**
Fe/Fe+Mg	**0.528**	**0.538**	**Fe/Fe+Mg**	**0.516**		
					An	**18**
					Ab	**81**
					Or	**0**

Table 2.8: Representative mineral chemistry for WW02C (Transition Unit metasedimentary rock)
(No refers to analysis presented in Appendix A)

	muscovite		**chlorite**		**staurolite**		**plagioclase**
No	31	**No**	26	**No**	6	**No**	10
	wt%		**wt%**		**wt%**		**wt%**
SiO_2	52.46	SiO_2	23.35	SiO_2	26.73	SiO_2	59.01
TiO_2	0.17	TiO_2	0.24	TiO_2	0.37	Al_2O_3	26.19
Al_2O_3	32.49	Al_2O_3	22.40	Al_2O_3	54.09	Fe_2O_3	0.09
FeO	1.06	FeO	32.66	FeO	13.61	CaO	7.73
MnO	0.03	MnO	0.11	MnO	0.22	Na_2O	7.08
MgO	0.28	MgO	8.22	MgO	0.73	K_2O	0.04
CaO	0.05	CaO	0.05	CaO	0.00	MgO	0.01
Na_2O	0.73	Na_2O	0.09	Na_2O	0.01	MnO	0.00
K_2O	9.15	K_2O	0.10	K_2O	0.03		
Cr_2O_3	0.05	Cr_2O_3	0.11	Cr_2O_3	0.06		
F	0.01	F	0.11				
Total	**96.48**	**Total**	**87.33**	**Total**	**95.84**	**Total**	**100.16**
no. of O	11	**no. of O**	14	**no. of O**	23	**no. of O**	8
	moles		**moles**		**moles**		**moles**
Si	3.384	Si	2.584	Si	3.788	Si	2.630
Al	0.616	Al	1.416	Ti	0.040	Al	1.376
ΣT	**4.000**	**ΣT**	**4.000**	Al	9.033	**Σ**	**4.0053**
Al	1.853	Al	1.505	Fe(ii)	1.612	Ca	0.369
Ti	0.008	Ti	0.020	Mn	0.026	Na	0.611
Fe(ii)	0.057	Fe(ii)	3.022	Mg	0.153	K	0.002
Mn	0.002	Mn	0.010	Ca	0.000	**ΣX**	**0.9830**
Mg	0.027	Mg	1.355	Na	0.002	Fe(iii)	0.001
ΣR	**1.948**	**ΣR**	**5.913**	K	0.005		
Ca	0.003	Ca	0.006				
Na	0.091	Na	0.019				
K	0.753	K	0.014				
ΣA	**0.847**	F	0.039				
F	0.002						
Total	**6.795**	**Total**	**9.952**	**Total**	**14.660**	**Total**	**4.989**
Fe/Fe+Mg	**0.677**	**Fe/Fe+Mg**	**0.690**	**Fe/Fe+Mg**	**0.913**		
						An	**38**
						Ab	**62**
						Or	**0**

Table 2.9: Representative mineral chemistry for WW05004 (Burwash Formation metasedimentary rock)
(No refers to analysis presented in Appendix A)

	biotite	muscovite		chlorite		plagioclase
No	2	8	**No**	10	**No**	4
	wt%	**wt%**		**wt%**		**wt%**
SiO_2	36.22	46.32	SiO_2	24.56	SiO_2	65.17
TiO_2	1.60	0.39	TiO_2	0.08	Al_2O_3	22.00
Al_2O_3	19.11	35.84	Al_2O_3	23.72	Fe_2O_3	0.14
FeO	17.19	0.73	FeO	23.46	CaO	3.04
MnO	0.14	0.00	MnO	0.23	Na_2O	9.71
MgO	10.73	0.59	MgO	15.65	K_2O	0.07
CaO	0.00	0.04	CaO	0.00	MgO	0.00
Na_2O	0.10	1.05	Na_2O	0.04	MnO	0.02
K_2O	10.17	10.18	K_2O	0.04		
Cr_2O_3	0.06	0.08	Cr_2O_3	0.000		
F	0.40	0.03	F	0.00		
Total	**95.32**	**95.22**	**Total**	**87.78**	**Total**	**100.14**
no. of O	11	11	**no. of O**	14	**no. of O**	8
	moles	**moles**		**moles**		**moles**
Si	2.734	3.076	Si	2.558	Si	2.865
Al	1.266	0.924	Al	1.442	Al	1.140
ΣT	4.000	4.000	**ΣT**	4.000	**Σ**	**4.0045**
Al	0.435	1.881	Al	1.471	Ca	0.143
Ti	0.091	0.020	Ti	0.006	Na	0.827
Fe(ii)	1.085	0.041	Fe(ii)	2.044	K	0.004
Mn	0.009	0.000	Mn	0.021	**ΣX**	**0.9747**
Mg	1.208	0.058	Mg	2.431	Fe(iii)	0.002
ΣR	2.827	2.000	**ΣR**	5.973		
Ca	0.000	0.003	Ca	0.000		
Na	0.014	0.135	Na	0.007		
K	0.980	0.862	K	0.006		
ΣA	0.994	1.000	F	0.000		
F	0.095	0.006				
Total	**7.821**	**7.000**	**Total**	**9.985**	**Total**	**4.981**
Fe/Fe+Mg	**0.473**	**0.410**	**Fe/Fe+Mg**	**0.457**		
					An	**15**
					Ab	**85**
					Or	**0**

2.7.2 Average P-T Estimates Using Conventional Thermobarometry

Appropriate mineral assemblages are not present in the metasedimentary rocks to use calibrated reactions (geothermometers and geobarometers) to compute pressure and temperature of peak metamorphism. However, since the metabasalt of the Giauque Lake Unit contains both garnet and biotite in equilibrium, the following reaction can be used as a geothermometer to compute the temperature of peak metamorphism:

$$\underset{\text{(phlogopite)}}{KMg_3AlSi_3O_{10}(OH)_2} + \underset{\text{(almandine)}}{Fe_3Al_2Si_3O_{12}} \leftrightarrow \underset{\text{(annite)}}{KFe_3AlSi_3O_{10}(OH)_2} + \underset{\text{(pyrope)}}{Mg_3Al_2Si_3O_{12}}$$

The exchange of Mg and Fe between garnet and biotite is dependent on temperature, and independent of pressure. By using the electron microprobe analyses of biotite and garnet in the rock, the Mg/Fe ratios of these coexisting minerals are used to determine the temperature at which the peak-metamorphic mineral assemblage crystallized.

The distribution of Fe and Mg between biotite and garnet was experimentally measured by Ferry and Spear (1978) at 2.07 kbar and the following relationship was found:

$$\ln K_D = (-2109/T) + 0.782$$
where K_D is the distribution coefficient = $K^{1/3} = (Mg/Fe)^{gt}/(Mg/Fe)^{bi}$

Using molar values for Fe and Mg in the above equation, a peak-metamorphic temperature of 568ºC was computed for the rocks of the Giauque Lake Unit. Ferry and Spear (1978) caution against applying this thermometer to systems containing significant amounts of Ca, Mn or Ti (up to ~ 0.2 (Ca + Mn)/(Ca + Mn + Fe + Mg) in garnet and up to ~ 0.15 $(Al^{VI} + Ti)/(Al^{VI} + Ti + Fe + Mg)$ in biotite). The ratios in the garnet used in this study are ~ 0.23 to 0.27, which is higher than ideal, likely resulting in a lower temperature estimate than the actual temperature of crystallization. The above ratios in the biotite are acceptably low (~ 0.11 to 0.12). In general, this thermometer has a maximum precision of ±50º where components other than Fe and Mg have appropriately low ratios and errors of ±0.001 in mole fractions (X) are propagated through the equation.

Although the result from the Ferry and Spear (1978) calibration seems reasonable several other popular calibrations were used as verification (Table 2.10). Using a pressure of 3 kbar, microprobe data were inputed into an Excel spreadsheet (grt-bt.xls) from Dave Waters' website (http://www.earth.ox.ac.uk/~davewa/pt/th_tools.html). The Ferry and Spear

(1978), as well as Thompson (1976), Holdaway and Lee (1977) and Perchuck and Lavrent'eva (1983) calibrations all treat the minerals as ideal solid solutions. Hodges and Spear (1982) incorporate the non-ideal behaviour of garnet, and Dasgupta et al. (1991) incorporate the non-ideal behaviour of garnet and biotite. Results presented in Table 2.10 show that the Ferry and Spear (1978) calibration is within 25ºC of the others. The exception is the Hodges and Spear (1982) calibrations, which give a temperature of 626ºC. This temperature is a little higher than expected for the rocks in this study. The Ferry and Spear (1978) calibration is presented herein because it is simple, commonly used and produces results that are generally consistent with other calibrations as well as predicted temperatures.

Table 2.10: Comparison of several garnet-biotite geothermometer calibrations

Ref P	Temperatures (ºC)					
(kbar)	FS78	T76	HL77	HS82	PL83	Dasg91
3	574	584	574	626	579	550

FS78 = Ferry and Spear, 1978; T76 = Thompson, 1976; HL77 = Holdaway and Lee, 1977; HS82 = Hodges and Spear, 1982; PL83 = Perchuk and Lavrent'eva, 1983; Dasg91 = Dasgupta et al., 1991

The rocks of the Giauque Lake Unit contain plagioclase in equilibrium with garnet and hornblende. The following geobarometer was attempted (but failed; see below – this section) to compute the pressure at which peak metamorphism took place:

$$6CaAl_2Si_2O_8 + 3Ca_2Fe_5Si_8O_{22}(OH)_2 \leftrightarrow 2Ca_3Al_2Si_3O_{12} + Fe_3Al_2Si_3O_{12} +$$
(anorthite) (Fe-cctinolite) (grossular) (almandine)

$$3Ca_2Fe_4Al_2Si_7O_{22}(OH)_2 + 18SiO_2$$
(Fe-tschermakite) (quartz)

The transfer of Al between tetrahedral and octahedral coordination sites is pressure sensitive and relatively insensitive to temperature. The following calibrations where determined by Kohn and Spear (1990), at equilibrated conditions of 2.5 to 13 kbar and 500 to 800ºC:

$$P = [35327 + T(56.09 + 8.314\ln K_{eq})]/11.906$$

$$K_{eq} = \mathbf{a}_{grs}^{2}\mathbf{a}_{alm}\mathbf{a}_{Fe\text{-}tsch}^{3}\mathbf{a}_{qtz}^{6}/\mathbf{a}_{an}^{6}\mathbf{a}_{Fe\text{-}act}^{3}$$

The pressure calculated is 7.9 kbars, which is completely unreasonable, being significantly higher than the predicted pressure of ≤4 kbars (based on the presence of andalusite rather than kyanite in the metasedimentary rocks) or the pressure calculated for the Transition Unit (sample WW05030) of 2.9 kbar (see below – this section). In every case, the analyses used meet the compositional criteria outlined by Kohn and Spear (1990). The only exception is with the Fe/(Fe + Mg) ratios in hornblende. Kohn and Spears (1990) recommend ratios between 0.4 and 0.6 whereas the ratios present in the samples used in this study are significantly higher (0.75-0.76). It is not clear why this calculation did not work, but it seems the barometer is not appropriate for the reactions present in the rocks used for this study.

2.7.3 Average P-T Estimates Using THERMOCALC

THERMOCALC (v.3.26) was used to estimate average P-T conditions for the formation of peak-metamorphic assemblages. THERMOCALC is a computer program consisting of an internally consistent dataset used for solving mineral equilibria problems. The concepts behind the *Average PT* function of the program are described in detail by Powell and Holland (1994). In general, the calculations involve a set of independent reactions (version: tcd 5.5) built into the software. Computing the average P-T formation of a rock is a statistical problem. Uncertainties in input data, particularly the activities of the end-members, propagate to control the position of the calculated P-T. A least-squares method is used to determine an optimal P-T from the thermodynamics of the reactions in an independent set, including uncertainties and correlations on the activities and enthalpies of formation of end-members (Powell and Holland, 1994). End-member activities were calculated using the *AX* software as part of THERMOCALC. (THERMOCALC and *AX* are freeware downloaded from Roger Powell's website: http://www.earthsci.unimelb.edu.au/tpg/thermocalc/.) Inputting weight percent microprobe data for each mineral in the peak-metamorphic assemblage yields activities and their uncertainties, which then are input into THERMOCALC to calculate average P and T. Although this program has improved the reliability of thermobarometric calculations, the uncertainties on calculated temperatures and pressures remain relatively large as a result of imprecision in thermodynamic data and activity-composition (a-x) relationships (Worley and Powell, 2000).

Transition Unit (sample WW05030; meta-sandstone) with the assemblage of biotite + andalusite + muscovite + quartz + oligoclase + chlorite was the only sample for which THERMOCALC was able to calculate an average T and P of 558ºC and 2.9 kbar. This is consistent with the prediction broad constraints of 500-600ºC, and ≤4 kbar based on that mineral assemblage.

Although THERMOCALC was unable to calculate an average P-T for the metabasalt, using the temperature (568ºC) obtained from conventional geothermometry (see above – this section), THERMOCALC computed pressure as a function of a provided temperature range (Figure 2.14). For temperatures between 550ºC and 600ºC, a pressure estimate of approximately 3.1 kbar was obtained (Figure 2.14). This is more reasonable than 7.9 kbar (computed above), and accepted as an average pressure. Data from the Burwash Formation (sample WW05028; meta-sandstone) yielded average temperature as a function of pressure (Figure 2.14). By all calculations and observations, average P-T formation of the rocks of the Giauque and Transition units on the property is most consistently estimated at about 560 ±50ºC, and 3 ±1 kbar.

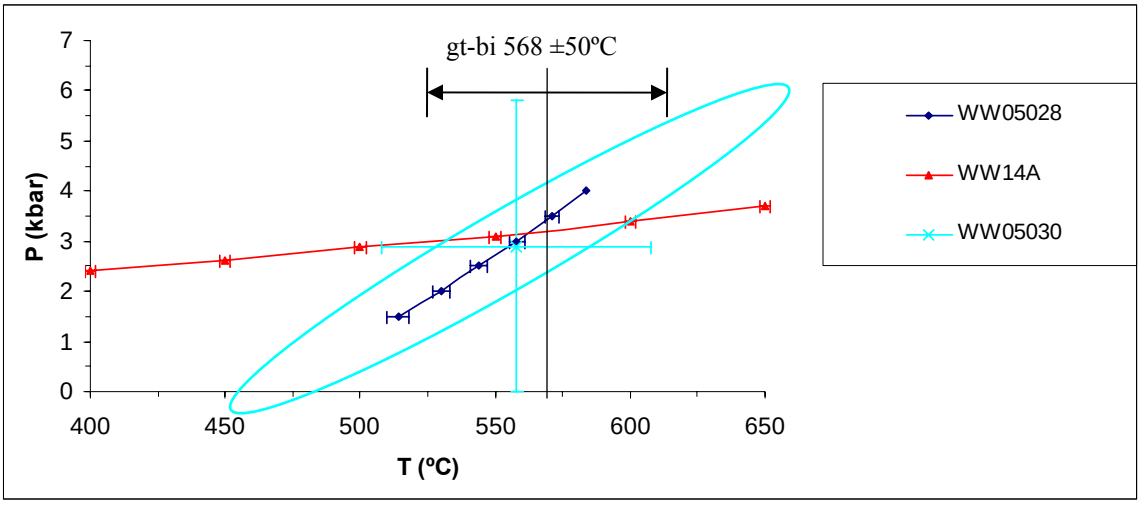

Figure 2.14: Data plots with uncertainties showing the metabasalt sample intersecting the metasedimentary samples at approximately 560ºC and 3 kbar. Sample WW05030 is shown at approximately the intercept with the calculated error ellipse (calculated using an Excel spreadsheet (avept.xls) from Dave Waters' website, http://www.earth.ox.ac.uk/~davewa/pt/th_tools.html). Temperature calculated from garnet-biotite geothermometer shown with approximate uncertainties.

2.8 Structure

Standard structural nomenclature is used to differentiate generations of related structures. Four generations of ductile deformation ($D_1 - D_4$) are preserved on the property and structures are associated with each generation using numerical subscripts. Four recognized foliations ($S_1 - S_4$), a composite lineation (L_C), and three generations of folds ($F_1 - F_3$) are mapped or identified petrographically.

The strongest fabric in outcrop is a penetrative foliation (S_1, subsequently re-aligned parallel to S_3) throughout the metabasalt (Figure 2.5 and 2.6) recognized by the vertical or near vertical dipping parallel alignment of stretched oblate metabasalt fragments and pillows as well as sub-parallel alignments of palagonite seams. The foliation is defined by the alignment of amphibole and mica crystals. It generally strikes NE (040-060º) and is steeply dipping. In the metasedimentary rocks, bedding and two generally weak foliations, defined by aligned mica, were measured in outcrop but clear mesoscopic overprinting relationships are uncommon. Bedding is demonstrably transposed locally (Figure 2.2 and 2.3), especially around the metabasalt bodies. How pervasive transposition affects the metasedimentary rocks away from the metabasalt is uncertain. Commonly, compositional bedding close to the metabasalt is continuous for the length of outcrops up to tens of metres.

Bedding (S_0) and foliation relationships observed in the field and from oriented thin sections indicate at least four fabric generations ($S_1 - S_4$; Table 2.11). All are vertical or near vertical dipping. As cross-cutting relationships between fabric elements are uncommon in outcrop, thin sections from oriented hand samples cut horizontal (looking down) and vertical (looking SW) were examined to define the sequence of events. Overprinting relationships such as fabrics kinked or rotated into younger fabrics, and foliation-porphyroblast/porphyroclast relationships are integrated with field data to define their sequence. The metasedimentary rocks were most useful to sequence the fabric-forming events as only one fabric is preserved in the metabasalt. That being said, most fabrics are weak and overprinting relationships are commonly equivocal.

The Ormsby and Discovery members are enveloped by more ductile metasedimentary rocks. These metabasalt bodies are more resistant to deformation and act like giant porphyroclasts in a more ductile matrix. This creates a “strain shadow” at their tips where older deformation is better preserved. This competency contrast is also seen at the outcrop

scale as the more competent Fe-rich layers in the Transition Unit are boudinaged and rotated into parallelism with the dominant planar fabric (S_3). Assuming deformation at outcrop scale is indicative of deformation at the regional scale, this observation reinforces the hypothesis that the Giauque Lake Unit occurs as layers within the Transition Unit (discussed in Chapter 4). This setting of more competent bodies surrounded by less competent metasedimentary rocks is a typical setting for Archean orogenic gold deposits (Groves et al., 1990). The contrasting competence of the rock units results in more concentrated deformation along the margins of the more rigid metabasalt bodies (see below – section 4.2) providing channels for gold-bearing fluid.

Table 2.11: Foliations
(Note: All the fabrics measured and observed have vertical or near vertical dips. 90º± 15º)

	Metasedimentary Rocks		**Metabasalt**	
	Outcrop	**Thin section**	**Outcrop**	**Thin Section**
S_0	bedding; generally striking NNE-ENE; more competent beds commonly dismembered and transposed into S_3			
S_1	Not Seen	Not Seen	NE alignment of stretched oblate fragments, pillows and palagonite seams	NE alignment of amphibole-rich and quartz-feldspar rich discontinuous layers, and by alternating layers of coarser-grained hornblende-rich layers and finer-grained actinolite-rich layers
S_2	uncommon, weak NW alignment of micas	WNW-WSW, preserved as aligned micas commonly at tips of quartz porphyroclasts, in places rotated into S_3	Not Seen	Not Seen
S_3	generally NNE alignment of micas	Generally NNE alignment of micas	Not Seen	Not Seen
S_4	rare - generally E-W crenulation	ESE weak crenulation of S_3	Not Seen	Not Seen

2.8.1 Foliations

S_1

The main fabric in the metabasalt is a NE (~ 040-060º) striking foliation assigned to S_1. This fabric is presently aligned with S_3 in the immediately adjacent metasedimentary rocks, but is interpreted to have formed synchronous with D_1 and is axial planar parallel to F_1 folds in the metasedimentary rocks at the tips of the metabasalt members. At thin section scale, the foliation is penetrative, overprinting the breccia fragments, pillows and palagonite seams. It is defined by the alignment of discontinuous amphibole-rich and quartz-feldspar rich layers (Figure 2.15), as well as amphibole and biotite (where present) crystals being aligned in the foliation. Where actinolite is present, the foliation is characterized by alternating layers of coarser-grained green hornblende-rich layers and finer-grained almost colourless actinolite-rich layers. Garnet appear to have grown syn-S_1.

S_2

In the metasedimentary rocks, S_2 is typically preserved as a weak alignment of micas, commonly at the tips of quartz porphyroclasts (Figure 2.16), ranging in strike from WNW to WSW. In places, S_2 was observed being rotated into S_3. Both east and west verging rotations are visible, but rare enough that a pattern to their distribution is not evident.

S_3

S_3 is commonly visible in outcrop and in most thin sections, and is defined by an approximate NNE alignment of micas in the metasedimentary rocks. S_3 curves into a more NE orientation along the contact with the metabasalt bodies. Garnet growth continued syn- S_3 (Figure 2.9). Cordierite in the Burwash Formation grew post-S_3, which is indicated by foliated mica inclusions.

S_4

S_4 is a weak ESE crenulation rarely measured in outcrop, but more commonly recognized in metasedimentary rocks by kinking of S_3 (Figure 2.17). S_4 overprints cordierite porphyroblasts in the Burwash Formation. Plagioclase porphyroblasts overprint S_4 in one sample, and are observed overprinting older fabrics in other samples.

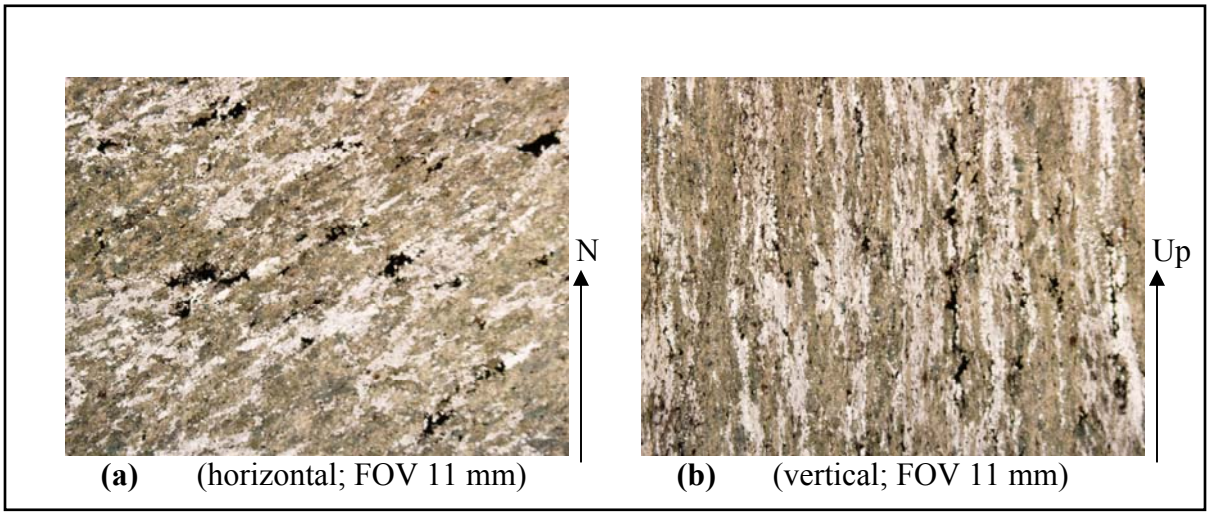

Figure 2.15: Ormsby metabasalt, showing discontinuous layers defining foliation (S_1); **(a)** horizontal section with north up; FOV 11 mm; **(b)** vertical section looking SW; FOV 11 mm; note strong fabric in vertical section representing the lineation.

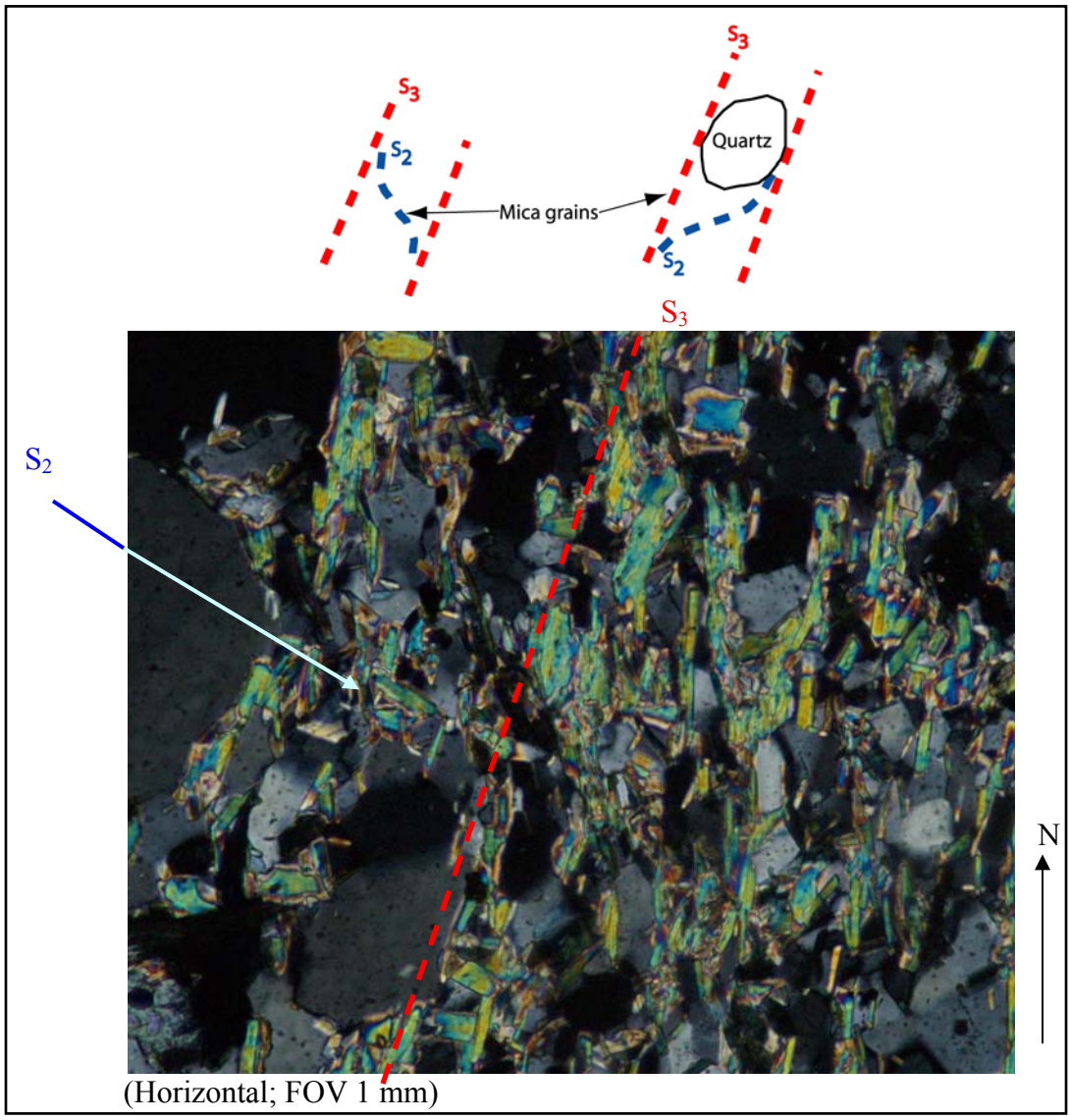

Figure 2.16: Line drawings and photomicrograph example showing how the micas define S_2 and S_3 as observed in thin section. S_2 is defined by rare mica crystals striking NW.

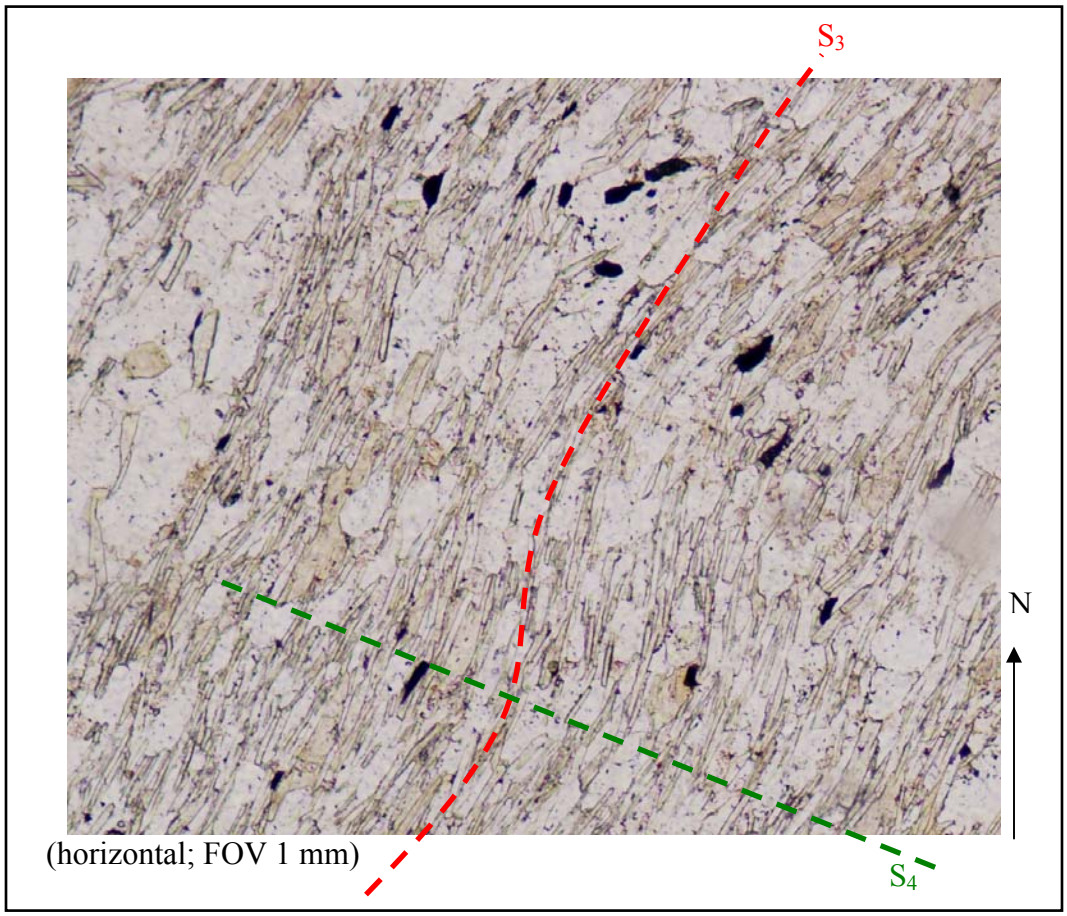

Figure 2.17: S_4 crenulating S_3

2.8.2 Lineation

A strong near vertical lineation (L_C) is present across the property. In the metabasalt, the fragments (Figure 2.18a) and relic pillows display an obvious vertical stretch. This lineation is visible in metabasalt thin sections as a vertical fabric defined by the alignment of amphibole crystals (Figure 2.15b).

The linear fabric is not observed in outcrop in the metasedimentary rocks, but is strong in thin section (Figure 2.18b-e). The lineation lies in the plane of the foliations and is a combination of the intersections of $S_2 - S_4$ as well as a vertical stretch indicated by elongate quartz porphyroclasts (Figure 2.18d-e). Vertical elongation is interpreted to have begun during D_1 where it is observed with S_1 in the metabasalt, and progressed through D_4, where is it observed with $S_2 - S_4$.

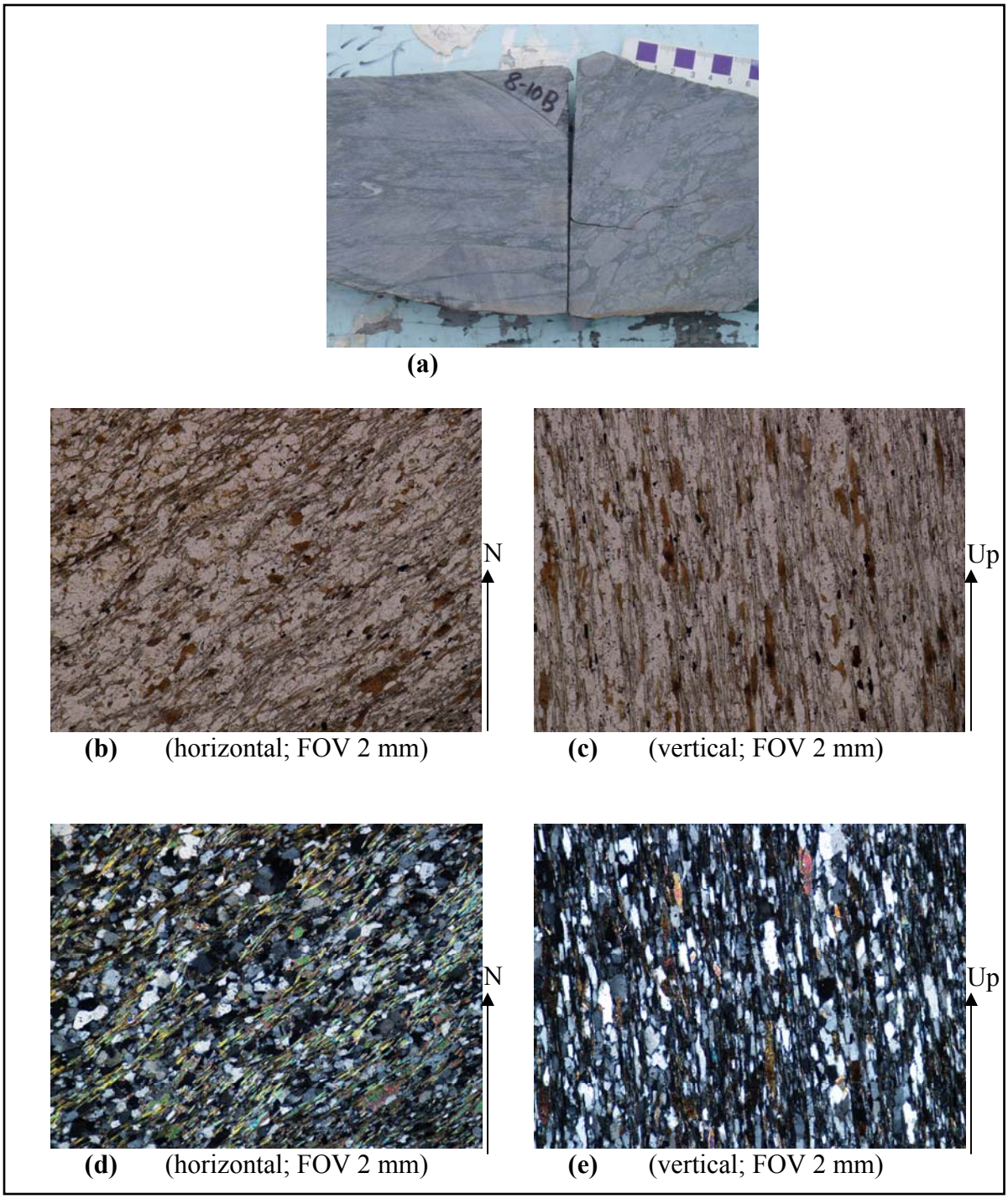

Fig 2.18: (a) Hand sample from Ormsby metabasalt cut to show the vertical elongation of fragments (left block is vertical, right block is horizontal; courtesy of P. Stewart, 2005). **(b)** to **(e)** Thin sections from a metasedimentary rock sample illustrating lineation. **(b)** and **(c)** are in PPL showing lineated biotite, **(d)** and **(e)** are in X-polar light to help show vertically elongated quartz.

2.8.3 Folds

Outcrop-scale folded bedding and quartz veins in the metasedimentary rocks are common at the tips of the metabasalt bodies. As well, the metasedimentary rocks are folded around the tips of the metabasalt bodies. Map scale folding is interpreted from cleavage-bedding asymmetry measured in the field (Figures. 2.19 and 2.20).

F_1

F_1 folds are identified from overprinting relationships and correlations described in the following paragraph. Folded bedding at the northern tip of the Discovery Member is presently aligned with S_3, but overprinted by S_2 (Figure 2.19) and therefore assigned to F_1. These folds are aligned axial planar parallel to S_3 as a result of subsequent deformation and interpreted as F_1 reactivated by D_3 and rotated into S_3 ($F_1/_{rS3}$). The North Vein (mined from 1950 to 1969) at the northern tip of the Discovery Member is folded (F_1 and F_2) with $F_1/_{rS3}$ (Figure 2.20 and 2.21). It is described by Tremblay (1952) as a west dipping anticline with a more shallowly dipping west limb. Outcrop scale Z-folds (facing north) across the property are assigned to $F_1/_{rS3}$ based on their similarity to the previously described folds, and suggest the Giauque Lake Unit occurs on the west limb of a regional scale F_1 fold. Folded bedding around the tips of, and between the metabasalt members with axial planes striking parallel to the members (NE), are assigned to F_1. They are preserved in the strain shadow of the metabasalt members where they have not been reoriented into regional S_3, as have many other F_1 folds. Regionally, F_1 is interpreted to have once been an inclined fold, with its hinge line trending northeast, based on overprinting relationships with F_2 (see below – this section).

F_2

Evidence of F_2 folding was observed in only two outcrop locations (Figure 2.20), between the metabasalt members, and along the SE side of the Discovery Member. In these locations, a Type-2 interference pattern (Figure 2.22) is preserved where F_2 folding with axial traces trending NW, folded older folds with axial traces trending NE. The F_2 axial trace is consistent with S_2 measured in thin section samples from both these general locations.

F_3

S_3 is interpreted as being axial planar parallel to a regional scale F_3 fold not visible on the property. Only four reliable instances of S_2/S_3 overprinting relationships were observed in thin section (Figure 2.23). Three of the four asymmetries show S_2 verging west into S_3, and

the fourth shows it verging east. Although this suggests that the property lies on the east limb of an F_3 fold, with minor reversals of vergence representing parasitic folds, more data are required to confirm this implied geometry.

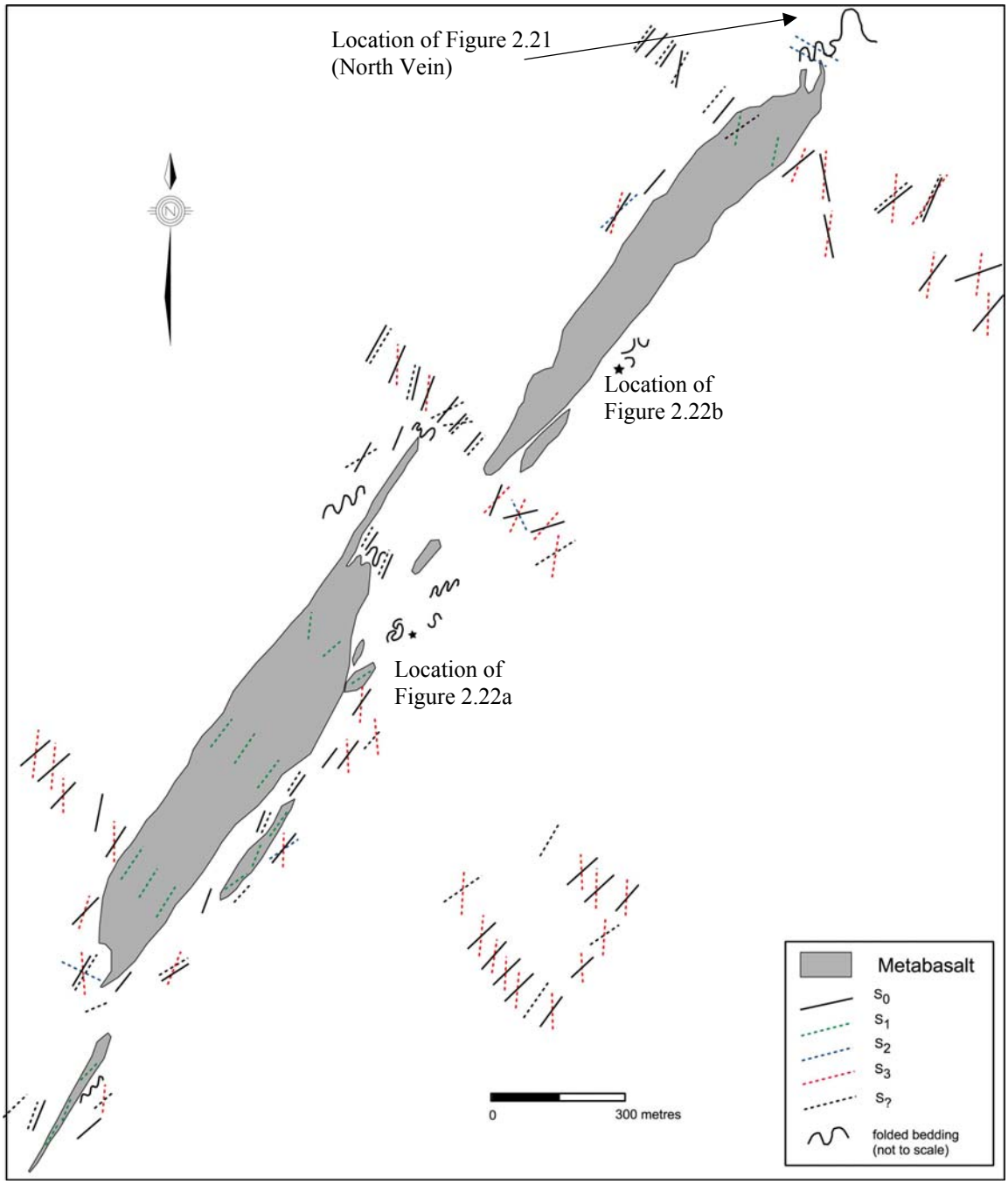

Figure 2.19: Bedding/foliation relationships measured in the field and outcrop scale folds (not to scale) as observed in the field. Note the locations of outcrop observations of F_2 (stars) and North Vein.

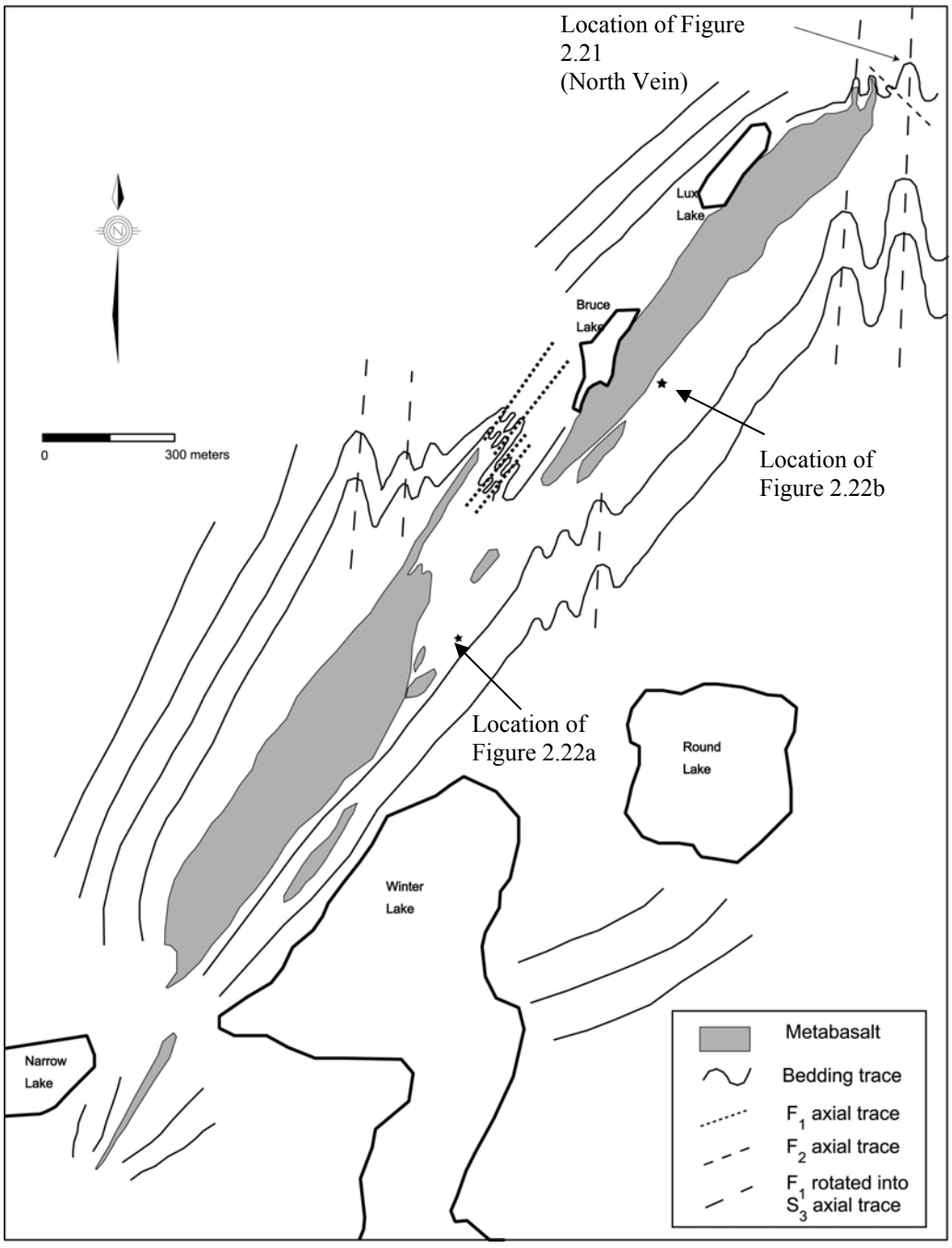

Figure 2.20: Interpretation of bedding trace with fold hinge lines for F_1 shown. Note the locations of outcrop observations of F_2 (stars) and the North Vein.

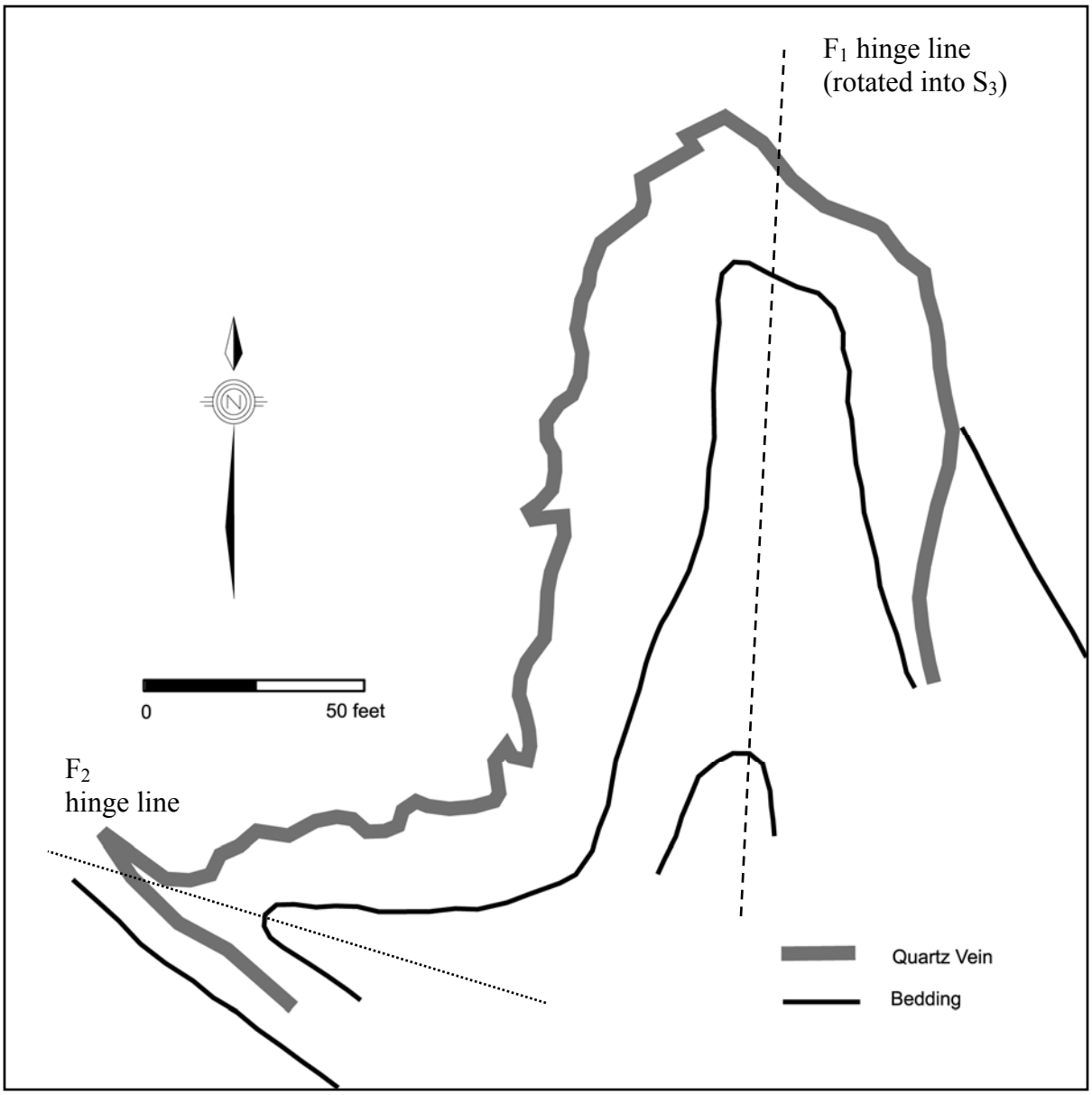

Figure 2.21: Past producing North Vein (location marked on Figure 2.19). It plunges northerly from 85º to 70º in the western limb. The east limb dips from 87º W to 90º, and the west limb dips about 73º to 65º W in its southwestern extremity (Tremblay, 1952).

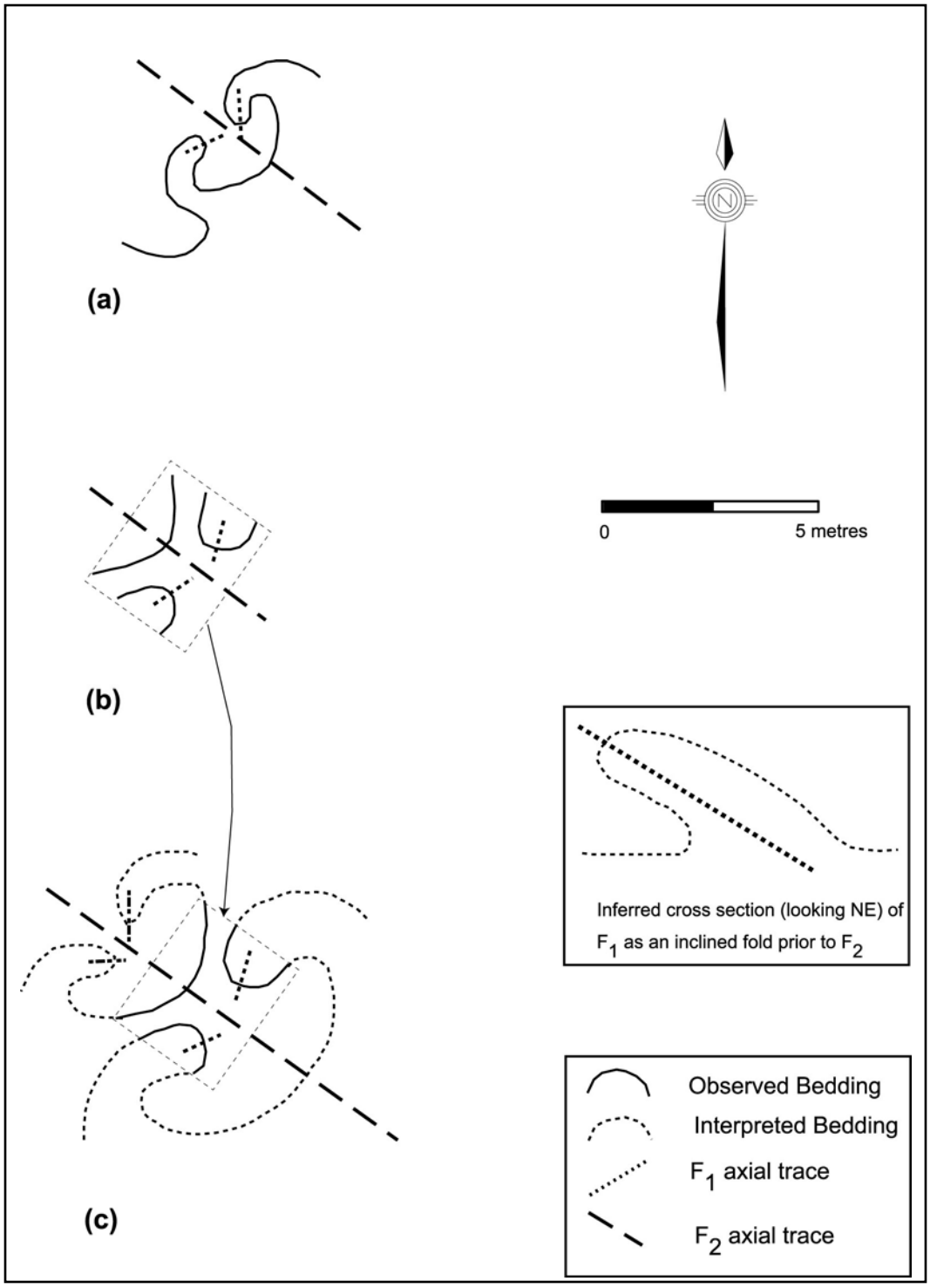

Figure 2.22: Refolded folds observed in outcrop (see Figure 2.19). **(a)** Type-2 interference pattern where inclined folds are refolded. **(b)** Part of a fold interference pattern. **(c)** Pattern (b) extrapolated with dashed lines to show compatibility with (a).

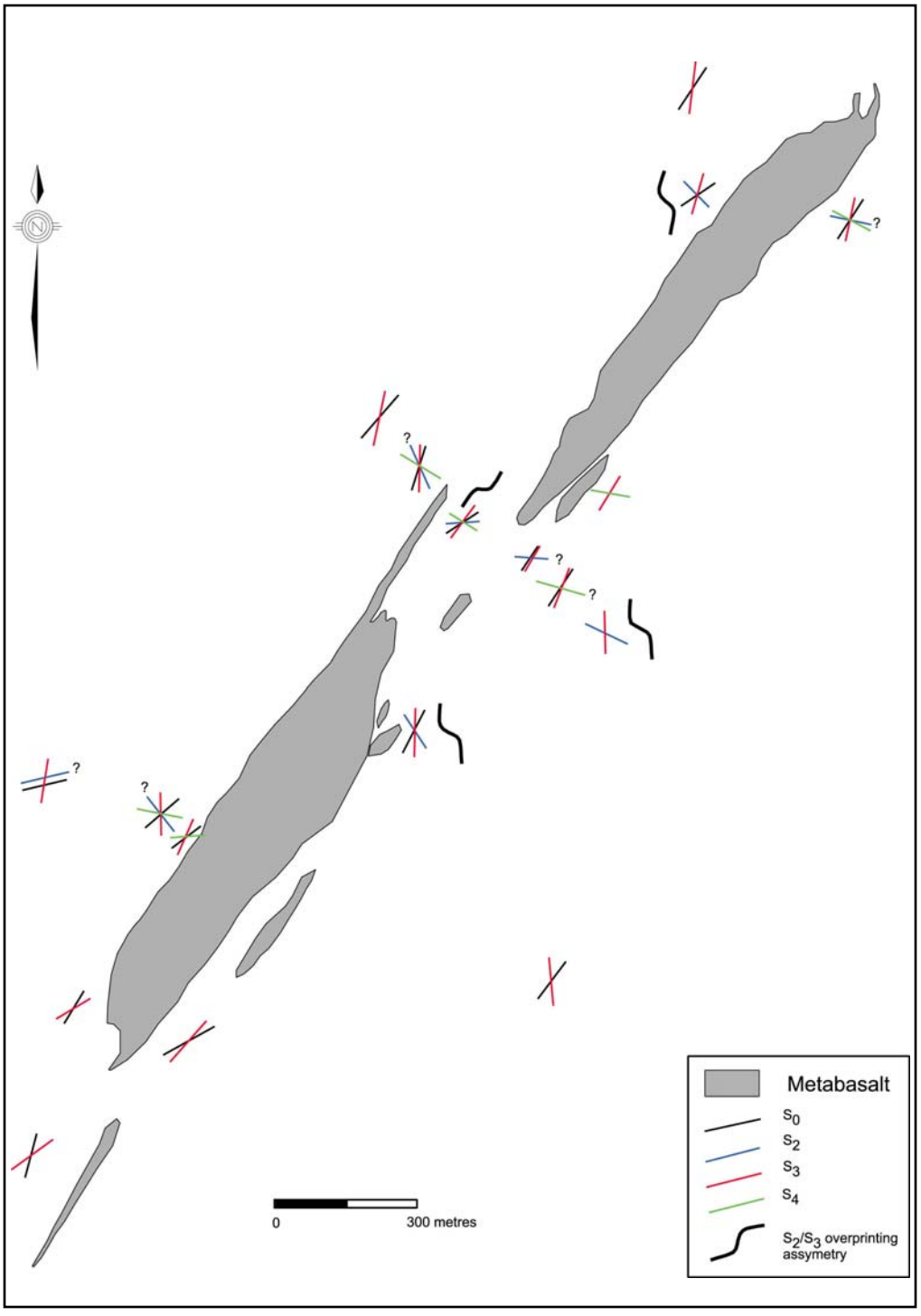

Figure 2.23: Foliation overprinting relationships observed in thin section and their spatial distribution. (Bedding orientations are mostly taken from outcrop measurements; "?" indicates very weak/questionable fabric/overprint.)

2.8.4 Faults

Metamorphic data (see above – section 2.7) suggest there may be a post-peak metamorphic fault separating rocks of the Burwash Formation from those of the Giauque Lake and Transition units. There is no evidence of a through-going fault in drill core or on surface, therefore if a fault is present, it is most likely a ductile fault overprinted by retrograde metamorphism.

Brittle faulting postdates all ductile deformation on the property. Lineaments seen from air photos correspond to ditches and discontinuities along the ground. These features, as well as locally centimetre wide brittle zones of gouge in outcrop were mapped by Stubley (1997) as brittle faults, and correspond to the faults in Figure 2.1 and Plate 1. Drill data show that some of these features are not through going faults (pers. comm. with Tyhee NWT Corp. staff). The only well document brittle fault on the property is the Discovery Fault (Figure 1.2), which offsets the North Vein. It is described by Tremblay (1952) as an oblique thrust fault with sinistral displacement. It has an average dip of 22º to the southeast, and has approximately 220 feet of horizontal displacement and 70 feet of vertical displacement (Tremblay, 1952). Tremblay (1952) states that many small brittle faults striking northwesterly and northeasterly occur throughout the area, and are probably characteristically similar to the Discovery Fault.

Zones of fine-grained crumbled rock observed in drill core might represent faults. Alternately, they could be bands of weaker rock more susceptible to deformation. In some cases, conformable contacts were observed between the crumbled rock and adjacent wall rock, suggesting the latter.

2.9 Summary

Three rock units are present on the Discovery Property: (1) the Burwash Formation composed of metamorphosed sandstone and siltstone turbidites; (2) the Transition Unit composed of metamorphosed sandstone, siltstone, (now graphitic) mudstone, and volcanic components; and (3) the Giauque Lake Unit composed of pillowed, brecciated and massive metabasalt. The Transition Unit is correlated to the Banting Group (occurring farther south) based on a U-Pb age of 2661 ±5 Ma. The Giauque Lake Unit is correlated to the Banting Group as well, based on its interpreted depositional relationship with the Transition Unit.

Peak-metamorphic assemblages of: quartz + plagioclase (oligoclase) + biotite + muscovite ± chlorite + cordierite, and quartz + plagioclase (oligoclase) + biotite ± muscovite ± chlorite in the Burwash Formation: quartz + plagioclase ± biotite ± muscovite ± graphite; quartz + plagioclase (andesine) + biotite + muscovite + chlorite + staurolite; quartz + plagioclase (oligoclase) + biotite + muscovite + chlorite + andalusite, and quartz + plagioclase + biotite ± chlorite ± epidote ± hornblende ± garnet in the Transition Unit; and: hornblende ± actinolite ± cummingtonite + quartz + plagiocalse ± garnet ± epidote ± biotite in the Giauque Lake Unit record greenschist to amphibolite facies metamorphism. Average pressure-temperature calculations give estimates of approximately 560 ±50ºC, and 3 ±1 kbar for peak metamorphism in the Giauque Lake and Transition units.

Four generations of ductile deformation are preserved on the property exposed as foliations, folds and a composite lineation. D_1 produced S_1, F_1, garnet and biotite growth; D_2 produced S_2, and F_2; D_3 rotated S_2 into S_3, rotated some F_1 into S_3, produced F_3, continued garnet growth and post-S_3 cordierite growth; D_4 produced a weak S_4 crenulation. L_C is the result of the combination of the intersections of $S_1 - S_4$ and a vertical stretch. Peak metamorphism is observed overprinting S_4 with late plagioclase growth. Retrograde phases of chlorite, calcite and sericite in the metabasalt, and chlorite in the metasedimentary rocks overprint ductile deformation. Potential ductile faulting and observed brittle faulting are the youngest deformation on the property.

Chapter 3: Gold

3.1 Introduction

Orogenic gold deposits in greenstone belts, as summarized in section 1.2 (see above), are commonly hosted in greenschist to amphibolite facies metamorphosed basalts. Gold deposition typically post-dates peak metamorphism and accompanies retrograde metamorphism in the greenschist facies host rocks (e.g., Hagemann and Cassidy, 2000, and references therein). Favourable structural settings include areas of competency contrast between adjacent rock units where faults and shears are likely to occur (Groves et al., 1990). Multiple styles of gold mineralization are associate with Archean orogenic gold deposits and commonly two or more styles occur together each representing a separate mineralization event (Robert et al., 2005). Quartz-carbonate veins and disseminated stockwork zones are the most common styles of mineralization, and the two that are most relevant to the current study.

The Ormsby Zone is hosted in upper greenschist to lower amphibolite facies, metamorphosed pillowed volcanic rocks surrounded by less competent metasedimentary rocks. Observations and data presented below show that mineralization and alteration assemblages are also typical of orogenic gold deposits.

The Discovery Property is underlain by two brecciated and pillowed metabasalt bodies (the Ormsby and Discovery members) enclosed in metasedimentary rocks (Figure 1.2). All the rocks have peak-metamorphic mineral assemblages recording greenschist to amphibolite facies. Four generations of fabric-forming ductile deformational events are preserved in the rocks including four foliations ($S_1 - S_4$), three generations of folds ($F_1 - F_3$) and a composite lineation (L_C). S_1 and L_C are the only fabrics preserved in the metabasalt. Retrograde metamorphism, producing mainly chlorite and carbonate, post-dates ductile fabrics. The Ormsby Member metabasalt body hosts Ormsby Zone gold mineralization described in this chapter. As of June 2007 the Ormsby Zone contains 936,000 (measured + indicated) ounces of gold with an average grade of 3.53 gpt (Tyhee Development Corp., NI 43-101 resource estimates).

Two types of gold mineralization occur in the region surrounding and including the Discovery Property (Tremblay, 1952). In the first type, gold occurs in smoky grey to black quartz veins in metasedimentary rocks, but restricted to locations where strata are folded and

faulted. The second type is associated with, but not restricted to within, smoky grey to almost black quartz veins and veinlets in volcanic (and dioritic – reported to occur in the region) rocks. Both these types of mineralization occur on the Discovery Property. Mineralization in the Ormsby Member appears to be typical of the second type where gold occurs both in smoky grey quartz veins and surrounding wall rock. Gold mineralization at the past producing Discovery Mine is an example of the first type, where gold mineralization occurs near the hinge of an F_1 folded quartz vein (the North Vein) in folded and faulted metasedimentary rocks. Gold deposition in the North Vein is interpreted by Stubley (1997) as predating vein deformation since grades are significantly reduced on the thinned eastern limb. The gold-bearing North Vein is offset by the Discovery Fault (see above – section 2.8.4), indicating gold was deposited prior to brittle faulting. Both occurrences of gold on the Discovery Property are free-milling. Gold in the North Vein is not accompanied by sulphide minerals (Tremblay, 1952), whereas gold at Ormsby is (see below – this chapter).

3.2 Gold Paragenesis

3.2.1 Outcrop Observations

Oxidation of sulphides to rusty weathering surfaces on outcrop (iron staining) of the metabasaltic Ormsby Member mark zones of gold mineralization, and are prime drill targets. Iron staining occurs throughout the Ormsby Member, but is concentrated on the ridge above the portal and to the north end of the Ormsby Member (Figure 3.1, Plate 1). In drill core, higher abundances of pyrrhotite correspond to higher gold grades, and oxidation of pyrrhotite is inferred to be reflected in iron-stained outcrop.

Two geometries of quartz veins were observed while outcrop mapping. The most common quartz veins on the property typically strike sub-parallel to bedding in the metasedimentary rocks and to S_1 (the dominant fabric) in the Ormsby Member. These veins dip almost vertically and are commonly folded. The second geometry occurs in the Ormsby Member, are informally referred to “Ormsby veins”, and are associated with gold. These veins are inclined, and strike, at most tens of metres, approximately perpendicular to S_1. “Ormsby veins” characteristically occur in the coherent pillowed part of the Ormsby Member.

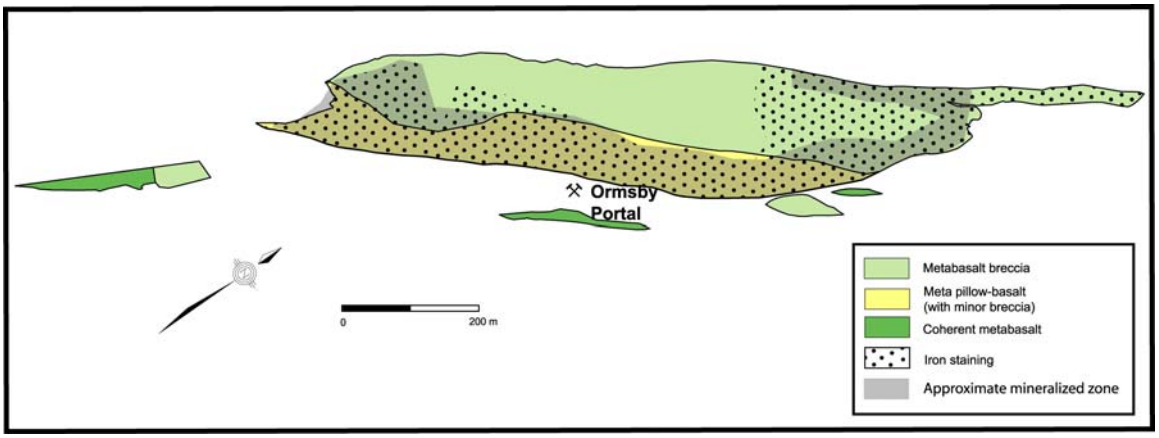

Figure 3.1: Simplified version the Ormsby Member of the Giauque Lake Unit showing gold mineralization relative to lithology and iron staining.

3.2.2 Drill Core Observations

Mineralized zones in Ormsby typically contain 3-10% pyrrhotite whereas unmineralized zones typically contain <2% pyrrhotite. For example a modal abundance of 2-5% pyrrhotite corresponds to approximately 2-4 gpt Au, and 5-10% pyrrhotite corresponds to approximately 4-8 gpt Au. Arsenopyrite, although not common, is only present in higher-grade zones. Pyrrhotite is generally aligned with the foliation (S_1), but also forms as semi-massive clumps and veins cross-cutting the metamorphic fabric. Arsenopyrite is typically not aligned with the foliation, is typically coarser grained, and appears to overprint pyrrhotite. Mineralized zones are characteristically more quartz-rich, having higher abundances of quartz veins and quartz in the host metamorphic rocks.

Visible gold in drill core is typically in or on the edges of smoky grey quartz veins and is associated most commonly with pyrrhotite, pyrite, and chlorite. Two distinctive colours of quartz veins were observed in drill core: older smoky grey and younger milky white quartz. Commonly both colours of quartz occur within the same vein with the milky white quartz overprinting the smoky grey quartz. Gold is associated with the grey quartz veins whereas the white quartz veins are barren. Calcite (identified as post-peak metamorphic in thin section) occurs on the margins of some smoky grey quartz veins and infilling fractures in the host rock. Quartz veins are typically several centimetres to tens of centimetres thick.

3.2.3 Thin Section Observations

Metallic minerals were identified in thin section under reflected light. Ilmenite is most abundant, followed by pyrrhotite. Pyrite is less common and chalcopyrite occurs only as trace amounts. Pyrrhotite and ilmenite are typically aligned with the dominant foliation (S_1, see above – section 2.8.1, Figure 3.2) but appear to be overgrowing minerals that define the foliation (S_1; Figure 3.3). Sulphides commonly occur in chlorite-rich (where chlorite is post peak-metamorphic) parts of the rock. Post peak-metamorphic sericite commonly occurs around pyrrhotite crystals.

Within thin sections of metabasalt, metallic minerals are somewhat segregated into layers that typically contain ilmenite without sulphides, alternating with layers predominated by pyrrhotite. Ilmenite rarely occurs in quartz or quartz veins, whereas pyrrhotite is common in quartz veins, commonly intergrown with, or as veinlets cutting quartz crystals (Figure 3.4). Trace chalcopyrite is intergrown with pyrrhotite. Visible gold in thin section occurs with pyrrhotite and quartz (Figure 3.5). Pyrite overprints pyrrhotite and ilmenite (Figure 3.6).

3.2.4 Implications

The sulphides are inferred as post peak-metamorphic and syn-retrograde metamorphism. This timing relation is based on their overprinting the metamorphic assemblages in the rocks, and their occurrences with retrograde phases of chlorite, calcite and sericite. Since the gold was deposited with the sulphides, gold mineralization is sequenced into the geological history of the property as post folding, post-peak metamorphism, and syn-retrograde metamorphism. Gold mineralization in the Ormsby Zone appears later than gold mineralization in the previously mined North Vein where mineralization is interpreted (Stubley, 1997) as pre-deformation (see above – section 3.1). The occurrence of two separate mineralization events, each with their own style, is not uncommon in Archean orogenic gold deposits (Robert et al., 2005).

Lithologically, highest gold grades occur in the pillowed part of the Ormsby Member (Figure 3.1). One explanation for this might be that the coherent pillowed rocks are more competent than the incoherent breccia and more prone to fracturing and jointing, and thus the formation of quartz veins.

Ormsby Member gold mineralization is typical of the disseminated stockwork style described in section 1.2 (see above). Gold is associated with 5-20% sulphides occurring along foliation-parallel planes and quartz veinlets. As well, the Ormsby Member lacks long strike extensive quartz veins, which are characteristically absent in this style of mineralization. The abundance of reduced phases, ilmenite and pyrrhotite, suggest a reduced fluid is associated with gold, as is common with Archean orogenic greenstone gold deposits (Goldfarb et al., 2005). In contrast, early gold mineralization in the North Vein fits the quartz-carbonate vein style consisting of quartz veins with <25% carbonate and <10% sulphides described in Chapter 1. The North Vein is a vertically extensive quartz vein, and lacks both carbonate and sulphide minerals.

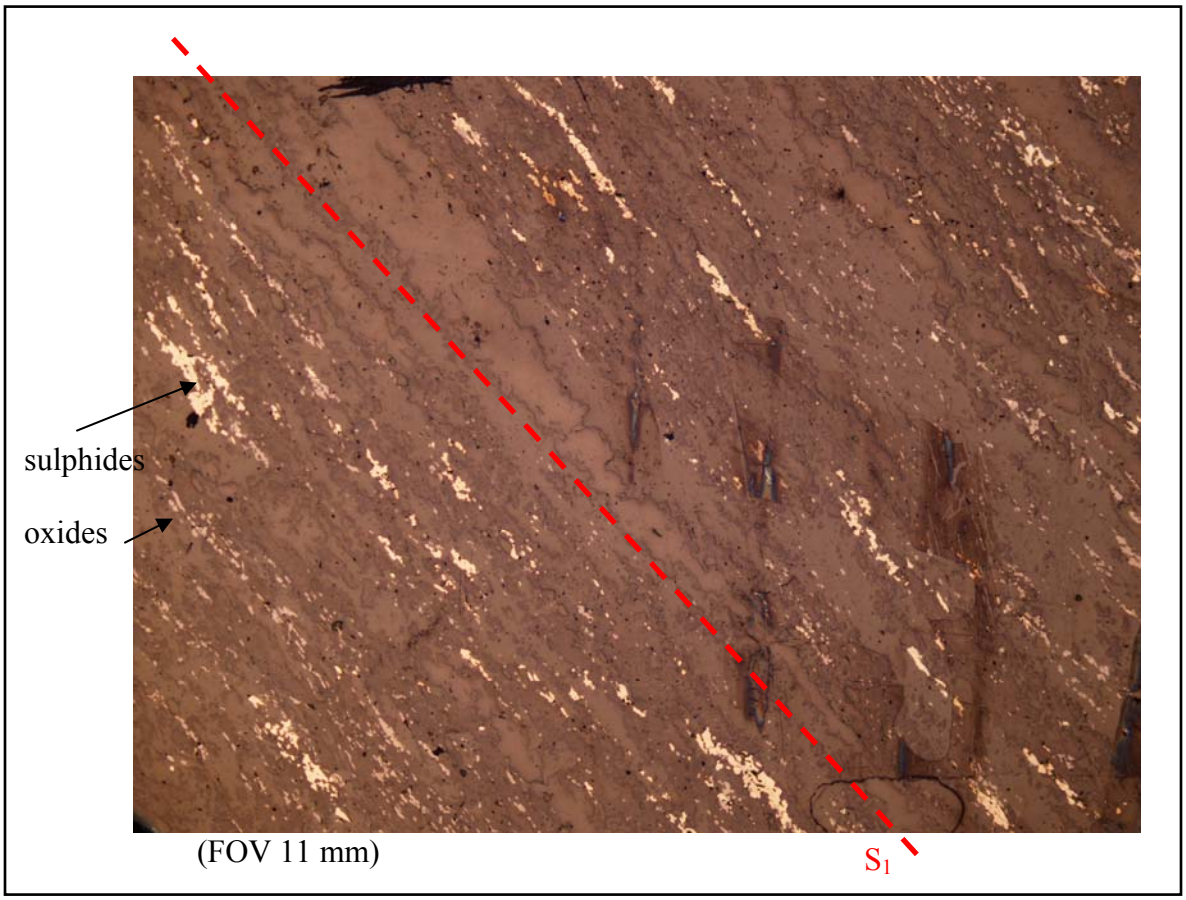

Figure 3.2: Oxides and sulphides in reflected light aligned with the dominant foliation (S_1).

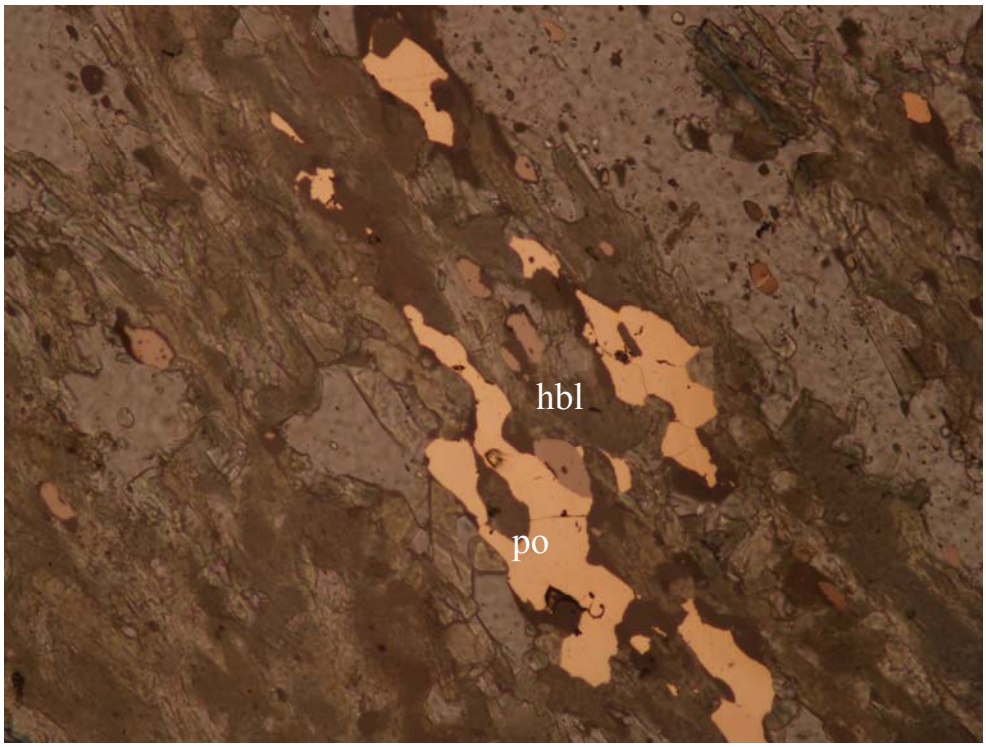

(a) (FOV 2 mm)

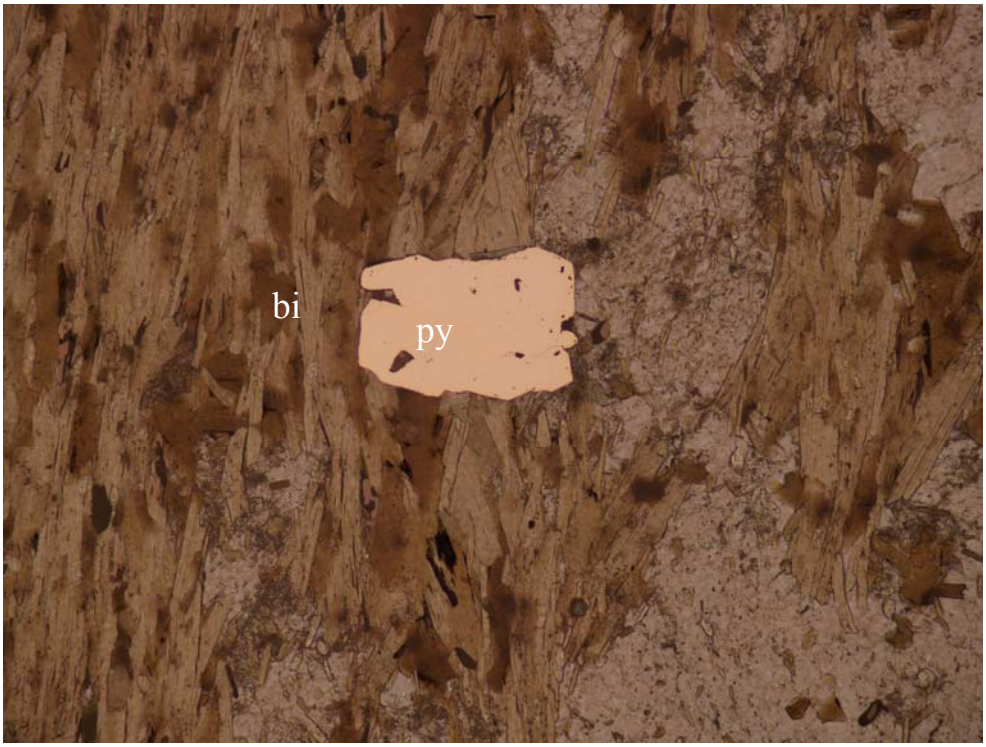

(b) (FOV 2 mm)

Figure 3.3: Sulphides (in reflected light) overprinting **(a)** hornblende and **(b)** biotite (po = pyrrhotite, py = pyrite, hbl = hornblende, bi = biotite)

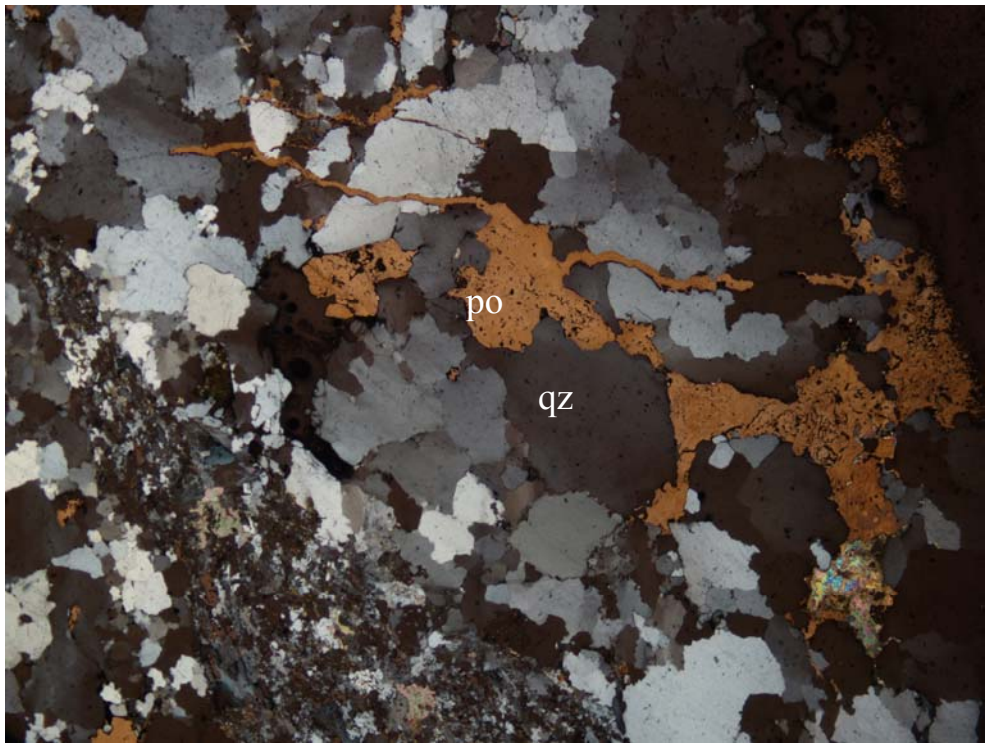

(a) (FOV 11 mm)

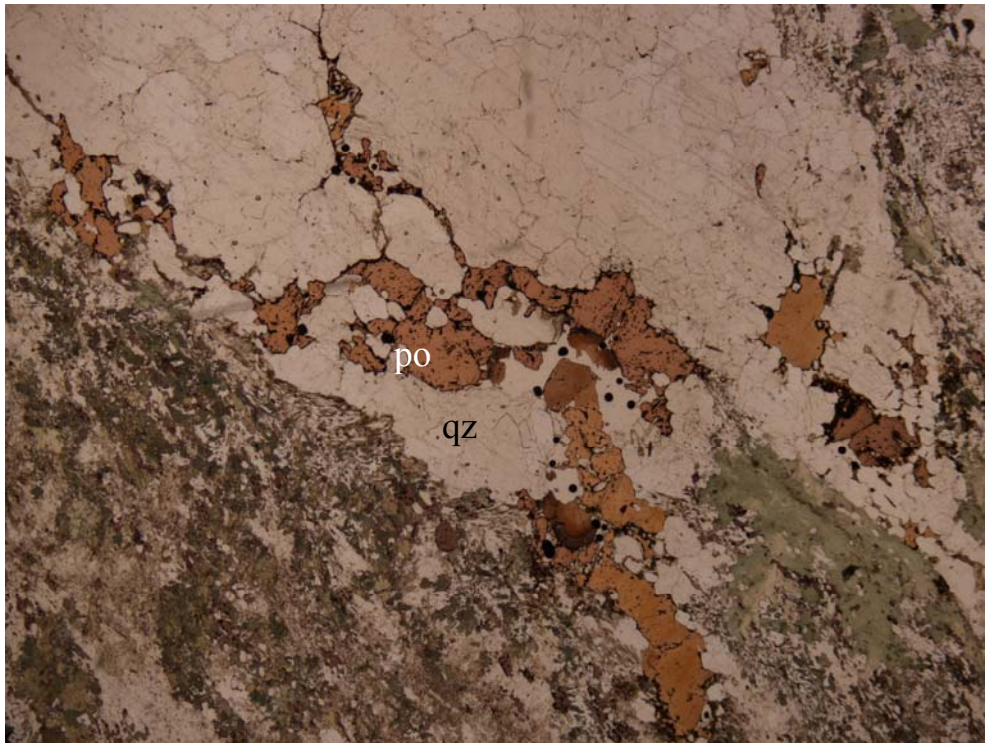

(b) (FOV 11 mm)

Figure 3.4: Pyrrhotite (in reflected light) cross-cutting **(a)** quartz and **(b)** infilling fractured quartz (po = pyrrhotite, qz = quartz).

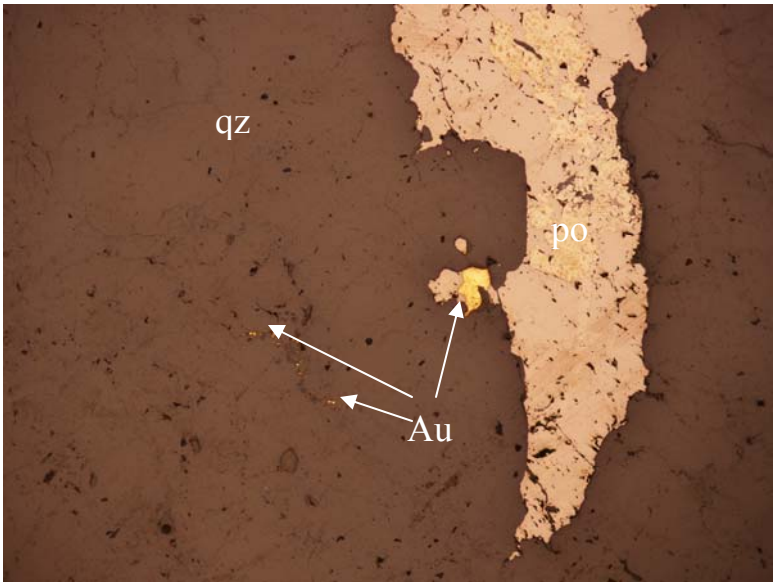

(a) (FOV 4 mm)

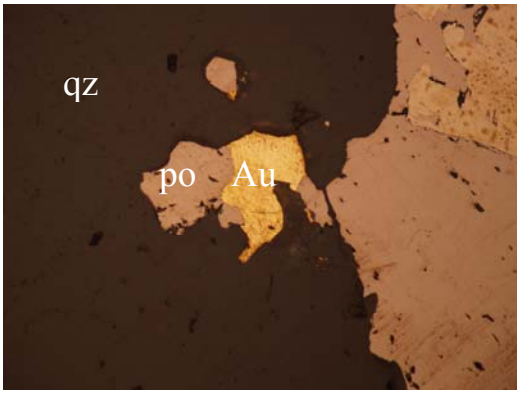

(b) (FOV 1 mm)

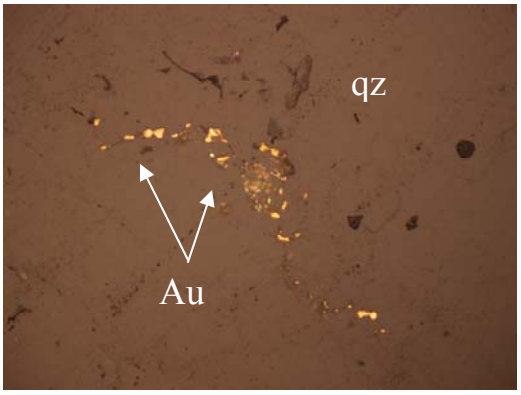

(c) (FOV 1 mm)

Figure 3.5: (a) Free gold (in reflected light) inter-grown with pyrrhotite in a quartz vein. **(b)** and **(c)** close ups of the gold from (a) (Au = gold, po = pyrrhotite, qz = quartz)

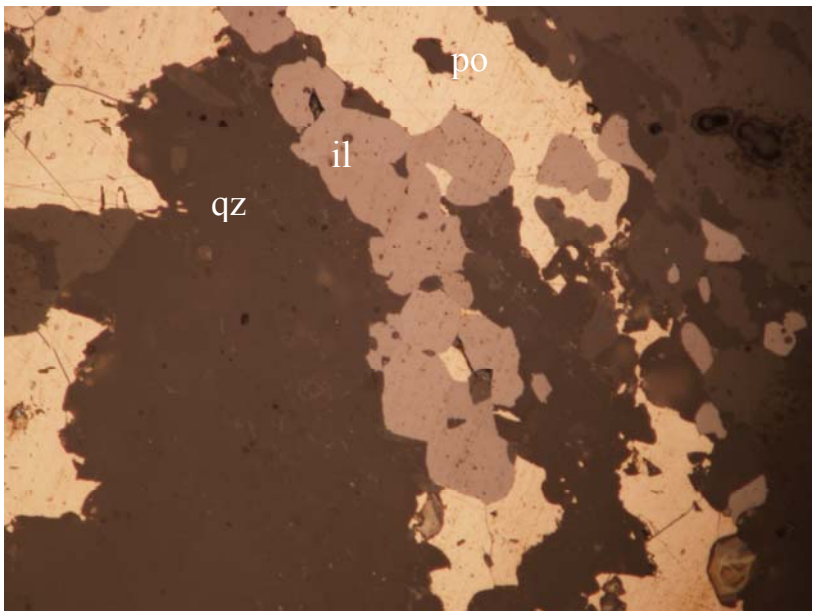

(a) (FOV 0.4 mm)

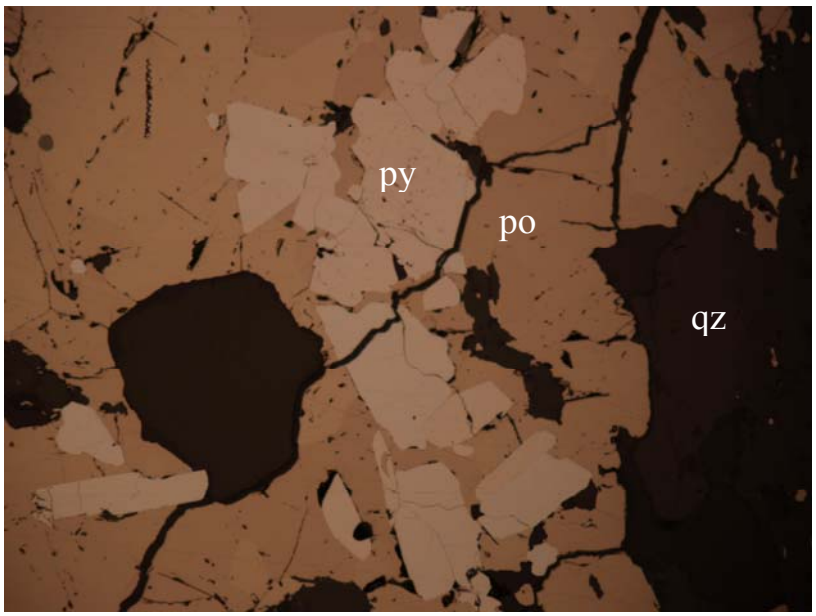

(b) (FOV 2 mm)

Figure 3.6: Overprinting relationships of oxides and sulphides in reflected light. **(a)** ilmenite growing on top of pyrrhotite **(b)** pyrite growing on top of pyrrhotite (il = ilemtite, po = pyrrhotite, py = pyrite, qz = quartz)

3.3 Summary

Gold mineralization in the Ormsby Zone occurs both in and around smoky grey quartz veins as free disseminated gold. Highest gold grades occur in the pillowed part of the Ormsby Member in close proximity to inclined quartz veins striking perpendicular to the length of the Ormsby Member. Alteration assemblages of pyrrhotite ± pyrite ± arsenopyrite ± chlorite ± sericite ± calcite are associated with gold. Pyrrhotite and gold always occur together, and arsenopyrite is always with gold, but not necessarily vice versa. Retrograde phases of chlorite, sericite and calcite typically occur with gold. Gold mineralization is interpreted to have occurred post folding, post-peak metamorphism, and syn-retrograde metamorphism based on sulphide relationships to host rock. The style of mineralization is typical of the disseminated stockwork style where mineralized zones consist of 5-20% sulphides occurring along foliation-parallel bands and quartz veinlets (Robert et al., 2005).

Chapter 4: Interpretations, Discussions and Conclusions

4.1 Introduction

Three rock units are present on the Discovery Property: (1) the Burwash Formation composed of metamorphosed sandstone and siltstone turbidites; (2) the Transition Unit composed of metamorphosed sandstone, siltstone, (now graphitic) mudstone, felsic tuff and reworked mafic volcanic components; and (3) the Giauque Lake Unit composed of pillowed, brecciated and massive metabasalts. The Giauque Lake and Transition units are interpreted to be part of the same sequence, and correlated to the Banting Group (occurring farther south) based on a U-Pb age of 2661 ±5 Ma from the Transition Unit, and lithological and depositional relationships between the two units. Peak metamorphism spans the transition from greenschist to amphibolite facies.

Four generations of ductile fabrics are preserved on the property as foliations, folds and a composite lineation. D_1 produced S_1, F_1, first stage garnet and biotite growth; D_2 produced S_2 and F_2; D_3 rotated S_2 into S_3, rotated some F_1 into S_3, produced F_3, continued garnet growth and post-S_3 cordierite growth; D_4 produced a weak S_4 crenulation. L_C is the result of the combination of the intersections of S_1 – S_4 and a vertical stretch. Peak metamorphism outlasted S_4. Retrograde phases of chlorite, calcite and sericite in the metabasalt, and chlorite in the metasedimentary rocks overprint ductile deformation. The possibility of a ductile fault with significant displacement is inferred to separate the Burwash Formation from the Giauque Lake and Transition units on the property. If this fault is present, it is interpreted to have occured post-peak metamorphism and pre-retrograde metamorphism. Gold mineralization in the Ormsby Zone is interpreted to have occurred syn-retrograde metamorphism, and is the younger of two mineralization events occurring on the property. Gold mineralization in the Ormsby Zone occurs both in and around smoky grey quartz veins as free disseminated gold. Highest gold grades occur in the pillowed rocks in close proximity to shallow dipping quartz veins striking perpendicular to the length of the Ormsby Member. Alteration assemblages of pyrrhotite ± pyrite ± arsenopyrite ± chlorite ± sericite ± calcite are associated with gold in the Ormsby Zone.

4.2 Proposed Structural Model

Regional (approximately E-W) contraction with syn- S_3 counterclockwise rotation is proposed to explain the orientation of fabrics and the Giauque Lake Unit on the Discovery Property. Deformation along the margins of the Giauque Lake Unit is interpreted as a result of competency contrast between the more rigid metabasalt bodies and the more ductile surrounding metasedimentary rocks. Figure 4.1 presents the progression of ductile fabric forming events, with (a) to (c) illustrating the geometry of the metabasalt bodies of the Giauque Lake Unit, bedding and foliations for D_1 through D_3 respectively. D_4 is omitted from Figure 4.1 since D_4 only produced a weak crenulation cleavage having no effect of the geometry of the rocks.

During D_1, NW-SE shortening folded bedding (F_1) and produced axial planar parallel S_1 (Figure 4.1a). The Giauque Lake Unit appears to lie on the west limb of a regional scale F_1 fold as suggested by the east-verging Z-folds on either side. The minor reversals in vergence represent parasitic folds. NE-SW shortening during D_2 produced S_2, and rare F_2 folds superimposed on F_1 (Figure 4.1b), and moved the Ormsby and Discovery members closer together. Regional F_3 folding caused rotation of the Giauque Lake Unit members, formed S_3 and realigned some F_1 folds into S_3 (Figure 4.1c). The more competent metabasalt bodies are interpreted to have responded to deformation by rotating counterclockwise within the less competent and more ductile metasedimentary rocks. This rotation resulted in localized higher strain in the immediately surrounding metasedimentary rocks. This high strain zone is characterized at map scale by a change in attitude of S_3 (Figure 4.1c). S_3 in the metasedimentary rocks generally strikes NNE, but near the margins of the Ormsby and Discovery members, it strikes NE, almost parallel to the length of the bodies. The foliation immediately surrounding the Ormsby and Discovery Members was aligned with the rotating metabasalt bodies.

More competent Fe-rich layers within the Transition Unit (described above – section 2.3.2) are in places boundinaged, transposed and rotated into S_3 (Figure 2.2 and 2.3). The boudins represent small scale analogies to the larger scale Ormsby and Discovery members, which are inferred to have had their geometry affected the same way. This fundamental observation supports the regional-scale rotation model.

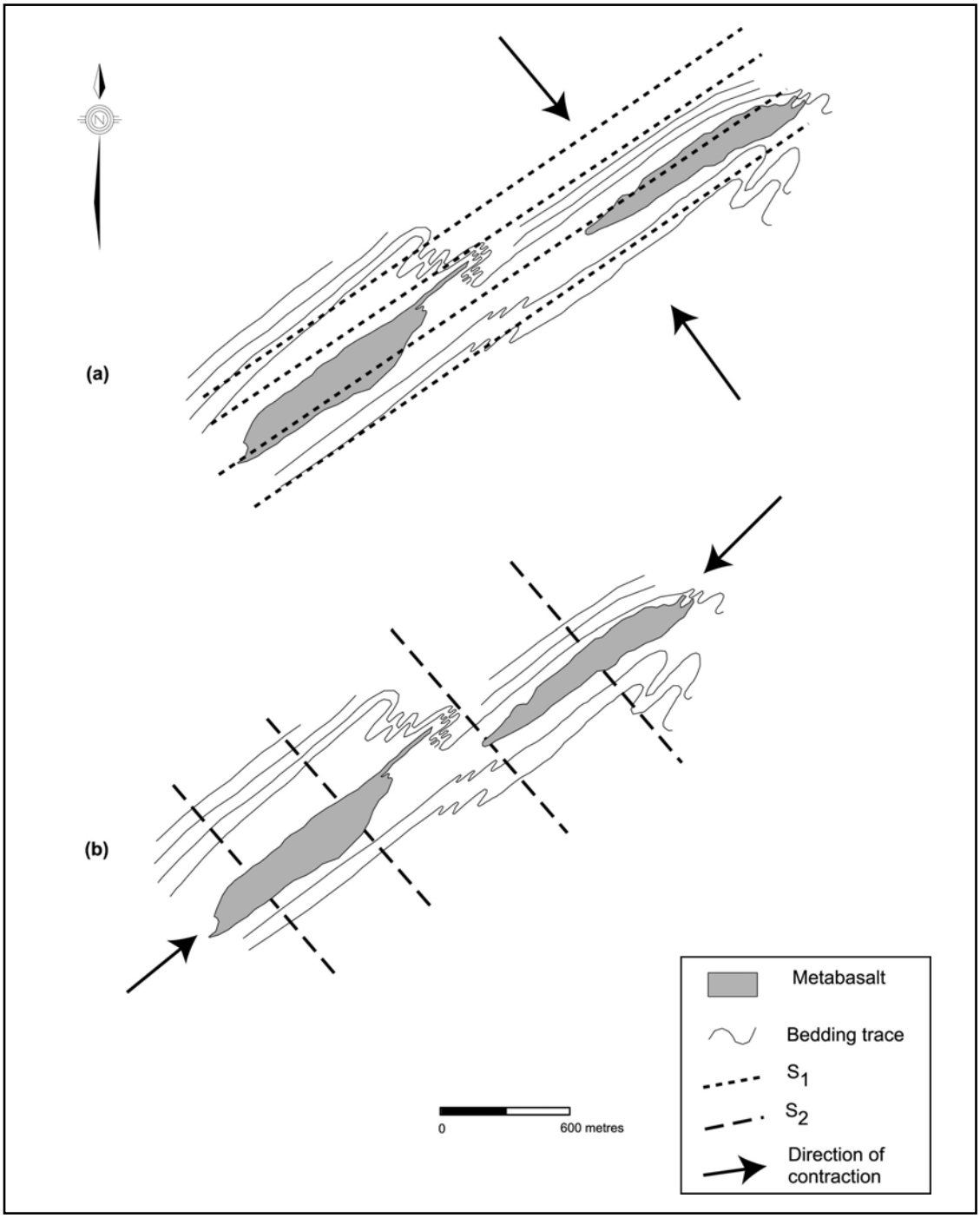

(continued on next page)

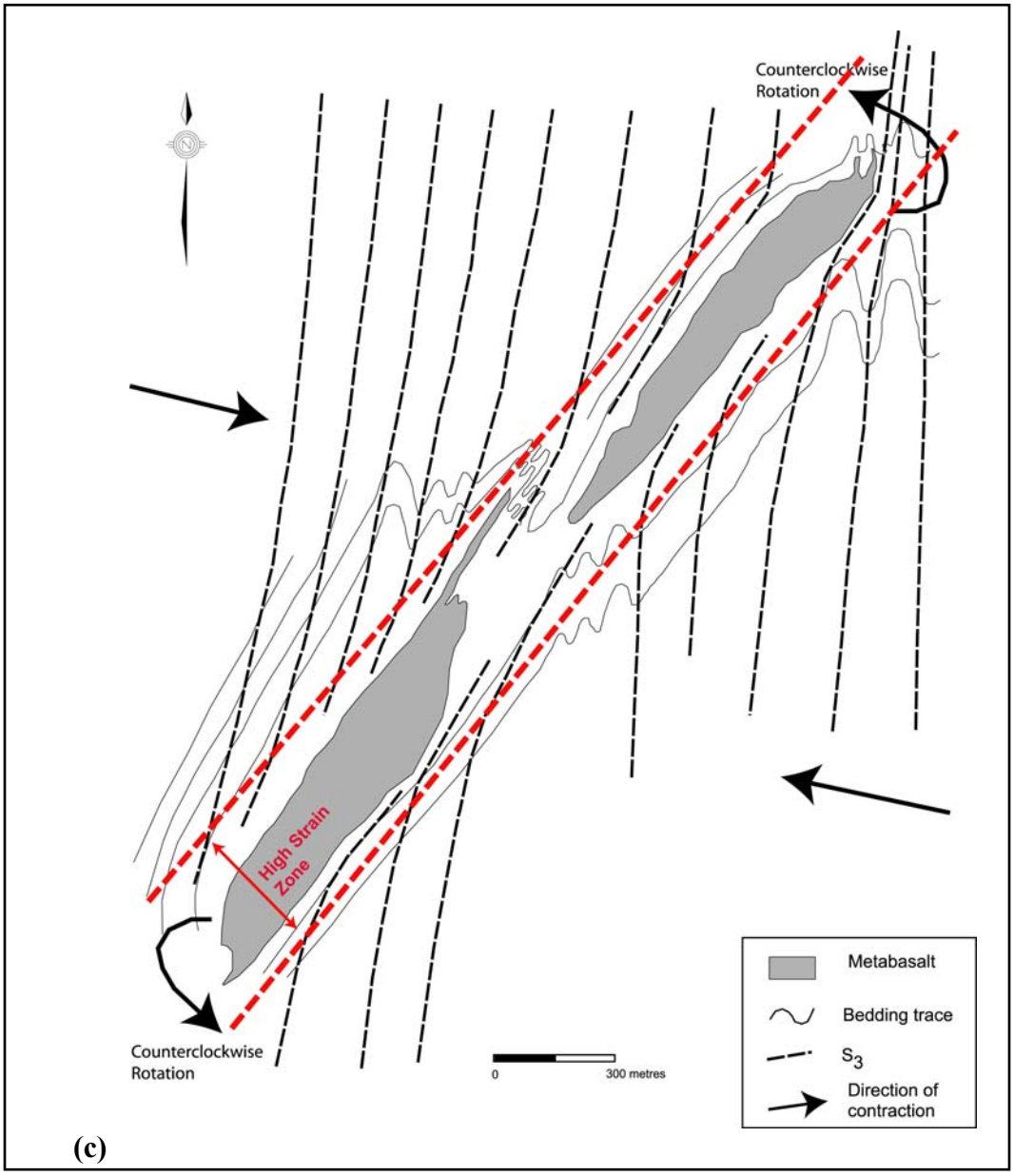

Figure 4.1: Proposed structural evolution of the rocks on the Discovery Property. **(a)** D_1: ductile deformation folds bedding into F_1 and forms S_1. The Giauque Lake Unit appears to lie on the west limb of a regional scale F_1 fold as suggested by the east-verging Z-folds on either side. The minor reversals present represent parasitic folds. **(b)** D_2: F_1 folds are refolded by F_2 and foliation S_2 is formed. **(c)** Regional F_3 folding caused rotation of the Giauque Lake Unit members, formed S_3 and realigned some F_1 folds into S_3. D_4 produced a weak almost E-W crenulation (not shown to enhance clarity), which has no effect on the geometry of the rocks.

4.3 Implications of a Post-Peak Metamorphic Fault

The presence of a regional scale post-peak metamorphic fault on the property, as suggested by the metamorphic data presented herein, has important implications for the regional geometry of the rock units in this study. Based on observations of Tremblay (1952) and Stubley (1997), the cordierte isograd (Figure 1.2) displays relatively little horizontal displacement from either side of the Giauque Lake and Transition units. If the Burwash Formation was juxtaposed with the Giauque Lake and Transition units along this interpreted post-peak metamorphic fault, a second (conjugate) fault of approximately equal displacement is required to explain the position of the of the cordierite isograd in the Burwash Formation northwest of the Giauque Lake Unit.

An interpretation of how these conjugate faults might explain how the older Transition and Giauque Lake units are completely enclosed in the younger Burwash Formation is presented in Figure 4.2. Figure 4.2a is a plan-view of the fault traces and cordierite isograd, and Figure 4.2b is a cross-section illustrating the relationship of the rocks during peak-metamorphism, prior to displacement. The cross-section in Figure 4.2c illustrates how faulting might have exposed the stratigraphically older rocks between the younger rocks through dip-slip movement.

Assumptions made are that peak metamorphic mineral assemblages observed in the Burwash Formation southeast of the Giauque Lake Unit also occur in the Burwash Formation exposed northwest of the Giauque Lake Unit, and that peak metamorphic mineral assemblages are constant across the width of the Transition Unit: this presents the same metamorphic discontinuity at the northwest contact between the Burwash Formation and Transition Unit, requiring a second, similar fault. For this scenario to work, interpretations of metamorphic data (see above – section 2.7) must be correct, as well as the assumption that all the minerals considered (including cordierite) grew in equilibrium as part of the peak metamorphic assemblage in a closed KFMASH system, prior to faulting. Even if the above interpretations and assumptions are correct, there is overlap in the uncertainty of estimated P-T presenting the possibility that this metamorphic discontinuity may not exit. All rocks in question are assumed to occur on the east limb of a regional fold (F_1, see above – section 2.8.3). Since no evidence of through-going brittle faulting was observed outcrop mapping or in drill core, the fault is assumed to be ductile and overprinted by retrograde metamorphism.

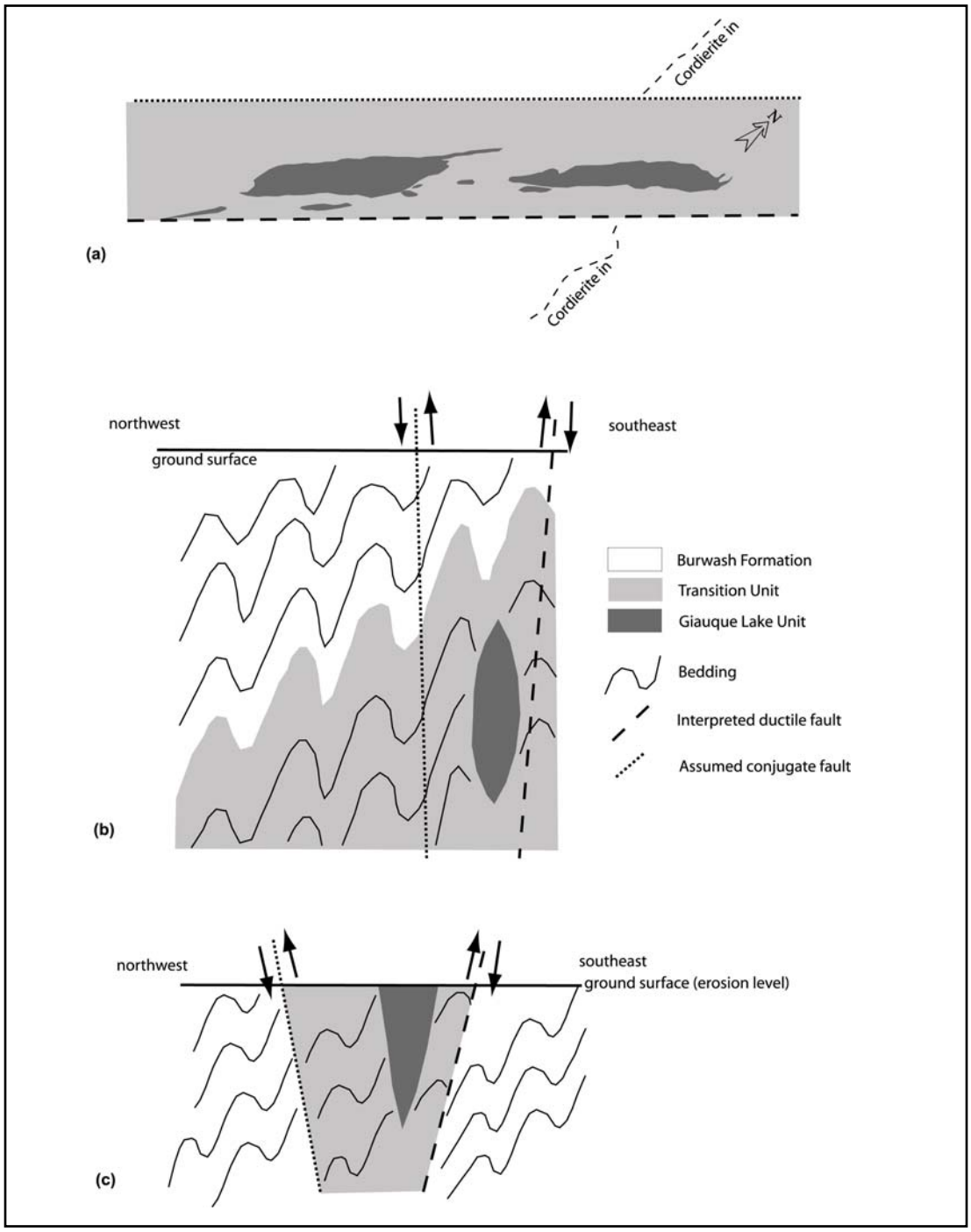

Figure 4.2: Interpretation of how post-peak metamorphic faulting might explain how the Giauque Lake and Transition units are exposed between the stratigraphically younger Burwash Formation (not to scale). **(a)** plan-view showing approximate fault traces and cordierite isograd, **(b)** Cross-section before displacement, **(c)** cross-section after displacement.

4.4 Correlation to Yellowknife Supergroup and Comparison with Previous Models

Previously the Giauque Lake Unit was interpreted as being stratigraphically lower than the Transition Unit because typically metabasalt underlie the metasedimentary rocks in the Yellowknife greenstone belt (Figure 1.5). Both the Giauque Lake and Transition units are inferred to be part of the same sequence, and correlated to the Banting Group based on a U-Pb age of 2661 ±5 Ma (see above – section 2.5). Based on data presented in this study, the Giauque Lake Unit is inferred to occur as discrete localized layers stratigraphically equal to and interfingered with the Transition Unit. The Giauque Lake Unit is inferred to have been deposited subaqueously as a basaltic lava flow sequence and formed both pillows and breccia while cooling on the sea floor (see above – section 2.6.1). During eruption and subsequent deposition the breccia was likely resedimented and reworked as it was eroded from the top of the lava flow. The more competent layers within the Transition Unit that deform more rigidly, similarly to the Giauque Lake Unit, are possibly resedimented or reworked basaltic material that originated from the Giauque Lake Unit.

The sandstone and siltstone layers of the Transition Unit are similar to the Burwash Formation. The Transition Unit links the Giauque Lake Unit and Burwash Formation together sedimentologically.

Dominant deformation documented in this study is correlated to documented regional deformation interpreted to have occurred in the southwestern Slave Province. D_3 deformation in this study is correlated to a regional approximately east-west compressive event described previously (D_2, see above – section 1.3). D_1 is this study can potentially be correlated to regional D_1 (see above – section 1.3), although in both cases original fabric orientations are uncertain, both interpretations of approximately northeast-southwest are compatible.

The Banting Group rocks on the Discovery Property (Transition and Giauque Lake units) crop out between the younger Burwash Formation on all sides. This exposure can only be explained by folding, faulting, or some combination of the two deformational styles, such as the two previously proposed models of Stubley (1997) and Stewart (2005; Figure 2.1). Results of the current study do not favour one model over the other, but rather modify the evidence used to support each. Data herein indicate the possibility of a metamorphic discontinuity, possibly representing a ductile fault, on the property separating the Banting

Group rocks from those of the Burwash Formation (Figure 4.2). This fault would likely be a ductile fault rather than a brittle one (in contrast to the "Ormsby Fault" proposed by Stubley, 1997), and strikes along the southeast side of the Discovery Member. Stubely's (1997) "Ormsby Fault" (Figure 2.1b) strikes between the two metabasalt members and along the northwest edge of the Discovery Member.

Both the Ormsby and Discovery members taper with depth. If the Giauque Lake Unit were stratigraphically lower than, and exposed between the surrounding Transition Unit in the hinge of an anticline as suggested by Stewart (2005), assuming no transposition on a regional scale, it would be expected to widen with depth. Moreover, the presence of thinner bands and discrete bodies of metavolcanic rocks similar to the Giauque Lake Unit occurring in the Transition Unit (Plate 1) suggest simultaneous deposition. Sufficient bedding/foliation overprinting relationships were not observed to be conclusive as to the Giauque Lake Unit's position relative to a regional F_1 fold hinge. Nonetheless, those that were observed generally have the same asymmetry on either side of the Giauque Lake Unit. As well, parasitic Z-folds on either side of the Giauque Lake Unit suggest it is located on the west limb on a regional F_1 fold.

The zone of deformation termed the "Ormsby Fault Zone" (Stubley, 1997, see above – section 2.2.1) is recognized in this study as a combination of ductile deformation resulting from contrasting rock competencies and potentially even a ductile fault. Stubley (1997) inferred it more as a brittle shear zone with sinistral displacement. Evidence presented herein does not support (or refute) Stubley's (1997) interpretation of bulk sinistral displacement.

4.5 Comparison with Other Deposits

The Ormsby Zone setting is typical of the Archean orogenic greenstone gold deposit model described previously (see above – section 1.2) in that it is hosted in a greenstone belt of greenschist to amphibolite facies metamorphosed pillowed basalts, where host rocks have undergone multiple fabric forming deformation events. Gold mineralization is late in the deformational history and associated with quartz veins and sulphide minerals.

Characteristics of selected deposits are compared in Table 1.1, and in conclusion the Ormsby Zone will be compared and contrasted with each of them. On a camp scale, the Con and Giant deposits are geologically similar to the Ormsby Zone, in that they are hosted in

poly-deformed greenschist to amphibolite facies metabasaltic rocks. The notable difference is that rocks hosting the Con and Giant deposits belong to the Kam Group whereas the Ormsby Zone is hosted in the stratigraphically younger Banting Group. Metal associations (gold with arsenopyrite) are similar as well, except that the arsenopyrite at Con-Giant contains refractory gold. The arsenopyrite at Ormsby does not affect gold recoveries. All the gold at Ormsby is free-milling whereas a substantial amount of gold recovered from Con-Giant was refractory; about 60% refractory from Giant (Chryssoulis, 1990), and a bit less from Con (Hubbard et al., 2006). Typical ore zones at Giant are 30-90% quartz (Canam, 2006). Ore Zones at Con consist of extremely common quartz veins up to 150 m long and from 1 m to 25 m wide (Hauser et al., 2006). Quartz veins at Ormsby are less common with the biggest veins being tens of metres long and less than 1 m wide. Free-milling gold at Con occurs within quartz or at vein margins (Hauser et al., 2006). Gold at Ormsby is associated with quartz and occurs as disseminations throughout silicified wall rock. Ore zones at Con and Giant are shear controlled while at Ormsby, mineralization does not appear to be structurally controlled.

Siddorn et al. (2006) propose that the Giant and Con deposits were once linked, and subsequently dismembered late in their deformational history. The Giant deposit and upper portions of the Con deposit are predominated by refractory gold. Younger free-milling gold occurs deeper within the Con deposit. Gold mineralization at these deposits is estimated to be ca. 2600 Ma (Ootes et al., 2007; see above – section 1.3), and early during the deformational history. The only absolute age constraint on mineralization at Ormsby is the U-Pb zircon age of 2661 ±5 Ma (see above – section 2.5) age of crystallization, but in contrast to Con-Giant, Ormsby mineralization is interpreted to have occurred late during the deformation history. The deformational event synchronous with the latest gold deposition at Con-Giant is correlated to D_3 in this study (see above – section 4.4). D_3 in this study is interpreted to have occurred before Ormsby gold mineralization, implying, based on this structural correlation, that gold at Ormsby is younger than gold of Con-Giant (2600 Ma).

The Discovery deposit is quite different from the Ormsby Zone. Not only is the gold restricted to a quartz vein hosted in a sedimentary sequence, but the relative timing of gold deposition is currently believed (Stubley, 1997) to be earlier in the deformational history. At Ormsby gold mineralization is late in the deformation history. As well, gold in the Discovery

deposit typically is not associated with sulphidation implying a different depositional mechanism.

Golden Mile in the Yilgarn Craton, Australia, is the largest known Archean greenstone gold vein system. It is hosted in primarily dolerite and basalt metamorphosed to greenschist facies where mineralization occurs within hundreds of shear zones (Shackleton, 2002). This is a typical Archean greenstone gold deposit, and differs from Ormsby with lower metamorphic grade and shear-zone controlled gold. Minimal pyrrhotite occurs at Golden Mile. Gold is mainly associated with pyrite (Shackleton, 2002), implying a more oxidized fluid than Ormsby.

The Hollinger-McIntyre deposit is located in the second richest (and largest Canadian producer) greenstone gold district, the Timmins-Porcupine gold district, Superior Province, Ontario. This deposit (along with the Hemlo deposit), although hosted in a typical Archean orogenic greenstone belt, is categorized by Groves et al. (2003) as "probably modified porphyry-epithermal systems". Although most ore is derived from quartz-carbonate veins, a minor proportion comes from porphyry style disseminated and stockwork Cu-Ag-Au-Mo, with Cu content and Au/Ag ratios completely unlike orogenic gold deposits (Groves et al., 2003). The overprinting quartz-carbonate veins have mineralogy, metal associations and wall-rock alteration typical of orogenic gold deposits.

Hemlo, Superior Province, Ontario, is atypical of Archean orogenic greenstone gold deposits in several ways. It lacks major quartz-carbonate veins, has a diverse metal suite (As, Ba, Hg, Mo, Sb, V) and lacks mafic volcanic rocks in the host sequence (Muir, 2002). As well, the moderate to high salinity ore fluid (Pan and Fleet, 1992) distinguish Hemlo from most orogenic gold deposits.

Lupin is the third largest gold producer in the Slave Province (behind Giant and Con). It differs from the Ormsby, and the other deposits discussed here in that it is hosted in an Archean banded iron formation (BIF). Gold was however deposited with pyrrhotite (Geusebroek and Duke, 2004), implying a reduced fluid source.

4.6 Remaining Work

Rocks assigned to the Banting Group in this study (Giauque Lake and Transition units) exposed between rocks of the younger Burwash Formation still present an enigma.

Folding, faulting or a combination of the two must exist, yet conclusive evidence to support one of these models remains elusive. Further structural mapping and analysis is required to solve this mystery. The potential post-peak metamorphic fault inferred herein may contribute to this model (Figure 4.2), but this hypothesis (see above – section 4.3) must be tested through a more detailed study, and the regional relationship between the Giauque Lake and Transition units, and the Burwash Formation understood. The detailed structural analysis of the current study needs to be supplemented with more regional work in order to understand the extent of the ductile fabrics defined herein, and hence regional folding. Closer inspection of better exposures in the area may prove beneficial. Recent burns in the region have left some areas well exposed. Brittle deformation should be mapped out in detail on the property, and faults, both brittle and ductile, traced regionally to understand their extent.

A detailed study of the Discovery Member would be beneficial for comparison with the Ormsby Member to help determine the relationship between the two bodies of rock. As well, a more detailed study of the Transition Unit must be completed to further support the link between all three units on the property. There are many lithological variations within the Transition Unit, most of which were not sampled or looked at in detail herein. A focused study of the Transition Unit would also contribute to understanding the metamorphic conditions by examining all the various mineral assemblages present in the different layers. Some of these assemblages may provide more reliable thermobarometry data.

More geochronology can be done on the metasedimentary rocks on the property to confirm the obtained age of the Transition Unit, and reinforce the assignment of the metaturbidites to the Burwash Formation. An age from the metabasalt would be extremely beneficial to confirm it's correlation with Banting Group. As well as geochronology, more detailed geochemical studies, following those of Cousens et al. (2002) and Cousens et al. (2006), on the metabasalt would not only be beneficial for correlating the Giauque Lake Unit to rocks farther south, but would help to determine their protoliths and depositional setting.

A focused study on the nature of the gold bearing fluid in order to compare it with typical fluid associated with other documented orogenic gold deposits is another potential area for research.

References

Baragar, W.R.A., Plant, A.G., Pringle, G.J., and Scau, M. 1979. Diagenic and post-diagenic changes in the composition of an Archean pillow. *Canadian Journal of Earth Sciences,* **16:** 2102-2121.

Bethune, K.M., Villeneuve, M.E., and Bleeker, W. 1999. Laser 40Ar/39Ar thermochronology of Archean rocks in the Yellowknife Domain, southwestern Slave Province: Insights into the cooling history of an Archean granite–greenstone terrane. *Canadian Journal of Earth Sciences,* **36**: 1189–1206.

Bleeker, W., 1996. Thematic structural studies in the Slave Province, Northwest Territories; the Sleepy Dragon Complex. *Geological Survey of Canada,* Current Research 1996-C, 37-48.

Bleeker, W. 2002. Archean tectonics: A review, with illustrations from the Slave Craton; *in* The Early Earth: Physical, Chemical and Biological Development, (ed.) C.M.R. Fowler, C.J. Ebinger, and C.J. Hawkesworth; *The Geological Society of London,* Special Publication, **199:** 151-181.

Bleeker, W., and Beaumont-Smith, C. 1995. Thematic structural studies in the Slave Province: preliminary results and implications for the Yellowknife Domain, Northwest Territories. *Geological Survey of Canada,* Current Research 1995-C, 87-96.

Böhkle, J.K. 1989. Comparison of metasomatic reactions between common CO_2-rich vein fluid and diverse wall rocks: Intensive variables, mass transfers, and Au mineralization, Alleghanny, California. *Economics Geology,* **84:** 291-327.

Bowring, S.A., Williams, I.S., and Compston, W. 1989. 3.96 Ga gneisses from the Slave Province, Northwest Territories, Canada. *Geology,* **17**: 971–975.

Bleeker, W., Ketchum, J.W.F., Jackson, V.A., and Villeneuve, M. 1999. The Central Slave Basement Complex, Part I: Its structural topology and autochthonous cover. *Canadian Journal of Earth Sciences,* **36**: 1083–1109.

Bloch, S., and Bishoff, J.L. 1979. The effect of low-temperature alteration of basal on the ocean budget of potassium. *Geology,* **7:** 193-196.

Bullen, W., and Robb, M. 2006. Economic contribution of gold mining in the Yellowknife mining district. Chapter 4 *in* Gold in the Yellowknife Greenstone Belt, Northwest Territories: Results of the EXTECH III Multidisciplinary Research Project, (ed.) C.D. Anglin, H. Falk, D.F. Wright, and E.J. Ambrose. *Geological Association of Canada, Mineral Deposits Division,* Special Publication #3, 38–49.

Canam, T.W. 2006. Discovery, mine production, and geology of the Giant mine. Chapter 13 *in* Gold in the Yellowknife Greenstone Belt, Northwest Territories: Results of the

EXTECH III Multidisciplinary Research Project, (ed.) C.D. Anglin, H. Falk, D.F. Wright, and E.J. Ambrose. *Geological Association of Canada, Mineral Deposits Division,* Special Publication #3, 188-196.

Cassidy, K.F., Groves, D.I., and McNaughton, N.J. 1998. Late-Archean granitoid-hosted lode-gold deposits, Yilgarn Craton, Western Australia: Deposit characteristics, crustal architecture, and implications for ore genesis. *Ore Geology Reviews,* **13:** 65-102.

Colvine, A.C. 1989. An empirical model for the formation of Archean gold deposits: Products of final cratonization of the Superior Province, Canada. *Economic Geology Monograph 6,* 37-53.

Cousens, B., Facey, K., Falk, H. 2002. Geochemistry of the late Archean Banting Group, Yellowknife greenstone belt, Slave Province, Canada: simultaneous melting of the upper mantle and juvenile mafic crust. *Canadian Journal of Earth Sciences.* **39:** 1635-1656.

Cousens, B., Falk, H., Ootes, L., Jackson, V., Mueller, W., Corcoran, P., Finnigan, C., van Hess, E., Facey, C., and Alcazar, A. 2006. Regional corrections, tectonic settings, and stratigraphic solutions in the Yellowknife greenstone belt and adjacent areas from geochemical and Sm-Nd isotopic analyses of volcanic and plutonic rocks. Chapter 7 *in* Gold in the Yellowknife Greenstone Belt, Northwest Territories: Results of the EXTECH III Multidisciplinary Research Project, (ed.) C.D. Anglin, H. Falk, D.F. Wright, and E.J. Ambrose. *Geological Association of Canada, Mineral Deposits Division,* Special Publication #3, 70-94.

Chryssoulis, S.L. 1990. Process Mineralogical Study of Au in Concentrator and Calcine Samples from Giant Yellowknife, NWT; Giant Mine. Internal Mining Report, 108p.

Dasgupta, S., Segupta, P., Guha, D., and Fukuoka, M. 1991. A refined garnet-biotite Fe-Mg exchange geothermometer and its application in amphibolites and granulites. *Contributions to Mineralogy and Petrology,* **109:** 130-137.

Davis, W., and Bleeker, W. 1999. Timing of plutonism, deformation, and metamorphism in the Yellowknife Domain. *Canadian Journal of Earth Sciences,* **36:** 1169-1187.

Drudy, S.A. 1977. Structures induced by granitic diapers in the Archean greenstone belt at Yellowknife, Canada: Implications for Archean geotectonics. *Journal of Geology,* **85:** 345-358.

Droop, G.T.R. 1987. A general equation for estimating Fe^{3+} concentrations in ferromagnesian silicates and oxides from microprobe analyses, using stoichiometric criteria. *Mineralogical Magazine,* **51:** 431-435.

Duke, N.A., Hauser, R., and Nauman, C.R. 1990. A guide to the geology of the NERCO Con Mine, Yellowknife, NWT; *in* Mineral Deposits of the Slave Province, Northwest Territories (Field Trip 13), 8th IAGOD Symposium Field Trip Guide Book, (ed.)

W.A. Padgham, and D. Atkinson; Geological Survey of Canada, Open File 2168: 41-52.

Dymoke, P., and Sandiford, M. 1992. Phase relationships in Buchan facies series politic assemblages: calculations with application to andalusite-staurolite paragenesis in the Mount Lofty Ranges, South Australia. *Contributions to Mineralogy and Petrology,* **110:** 121-132.

Ferry, J.M., and Spear, F.S. 1978. Experimental calibration of the partitioning of Fe and Mg between biotite and garnet. *Contributions to Mineralogy and Petrology,* **66:** #2, 113-117.

Geusbroek, P.A. and Duke, N.A. 2004. An Update on the Geology of the Lupin Gold Mine, Nunavut, Canada. *Exploration and Mining Geology,* **13:** #1-4, 1-13.

Gifkins, C., Herrmann, W., and Large, R. Altered Volcanic Rocks: A guide to description and interpretation. Centre for Ore Deposit Research, University of Tasmania, Australia: 2005.

Goldfarb, R.J., Baker, T., Dubé, B., Groves, D.I., Hart, C.J.R., and Gosselin, P. 2005. Distribution, character, and genesis of gold deposits in metamorphic terranes. *Economic Geology 100th Anniversary Volume*, 407-450.

Groves, D.I., Ridley, J.R., Bloem, E.J.M., Gebre-Mariam, M., Hagemann, S.G., Hronsky, J.M.A., Knight, J.T., McNaughton, N.J., Ojala, V.J., Vielreicher, R.M., McCuaig, T.C., and Holyland, P.W. 1995. Lode gold deposits of the Yilgarn block: Products of Late-Archean crustal-scale over pressured hydrothermal systems. *Geological Society of Special Publication* 95, 155-172.

Groves, D.I., Goldfarb, R.J., Gebre-Mariam, M., Hagemann, S.G., and Robert, F. 1998. Orogenic gold deposits: A proposed classification in the context of their crustal distribution and relationship to other gold deposit types. *Ore Geology Reviews,* **13:** 7-27.

Groves, D.I., Goldfarb, R.J., Knox-Robinson, C.M., Ojala, J. Gardoll, S., Yun, G.Y., and Holyland, P. 2000. Late-kinematic timing of orogenic gold deposits and significance for computer based exploration techniques with emphasis on the Yilgarn block, Western Australia. *Ore Geology Reviews,* **17:** 1-38.

Groves, D.I., Goldfarb, R.J., Roberts, F., and Hart, C.J.R. 2003. Gold deposits in metamorphic belts: Overview, understanding, outstanding problems, future research, and exploration significance. *Economic Geology,* **89:** 1-29.

Hagemann, S.G., and Cassidy, K.F. 2000. Archean Orogenic Lode Gold Deposits. *SEG Reviews,* **13:** 9-68.

Hauser, R.L., McDonald, D.W., and Siddorn, J.P. 2006. Geology of the Miramar Con Mine. Chapter 12 *in* Gold in the Yellowknife Greenstone Belt, Northwest Territories:

Results of the EXTECH III Multidisciplinary Research Project, (ed.) C.D. Anglin, H. Falk, D.F. Wright, and E.J. Ambrose. *Geological Association of Canada, Mineral Deposits Division,* Special Publication #3, 173-187.

Helmstaedt, H., and Padgham, W.A. 1986. A new look at the stratigraphy of the Yellowknife Supergroup at Yellowknife, N.W.T.—Implications for the age of gold-bearing shear zones and Archean basin evolution. *Canadian Journal of Earth Sciences*, **23**: 454-475.

Helmstaedt, H., Padgham, W.A., and Brophy, J.A. 1986. Multiple dikes in Lower Kam Group, Yellowknife greenstone belt: evidence for Archean sea-floor spreading? *Geology*, **14**: 562–566.

Henderson, J.B. 1970. Stratigraphy of the Yellowknife Supergroup, Yellowknife Bay – Prosperous Lake area, District of Mackenzie. *Geological Survey of Canada*, Paper 70-26.

Henderson, J.B. 1985. Geology of the Yellowknife–Hearne Lake Area, District of Mackenzie: A segment across an Archean basin. *Geological Survey of Canada*, Memoir 414.

Hodges, K.V., and Spear, F.S. 1982. Geothermometry, geobarometry and the Al_2SiO_5 triple point at Mt. Moosilauke, New Hampshire. *American Mineralogist,* **67:** 1118-1134.

Holdaway, M.J., and Lee, S.M. 1977. Fe-Mg cordierite stability based on experimental, theoretical, and natural observations. *Contributions to Mineralogy and Petrology,* **63:** 25-43.

Hubbard, L., Marshall, D., Anglin, C.D., Thorkelson, D., and Robinson, M.H. 2006. Giant mine: Alteration, mineralization, and ore-zone structures with an emphasis on the Supercrest zone; Chapter 14 *in* Gold in the Yellowknife Greenstone Belt, Northwest Territories: Results of the EXTECH III Multidisciplinary Research Project, (ed.) C.D. Anglin, H. Falk, D.F. Wright, and E.J. Ambrose. *Geological Association of Canada, Mineral Deposits Division,* Special Publication #3, 197-212.

Isachsen, C.E. 1992. U-Pb zircon geochronology of the Yellowknife Volcanic Belt and subajencent rocks, N.W.T., Canada: constraints on the timing, duration, and mechanics of greenstone belt formation. Ph.D. thesis, Washington University, St. Louis, Mo., 164 pp.

Isachsen, C.E., and Bowring, S.A. 1994. Evolution of the Slave Craton. *Geology,* **22:** 917-920.

Isachsen, C.E., and Bowring, S.A. 1997. The Bell Lake group and Anton Complex: a basement-cover sequence beneath the Archean Yellowknife greenstone belt revealed and implicated in greenstone belt formation. *Canadian Journal of Earth Sciences*, **34:** 2, 169-189.

Isachsen, C.E., Bowring, S.A., and Padgham, W.A. 1991. U-Pb zircon geochronology of the Yellowknife Volcanic Belt, NWT., Canada: new constraints on the timing and duration of greenstone belt magmatism. *Journal of Geology,* **99:** 55-67.

Jackson, V.A., and Cousens, B.L. 2006. Geology and geochemistry of the Bell Lake volcanic complex and its relationaship to the Yellowknife greenstone belt. Chapter 5 *in* Gold in the Yellowknife Greenstone Belt, Northwest Territories: Results of the EXTECH III Multidisciplinary Research Preject, (ed.) C.D. Anglin, H. Falk, D.F. Wright, and E.J. Ambrose. *Geological Association of Canada, Mineral Deposits Division,* Special Publication #3, 49-57.

Kerrich, R., Goldfarb, R., Groves, D., and Garwin, S. 2000. The Geodynamics of World-Class Gold Deposits: Characteristics, Space-Time Distribution, and Origins. *SEG Reviews,* **13:** 501-551.

Kohn, M.J., and Spear, F.S. 1990. Two new geobarometers for garnet amphibolites, with applications to southeastern Vermont. *American Mineralogist,* **75:** #1-2, 89-96.

Kusky, T.M. 1989. Accretion of the Archean Slave province. *Geology*, **17:** 63-67.

Kusky, T.M. 1990. Evidence for Archean ocean opening and closing in the southern Slave Province. *Tectonics,* **9:** 1533–1563.

Mahar, E.M., Baker, J.M., Powell, R., Holland, T.J.B., and Howell, N. 1997. The effect of Mn on mineral stability in metapelites. *Journal of Metamorphic Geology,* **15:** 223-238.

Martel, E. 2003. The Structural Evolution of the Yellowknife Greenstone Belt, Slave Province, NWT: New Insights on Its Stratigraphy and the Potential for Gold in the Jackson Lake Formation. M.Sc. thesis, University of Waterloo, Waterloo, On. 101 pp.

Martel, E., and Lin, S. 2006. Structural evolution of the Yellowknife greenstone belt, with emphasis on the Yellowknife River Fault Zone and the Jackson Lake Formation. Chapter 8 *in* Gold in the Yellowknife Greenstone Belt, Northwest Territories: Results of the EXTECH III Multidisciplinary Research Project, (ed.) C.D. Anglin, H. Falk, D.F. Wright, and E.J. Ambrose. *Geological Association of Canada, Mineral Deposits Division,* Special Publication #3, 95-115.

McCuaig, T.C., and Kerrich, R. 1998. P-T-t-deformation-fluid characteristics of lode gold deposits: Evidence from alteration systematics. *Ore Geology Reviews,* **12:** 381-435.

McDonald, D.W., Duke, N.A., and Hauser, R.L. 1993. Geological Setting of the NERCO Con Mine and the Relationship of Gold Mineralization to Metamorphism, Yellowknife, N.W.T. *Exploration and Mining Geology,* **2:** 139-154.

McPhie, J., Doyle, M., and Allen, R. Volcanic Textures: A guide to the interpretation of textures in volcanic rocks. Centre for Ore Deposit and Exploration Studies, University of Tasmania, Australia: 1993.

Muir, T.L. 2002. The Hemlo gold deposit, Ontario, Canada: principle deposit characteristics and constraints on mineralization. *Ore Geology Reviews,* **21:** 1-66.

Muir, T.L. 2003. Structural evolution of the Hemlo greenstone belt in the vicinity of the world-class Hemlo gold deposit. *Canadian Journal of Earth Sciences,* **40:** 395-430.

Ootes, L., Lentz, D.R., Creaser, R.A., Ketchum, J.W.F., and Falck, H. 2007. Re-Os molybdenite ages from the Archean Yellowknife greenstone belt: comparison to U-Pb ages evidence for metal introduction at ~2675 Ma. *Economic Geology,* **102:** 511-518.

Pan, Y., and Fleet, M.E., 1992. Calc-silicate alteration in the Hemlo gold deposit, Ontario: Mineral assemblages, P-T-X constraints, and significance. *Economic Geology*, **87:** 1104-1120.

Perchuk, L.L., and Lavrent'eva, I.V. 1983. Experimental investigation of exchange equilibria in the system cordierite-garnet-biotite. *In* Kinetics and Equilibrium in Mineral reactions. Advances in Physical Geochemistry, vol 3, (ed.) Saxena, S.K. Springer-Verlag, New York, pp. 199-239.

Phillips, G.N., Groves, D.I., and Martyn, J.E. 1984. An epigenetic origin for Archean banded iron-formation hosted gold deposits. *Economic Geology,* **79:** 162-171.

Poulsen, K.H., Robert, F., and Dubé, B. 2000 Geological Classification of Canadian Gold Deposits. *Geological Survey of Canada,* Bulletin **540:** 106 pp.

Powell, R., and Holland, T. 1994. Optimal geothermometry and geobarometry. *American Mineralogist,* **79:** 120-133.

Ramsey, C.R. 1973. Controls on biotite zone mineral chemistry in Archean metasediments near Yellowknife, N.W.T. Canada, *Journal of Petrology,* **14:** 467-488.

Robert, F., and Poulsen, K.H. 1997. World-class Archean gold deposits in Canada: An overview. *Australian Journal of Earth Sciences,* **44:** 329-351.

Robert, F., Poulsens, K.H., Cassidy, K.F., and Hodgson, C.J. 2005. Gold Metallogeny of the Superior and Yilgarn Cratons. *Economic Geology 100th Anniversary Volume,* 1001-1033.

Roberts, R.G. 1988. Archean lode gold deposits. *In* Ore deposit models, (ed.) Roberts, R.G. and Sheahan, P.A. *Geoscience Canada*, Reprint Series 3, 1-19.

Ridley, J.R., and Diamond, L.W. 2000. Fluid Chemistry of Orogenic Lode Gold Deposits and Implications for Genetic Models. *SEG Reviews,* **13:** 141-162.

Shackleton, J. Telluride mineralogy of the Golden Mile, Kalgoorie, Western Australia. M.Sc. thesis, Iowa State University of Science and Technology, Ames, IA, USA.

Shelton, K., McMenamy, T.A., van Hees, E.H.P., and Falk, H. 2004. Deciphering the complex fluid history of a greenstone-hosted gold deposit; fluid inclusion and stable isotope studies of the Giant Mine, Yellowknife, Northwest Territories, Canada. *Economic Geology and the Bulletin of the Society of Economic Geologists,* **99:** #8, 1643-1663.

Siddorn, J.P., Cruden, A.R., Hauser, R.L., Armstrong, J.P., and Kirkham, G. 2006. The Giant-Con gold deposits: Preliminary integrated structural and mineralization history. Chapter 15 *in* Gold in the Yellowknife Greenstone Belt, Northwest Territories: Results of the EXTECH III Multidisciplinary Research Project, (ed.) C.D. Anglin, H. Falk, D.F. Wright, and E.J. Ambrose. *Geological Association of Canada, Mineral Deposits Division,* Special Publication #3, 213-231.

Snyder, D.B., Bleeker, W. Roberts, B.J., and Salisbury, M.D. 2006. Structure and crustal architecture of the Yellowknife greenstone belt SNORCLE geophysical survey data. Chapter 9 *in* Gold in the Yellowknife Greenstone Belt, Northwest Territories: Results of the EXTECH III Multidisciplinary Research Project, (ed.) C.D. Anglin, H. Falk, D.F. Wright, and E.J. Ambrose. *Geological Association of Canada, Mineral Deposits Division,* Special Publication #3, 116-145.

Stern, R.A., and Bleeker, W. 1998. Age of the world's oldest rocks refined using Canada's SHRIMP: The Acasta Gneiss complex, Northwest Territories, Canada. *Geoscience Canada*, **25**: 27–32.

Stewart, P.W. 2005. Report on Geological Mapping at the Yellowknife Gold Project, Northwest Territories, Canada. Unpublished report for Tyhee NWT Corp. 85 pp. and accompanying 1:10,000 scale geological map.

Stroncik, N.A., and Schmincke, H. 2002. Palagonite – a review. *International Journal of Earth Sciences,* **91:** 680-697.

Stubley, M.P. 1997. Geology of the Discovery Property. Unpublished report to GMD Resource Corp. 23 pp. and accompanying 1:2400 scale geological map.

Sun, S.-s, and McDonough, W.F. 1989. Chemical and isotopic systematics of ocean basalts: implications for mantle composition and Processes. *In* Magmatism in the ocean basins, (ed.) A.D. Saunders, and M.J. Norry. *Geological Societey of London,* Special Publication 42, 313-345.

Thompson, A.B. 1976. Mineral reactions in pelitic rocks: II. Calculations of some P-T-X(Fe-

Mg) phase relations. *American Journal of Science*, **276:** 425-454.

Thompson, P.H. 2006. Metamorphic constraints on the geological setting, thermal regime, and timing of alteration and gold mineralization in the Yellowknife greenstone belt, N.W.T., Canada. Chapter 11 *in* Gold in the Yellowknife Greenstone Belt, Northwest Territories: Results of the EXTECH III Multidisciplinary Research Project, (ed.) C.D. Anglin, H. Falk, D.F. Wright, and E.J. Ambrose. *Geological Association of Canada, Mineral Deposits Division,* Special Publication #3, 142-172.

Tremblay, L.P. 1952. Giauque Lake map-area, Northwest Territories; *Geological Survey of Canada*, Memoir 266, 74 pp and accompanying 1:24,000 scale geological map.

van Breemen, O., Davis, W.J., and King, J.E. 1992. Temporal distribution of granitoid plutonic rocks in the Archean Slave Province, northwest Canadian Shield. *Canadian Journal of Earth Sciences,* **29**: 2186–2199.

van der Veldon, A.J., and Cook, F.A. 2002. Products of a 2.65-2.58 Ga orogenesis in the Slave Province correlated with Slave – Northern Cordillera Lithospheric Evolution (SNORCLE) seismic pattern. *Canadian Journal of Earth Sciences*, **38:** 1189-1200.

Wei, C.J., Powell, R., and Clake, L. 2004. Calculated phase equilibria for low- and medium-pressure metapelites in the KFMASH systems. *Journal of Metamorphic Geology,* **22:** 495-508.

Worley, B., and Powell, R. 2000. High-precision relative thermobarometry: theory and a worked example. *Journal of Metamorphic Geology,* **18:** 91-101.

Yamashita, K., Creaser, R.A., Jensen, J.E., and Heaman, L.M. 2000. Origin and evolution of mid- to late-Archean crust in the Hanikahimajuk Lake area, Slave Province, Canada: Evidence from U-Pb geochronological, geochemical and Nd-Pb isotopic data. *Precambrian Research,* **99**: 197–224.

Appendix A: Mineral Chemistry

(obtained from a Cameca SX-50 electron microprobe;
mineral recalculations done using Excel spreadsheets of:
Jeremy Preston (2001), v1.2, U of Aberdeen,
http://www.abdn.ac.uk/geology/profiles/analysis/software.htm)

Table A1

WW02C (Transition Unit Metasedimentary Rock): Staurolite

Label	**02C-13**	**02C-14**	**02C-15**	**02C-16**	**02C-17**	**02C-18**	**02C-19**
No	**1**	**2**	**3**	**4**	**5**	**6**	**7**
wt %							
SiO_2	26.87	27.03	26.92	27.26	26.58	26.73	27.04
TiO_2	0.35	0.42	0.40	0.35	0.39	0.37	0.32
Al_2O_3	53.96	53.96	53.85	54.55	54.64	54.09	54.55
FeO	13.18	13.32	13.65	13.02	13.29	13.61	13.25
MnO	0.20	0.23	0.21	0.27	0.28	0.22	0.20
MgO	0.69	0.79	0.79	0.54	0.44	0.73	0.75
CaO	0.00	0.02	0.03	0.01	0.02	0.00	0.00
Na_2O	0.02	0.03	0.00	0.01	0.00	0.01	0.04
K_2O	0.00	0.01	0.00	0.00	0.00	0.03	0.01
Cr_2O_3	0.08	0.07	0.03	0.04	0.06	0.06	0.06
Total	**95.36**	**95.86**	**95.90**	**96.05**	**95.70**	**95.84**	**96.23**
moles	(based on 23 O)						
Si	3.817	3.822	3.812	3.837	3.765	3.788	3.806
Ti	0.038	0.045	0.043	0.037	0.041	0.040	0.034
Al	9.034	8.993	8.985	9.048	9.122	9.033	9.049
Fe(ii)	1.566	1.576	1.616	1.533	1.575	1.612	1.560
Mn	0.024	0.027	0.025	0.032	0.034	0.026	0.024
Mg	0.147	0.166	0.168	0.113	0.092	0.153	0.157
Ca	0.000	0.003	0.005	0.001	0.003	0.000	0.000
Na	0.005	0.008	0.000	0.002	0.001	0.002	0.011
K	0.000	0.001	0.000	0.000	0.000	0.005	0.001
Total	**14.631**	**14.642**	**14.653**	**14.603**	**14.633**	**14.660**	**14.642**
Fe/Fe+Mg	**0.914**	**0.905**	**0.906**	**0.931**	**0.945**	**0.913**	**0.908**

Table A2

WW05028 (Burwash Formation Metasedimentary Rock): Cordierite

Label	**28-1**	**28-2**	**28-3**	**28-4**
No	**8**	**9**	**10**	**11**
wt %				
SiO_2	47.62	47.46	47.56	47.51
TiO_2	0.00	0.00	0.01	0.01
Al_2O_3	32.28	32.03	32.37	32.38
FeO	8.25	8.47	8.15	7.97
MnO	0.33	0.32	0.34	0.36
MgO	8.20	7.99	8.15	8.16
CaO	0.02	0.02	0.02	0.00
Na_2O	0.27	0.28	0.21	0.24
K_2O	0.02	0.01	0.01	0.01
Cr_2O_3	0.00	0.03	0.03	0.00
F	0.10	0.00	0.00	0.00
Total	**97.00**	**96.60**	**96.84**	**96.64**
moles	(based on 18 O)			
Si	4.984	4.992	4.982	4.982
Ti	0.000	0.000	0.001	0.001
Al	3.981	3.971	3.997	4.002
Fe(ii)	0.722	0.745	0.713	0.699
Mn	0.029	0.029	0.030	0.032
Mg	1.279	1.254	1.272	1.276
Ca	0.002	0.002	0.002	0.001
Na	0.056	0.056	0.043	0.048
K	0.003	0.001	0.002	0.001
Total	**11.055**	**11.051**	**11.041**	**11.041**
Fe/Fe+Mg	**0.361**	**0.373**	**0.359**	**0.354**

Table A3 WW14A (Giauque Lake Unit Metabasalt): Garnet

Label	**14A-1**	**14A-2**	**14A-3**	**14A-4**	**14A-5**	**14A-6**	**14A-7**	**14A-8**	**14A-9**
No	**1**	**2**	**3**	**4**	**5**	**6**	**7**	**8**	**9**
wt %									
SiO_2	35.91	35.32	35.90	35.15	35.47	35.51	36.03	36.43	35.24
TiO_2	0.10	0.22	0.08	0.09	0.15	0.12	0.13	0.13	0.12
Al_2O_3	20.94	20.73	20.71	20.86	20.57	21.07	20.90	20.93	20.76
FeO	31.54	31.23	31.04	31.41	30.32	31.46	30.95	31.19	30.63
MnO	4.78	5.27	4.72	4.69	4.19	4.70	5.25	4.89	5.00
MgO	1.07	1.17	1.08	1.09	1.15	1.06	1.14	1.09	0.86
CaO	4.66	4.20	3.96	4.18	5.76	4.31	4.32	4.08	5.48
Na_2O	0.01	0.02	0.13	0.06	0.09	0.05	0.04	0.00	0.03
Cr_2O_3	0.00	0.03	0.00	0.02	0.03	0.00	0.00	0.00	0.00
Total	**99.02**	**98.19**	**97.63**	**97.54**	**97.72**	**98.27**	**98.75**	**98.74**	**98.12**
moles	(based on 12 O)								
Si	2.952	2.935	2.984	2.936	2.949	2.940	2.964	2.989	2.930
Al	0.048	0.065	0.016	0.064	0.051	0.060	0.036	0.011	0.070
ΣT	**3.000**	**3.000**	**3.000**	**3.000**	**3.000**	**3.000**	**3.000**	**3.000**	**3.000**
Al	1.980	1.964	2.013	1.990	1.965	1.996	1.991	2.012	1.963
Ti	0.006	0.014	0.005	0.005	0.009	0.007	0.008	0.008	0.007
Fe	0.014	0.022	0.000	0.004	0.026	0.000	0.001	0.000	0.029
ΣY	**2.000**	**2.000**	**2.018**	**2.000**	**2.000**	**2.003**	**2.000**	**2.020**	**2.000**
Fe	2.154	2.148	2.158	2.190	2.082	2.178	2.129	2.140	2.099
Mn	0.333	0.371	0.332	0.332	0.295	0.330	0.366	0.340	0.352
Mg	0.131	0.145	0.134	0.135	0.143	0.131	0.139	0.133	0.107
Ca	0.411	0.374	0.353	0.375	0.513	0.382	0.381	0.358	0.488
ΣX	**3.028**	**3.037**	**2.978**	**3.031**	**3.033**	**3.021**	**3.014**	**2.972**	**3.046**
Total	**8.028**	**8.037**	**7.996**	**8.031**	**8.033**	**8.025**	**8.014**	**7.992**	**8.046**
Fe/Fe+Mg	**0.943**	**0.937**	**0.941**	**0.942**	**0.936**	**0.943**	**0.939**	**0.941**	**0.952**
Py	**4**	**5**	**5**	**4**	**5**	**4**	**5**	**4**	**3**
Alm	**71**	**71**	**72**	**72**	**69**	**72**	**71**	**72**	**69**
Gro	**13**	**12**	**12**	**12**	**17**	**13**	**13**	**12**	**16**
Sp	**11**	**12**	**11**	**11**	**10**	**11**	**12**	**11**	**11**

Table A4

(Giauque Lake Unit Metabasalt) Hornblende

	WW14A		WW05068				
Label	**14A-8**	**14A-13**	**68-1**	**68-2**	**68-3**	**68-4**	**68-9**
No	**19**	**24**	**25**	**26**	**27**	**28**	**33**
wt %							
SiO_2	38.96	38.59	42.24	40.34	40.89	41.16	42.64
TiO_2	0.32	0.37	0.65	0.50	0.65	0.56	0.68
Al_2O_3	16.15	14.61	10.90	11.20	10.54	11.75	10.58
Cr_2O_3	0.00	0.02	0.00	0.00	0.00	0.00	0.02
FeO	25.14	24.41	23.66	24.77	23.58	24.34	23.74
MnO	0.26	0.38	0.69	0.64	0.64	0.54	0.64
MgO	3.38	3.84	5.64	5.71	5.61	5.28	5.78
CaO	10.70	12.07	11.44	10.20	11.54	11.12	11.62
Na_2O	1.59	1.67	1.12	1.03	1.21	1.16	1.18
K_2O	0.50	0.41	0.69	0.61	0.72	0.79	0.76
F	0.09	0.17	0.12	0.00	0.10	0.14	0.06
Total	**96.99**	**96.37**	**97.01**	**95.00**	**95.37**	**96.69**	**97.65**
moles	(based on 23 O; 13 cations exclusive of K, Na, Ca; Fe(iii) estimates using equation (6) of Droop (1987))						
Si	5.994	6.077	6.511	6.267	6.450	6.363	6.549
Al	2.006	1.923	1.489	1.733	1.550	1.637	1.451
ΣT	**8.000**	**8.000**	**8.000**	**8.000**	**8.000**	**8.000**	**8.000**
Al	0.921	0.788	0.491	0.318	0.408	0.503	0.464
Ti	0.037	0.044	0.075	0.059	0.077	0.065	0.079
Cr	0.000	0.003	0.000	0.000	0.000	0.000	0.002
Fe(iii)	0.912	0.377	0.599	1.471	0.575	0.819	0.502
Fe(ii)	2.321	2.837	2.450	1.746	2.535	2.327	2.547
Mn	0.034	0.050	0.089	0.084	0.085	0.071	0.083
Mg	0.774	0.901	1.295	1.323	1.319	1.216	1.323
ΣC	**5.000**	**5.000**	**5.000**	**5.000**	**5.000**	**5.000**	**5.000**
Ca	1.763	2.037	1.889	1.698	1.949	1.841	1.913
Na	0.474	0.511	0.335	0.311	0.369	0.348	0.351
K	0.098	0.082	0.135	0.121	0.144	0.156	0.149
ΣA	**2.336**	**2.630**	**2.359**	**2.129**	**2.463**	**2.345**	**2.413**
Total	**15.336**	**15.630**	**15.359**	**15.129**	**15.463**	**15.345**	**15.413**
Fe/Fe+Mg	**0.750**	**0.759**	**0.654**	**0.569**	**0.658**	**0.657**	**0.658**
Species	**Ferro-tschermakite**	**Ferro-pargasite**	**Ferro-hornblende**	**Ferro-tschermakite**	**Ferro-tschermakite**	**Ferro-tschermakite**	**Ferro-hornblende**

Table A5
WW14A (Giauque Lake Unit Metabasalt): Commingtonite

Label	14A-1	14A-3	14A-6	14A-11
No	**12**	**14**	**17**	**22**
wt %				
SiO_2	50.90	50.81	51.23	50.17
TiO_2	0.00	0.00	0.02	0.03
Al_2O_3	0.45	0.26	0.29	0.35
Cr_2O_3	0.04	0.00	0.00	0.05
FeO	35.51	35.90	35.59	34.82
MnO	1.20	1.19	1.11	1.15
MgO	9.17	9.10	9.23	9.23
CaO	0.45	0.57	0.59	0.64
Na_2O	0.11	0.05	0.10	0.90
K_2O	0.01	0.01	0.02	0.08
F	0.09	0.03	0.00	0.00
Total	**97.85**	**97.90**	**98.20**	**97.41**
moles	(based on 23 O; 15 cations exclusive of K; Fe(iii) estimates using equation (5) of Droop (1987))			
Si	7.926	7.912	7.947	7.876
Al	0.074	0.047	0.053	0.064
ΣT	**8.000**	**7.959**	**8.000**	**7.940**
Al	0.009	0.000	0.000	0.000
Ti	0.000	0.000	0.003	0.003
Cr	0.005	0.000	0.000	0.006
Fe(iii)	0.022	0.111	0.013	0.000
Fe(ii)	4.602	4.564	4.604	4.571
Mn	0.159	0.157	0.146	0.153
Mg	2.128	2.113	2.136	2.161
ΣC	**6.926**	**6.945**	**6.901**	**6.894**
Ca	0.074	0.096	0.099	0.107
Na	0.034	0.015	0.030	0.273
K	0.003	0.003	0.004	0.016
ΣA	**0.111**	**0.113**	**0.134**	**0.397**
Total	**15.037**	**15.017**	**15.035**	**15.231**
Fe/Fe+Mg	**0.684**	**0.684**	**0.683**	**0.679**

Table A6

Biotite

	WW05004 (Burwash Metased.)				WW05030 (Trans. Metased.)				WW05028 (Burwash Metased.)				WW14A (Giauque L. Metavolc.)			
Label	**04-1**	**04-2**	**04-3**	**04-4**	**30-2**	**30-3**	**30-7**	**30-11**	**28-1**	**28-2**	**28-3**	**28-10**	**14A-1**	**14A-2**	**14A-3**	**14A-4**
No	**1**	**2**	**3**	**4**	**14**	**15**	**17**	**20**	**46**	**47**	**48**	**54**	**59**	**60**	**61**	**62**
wt %																
SiO_2	35.87	36.22	35.81	36.22	38.97	35.76	35.93	35.72	35.81	35.22	35.72	36.13	32.58	32.18	32.87	33.71
TiO_2	1.90	1.60	2.09	1.55	1.22	1.37	1.50	2.32	1.46	1.19	1.36	1.39	2.19	2.54	2.35	2.29
Al_2O_3	19.43	19.11	18.64	18.68	25.06	20.64	20.13	18.84	19.92	19.81	19.79	20.19	15.28	15.90	15.56	15.96
FeO	17.12	17.19	18.19	17.39	14.15	18.43	18.28	18.56	19.07	19.24	18.64	17.86	28.08	27.69	29.31	28.26
MnO	0.11	0.14	0.11	0.10	0.03	0.13	0.05	0.10	0.07	0.12	0.10	0.08	0.12	0.08	0.07	0.15
MgO	10.81	10.73	10.80	10.78	6.74	9.25	9.20	9.84	9.84	9.84	9.44	10.17	5.58	5.44	5.20	5.85
CaO	0.01	0.00	0.01	0.00	0.00	0.04	0.00	0.04	0.01	0.00	0.02	0.03	0.02	1.21	0.06	0.01
Na_2O	0.07	0.10	0.03	0.10	0.45	0.16	0.11	0.16	0.35	0.22	0.29	0.24	0.04	0.13	0.03	0.06
K_2O	9.55	10.17	9.63	9.84	9.50	9.33	9.88	9.51	9.16	9.07	8.85	9.36	7.43	7.97	8.45	8.43
Cr_2O_3	0.02	0.06	0.12	0.00	0.11	0.16	0.08	0.11	0.23	0.16	0.24	0.05	0.01	0.02	0.00	0.03
F	0.42	0.40	0.32	0.65	0.41	0.63	0.53	0.59	0.20	0.18	0.13	0.12	0.08	0.09	0.21	0.08
Total	**94.88**	**95.32**	**95.42**	**94.66**	**96.24**	**95.26**	**95.16**	**95.20**	**95.92**	**94.87**	**94.45**	**95.50**	**91.34**	**93.15**	**93.88**	**94.77**
moles	(based on 11 O)															
Si	2.709	2.734	2.711	2.750	2.811	2.703	2.722	2.714	2.700	2.688	2.725	2.714	2.711	2.640	2.687	2.706
Al	1.291	1.266	1.289	1.250	1.189	1.297	1.278	1.286	1.300	1.312	1.275	1.286	1.289	1.360	1.313	1.294
ΣT	**4.000**	**4.000**	**4.000**	**4.000**	**4.000**	**4.000**	**4.000**	**4.000**	**4.000**	**4.000**	**4.000**	**4.000**	**4.000**	**4.000**	**4.000**	**4.000**
Al	0.439	0.435	0.374	0.422	0.942	0.542	0.520	0.401	0.470	0.470	0.505	0.501	0.210	0.176	0.186	0.216
Ti	0.108	0.091	0.119	0.089	0.066	0.078	0.086	0.133	0.083	0.068	0.078	0.079	0.137	0.157	0.144	0.138
Fe(ii)	1.081	1.085	1.152	1.104	0.854	1.165	1.159	1.179	1.202	1.228	1.189	1.122	1.954	1.899	2.004	1.897
Mn	0.007	0.009	0.007	0.006	0.002	0.008	0.003	0.006	0.005	0.008	0.007	0.005	0.008	0.005	0.005	0.010
Mg	1.217	1.208	1.219	1.220	0.725	1.042	1.039	1.115	1.106	1.120	1.074	1.139	0.693	0.665	0.633	0.700
ΣR	**2.852**	**2.827**	**2.870**	**2.841**	**2.589**	**2.835**	**2.807**	**2.834**	**2.866**	**2.895**	**2.853**	**2.846**	**3.002**	**2.902**	**2.972**	**2.962**
Ca	0.001	0.000	0.000	0.000	0.000	0.003	0.000	0.003	0.001	0.000	0.001	0.002	0.002	0.107	0.005	0.001
Na	0.010	0.014	0.005	0.014	0.063	0.024	0.016	0.024	0.051	0.032	0.044	0.035	0.007	0.020	0.005	0.010
K	0.920	0.980	0.930	0.953	0.874	0.899	0.955	0.921	0.881	0.883	0.862	0.896	0.789	0.833	0.881	0.864
ΣA	**0.931**	**0.994**	**0.935**	**0.967**	**0.937**	**0.927**	**0.971**	**0.948**	**0.933**	**0.915**	**0.907**	**0.934**	**0.798**	**0.960**	**0.891**	**0.875**
F	0.101	0.095	0.077	0.156	0.093	0.151	0.126	0.143	0.047	0.043	0.032	0.028	0.022	0.022	0.054	0.020
Total	**7.783**	**7.821**	**7.806**	**7.808**	**7.526**	**7.761**	**7.779**	**7.782**	**7.799**	**7.810**	**7.759**	**7.779**	**7.800**	**7.862**	**7.862**	**7.837**
Fe/Fe+Mg	**0.470**	**0.473**	**0.486**	**0.475**	**0.541**	**0.528**	**0.527**	**0.514**	**0.521**	**0.523**	**0.526**	**0.496**	**0.738**	**0.741**	**0.760**	**0.730**

Table A7

Muscovite

	WW05004 (Burwash Metased.)				WW05030 (Trans. Metased.)				WW05028 (Burwash Metased.)				WW02C (Trans. Metased.)		
Label	**04-5**	**04-6**	**04-7**	**04-8**	**30-1**	**30-5**	**30-10**	**30-12**	**28-5**	**28-6**	**28-11**	**28-12**	**02C-5**	**02C-6**	**02C-7**
No	**5**	**6**	**7**	**8**	**13**	**16**	**19**	**21**	**49**	**50**	**55**	**56**	**28**	**29**	**30**
wt %															
SiO_2	46.36	47.18	46.01	46.32	46.46	46.76	45.89	46.13	45.81	45.32	46.56	46.07	45.69	46.94	45.53
TiO_2	0.40	0.21	0.39	0.39	0.09	0.22	0.16	0.15	0.31	0.36	0.34	0.34	0.32	0.26	0.31
Al_2O_3	35.88	35.39	35.78	35.84	36.55	36.11	36.08	36.59	36.29	36.00	36.12	36.30	35.85	36.47	36.82
FeO	0.75	0.75	0.70	0.73	0.97	1.03	1.22	0.82	0.66	0.98	0.79	0.70	1.37	1.09	1.05
MnO	0.02	0.06	0.00	0.00	0.00	0.02	0.01	0.03	0.00	0.01	0.03	0.03	0.00	0.00	0.02
MgO	0.50	0.77	0.51	0.59	0.59	0.44	0.59	0.36	0.39	0.53	0.45	0.40	0.36	0.37	0.20
CaO	0.00	0.00	0.00	0.04	0.02	0.00	0.00	0.00	0.03	0.03	0.03	0.00	0.00	0.00	0.02
Na_2O	0.76	0.75	0.87	1.05	1.13	1.17	1.23	1.21	1.31	1.37	1.19	1.45	0.96	0.91	1.11
K_2O	10.34	10.28	10.47	10.18	10.07	9.94	9.78	9.85	9.12	9.11	9.37	9.14	9.76	10.17	10.18
Cr_2O_3	0.08	0.00	0.04	0.08	0.05	0.03	0.11	0.00	0.34	0.18	0.04	0.03	0.05	0.07	0.09
F	0.00	0.00	0.07	0.03	0.07	0.02	0.03	0.10	0.09	0.10	0.08	0.10	0.01	0.17	0.23
Total	**95.09**	**95.38**	**94.77**	**95.22**	**95.93**	**95.72**	**95.07**	**95.14**	**94.25**	**93.90**	**94.91**	**94.45**	**94.36**	**96.28**	**95.34**
moles	(based on 11 O)														
Si	3.082	3.120	3.073	3.076	3.062	3.086	3.057	3.059	3.064	3.047	3.085	3.067	3.063	3.081	3.028
Al	0.918	0.880	0.927	0.924	0.938	0.914	0.943	0.941	0.936	0.953	0.915	0.933	0.937	0.919	0.972
ΣT	**4.000**	**4.000**	**4.000**	**4.000**	**4.000**	**4.000**	**4.000**	**4.000**	**4.000**	**4.000**	**4.000**	**4.000**	**4.000**	**4.000**	**4.000**
Al	1.893	1.878	1.888	1.881	1.901	1.894	1.889	1.919	1.924	1.899	1.906	1.914	1.896	1.903	1.914
Ti	0.020	0.010	0.019	0.020	0.005	0.011	0.008	0.007	0.016	0.018	0.017	0.017	0.016	0.013	0.015
Fe(ii)	0.042	0.041	0.039	0.041	0.053	0.057	0.068	0.045	0.037	0.055	0.044	0.039	0.077	0.060	0.059
Mn	0.001	0.003	0.000	0.000	0.000	0.001	0.000	0.002	0.000	0.001	0.002	0.002	0.000	0.000	0.001
Mg	0.050	0.076	0.051	0.058	0.058	0.043	0.058	0.036	0.039	0.053	0.045	0.039	0.036	0.036	0.020
ΣR	**2.005**	**2.009**	**1.997**	**2.000**	**2.017**	**2.006**	**2.024**	**2.009**	**2.015**	**2.026**	**2.013**	**2.011**	**2.025**	**2.011**	**2.009**
Ca	0.000	0.000	0.000	0.003	0.001	0.000	0.000	0.000	0.002	0.002	0.002	0.000	0.000	0.000	0.001
Na	0.098	0.096	0.113	0.135	0.145	0.149	0.159	0.155	0.169	0.179	0.153	0.187	0.124	0.116	0.144
K	0.876	0.867	0.892	0.862	0.847	0.836	0.831	0.833	0.778	0.782	0.792	0.776	0.835	0.851	0.864
ΣA	**0.975**	**0.963**	**1.005**	**1.000**	**0.993**	**0.986**	**0.991**	**0.989**	**0.949**	**0.963**	**0.947**	**0.963**	**0.959**	**0.968**	**1.008**
F	0.000	0.000	0.014	0.006	0.014	0.004	0.006	0.022	0.018	0.020	0.016	0.022	0.002	0.036	0.048
Total	**6.980**	**6.972**	**7.003**	**7.000**	**7.010**	**6.992**	**7.014**	**6.998**	**6.964**	**6.989**	**6.960**	**6.974**	**6.984**	**6.979**	**7.017**
Fe/Fe+Mg	**0.456**	**0.353**	**0.432**	**0.410**	**0.478**	**0.570**	**0.538**	**0.560**	**0.489**	**0.511**	**0.494**	**0.499**	**0.681**	**0.621**	**0.745**

(Table A7 continued)

Muscovite

	WW02C (Transition Unit Metasedimentary Rock)							
Label	**02C-8**	**02C-9**	**02C-10**	**02C-11**	**02C-28**	**02C-29**	**02C-30**	**02C-31**
No	**31**	**32**	**33**	**34**	**40**	**41**	**42**	**43**
wt %								
SiO_2	52.46	45.56	46.56	49.33	45.33	46.00	45.62	45.91
TiO_2	0.17	0.23	0.04	0.18	0.17	0.27	0.19	0.27
Al_2O_3	32.49	35.68	36.15	33.81	36.01	36.09	35.63	35.49
FeO	1.06	1.12	0.67	0.97	1.00	1.07	0.84	1.27
MnO	0.03	0.00	0.00	0.03	0.00	0.00	0.01	0.02
MgO	0.28	0.34	0.24	0.30	0.34	0.38	0.36	0.42
CaO	0.05	0.02	0.01	0.03	0.02	0.00	0.00	0.03
Na_2O	0.73	0.92	1.09	0.82	0.90	1.00	1.03	0.84
K_2O	9.15	10.41	10.11	10.06	10.14	10.14	9.83	10.31
Cr_2O_3	0.05	0.08	0.05	0.00	0.02	0.09	0.02	0.07
F	0.01	0.15	0.02	0.05	0.18	0.15	0.18	0.05
Total	**96.48**	**94.36**	**94.93**	**95.55**	**93.92**	**95.04**	**93.52**	**94.63**
moles	(based on 11 O)							
Si	3.384	3.065	3.094	3.245	3.054	3.065	3.078	3.078
Al	0.616	0.935	0.906	0.755	0.946	0.935	0.922	0.922
ΣT	**4.000**	**4.000**	**4.000**	**4.000**	**4.000**	**4.000**	**4.000**	**4.000**
Al	1.853	1.893	1.925	1.865	1.913	1.899	1.912	1.881
Ti	0.008	0.011	0.002	0.009	0.009	0.013	0.009	0.014
Fe(ii)	0.057	0.063	0.037	0.053	0.056	0.060	0.047	0.071
Mn	0.002	0.000	0.000	0.002	0.000	0.000	0.001	0.001
Mg	0.027	0.034	0.024	0.030	0.034	0.037	0.036	0.042
ΣR	**1.948**	**2.002**	**1.989**	**1.959**	**2.012**	**2.009**	**2.005**	**2.009**
Ca	0.003	0.001	0.001	0.002	0.001	0.000	0.000	0.002
Na	0.091	0.120	0.141	0.105	0.117	0.129	0.135	0.109
K	0.753	0.893	0.857	0.844	0.871	0.862	0.846	0.882
ΣA	**0.847**	**1.014**	**0.999**	**0.951**	**0.990**	**0.991**	**0.981**	**0.993**
F	0.002	0.032	0.004	0.010	0.039	0.032	0.039	0.010
Total	**6.795**	**7.016**	**6.987**	**6.911**	**7.002**	**7.001**	**6.986**	**7.002**
Fe/Fe+Mg	**0.677**	**0.646**	**0.607**	**0.643**	**0.621**	**0.615**	**0.567**	**0.630**

Table A8

Chlorite

	WW05004 (Burwash Metased.)				WW04030 (Trans. M-sed.)			WW05028 (Burwash Metased.)			
Label	**04-9**	**04-10**	**04-11**	**04-12**	**30-8**	**30-13**	**30-14**	**28-7**	**28-8**	**28-13**	**28-14**
No	**9**	**10**	**11**	**12**	**18**	**22**	**23**	**51**	**52**	**57**	**58**
wt %											
SiO_2	24.81	24.56	28.35	25.32	24.86	27.45	24.68	24.49	24.49	24.49	25.03
TiO_2	0.11	0.08	0.09	0.10	0.06	0.22	0.09	0.09	0.04	0.14	0.05
Al_2O_3	23.25	23.72	23.83	22.44	24.15	23.78	23.65	23.76	23.74	23.53	23.82
FeO	23.71	23.46	19.85	22.98	24.69	23.97	25.99	24.37	24.30	23.90	24.04
MnO	0.20	0.23	0.14	0.17	0.23	0.12	0.11	0.25	0.16	0.17	0.17
MgO	15.21	15.65	13.62	15.94	13.76	12.63	13.49	14.46	14.37	14.60	13.99
CaO	0.01	0.00	0.00	0.03	0.00	0.02	0.02	0.01	0.00	0.03	0.05
Na_2O	0.04	0.04	0.11	0.06	0.09	0.07	0.00	0.05	0.07	0.01	0.02
K_2O	0.04	0.04	1.44	0.07	0.01	0.81	0.01	0.04	0.02	0.03	0.00
Cr_2O_3	0.059	0.000	0.024	0.047	0.06	0.06	0.00	0.04	0.03	0.03	0.02
F	0.05	0.00	0.09	0.06	0.17	0.17	0.04	0.00	0.00	0.04	0.02
Total	**87.44**	**87.78**	**87.45**	**87.16**	**87.90**	**89.14**	**88.05**	**87.56**	**87.23**	**86.93**	**87.20**
moles	(based on 14 O)										
Si	2.599	2.558	2.897	2.651	2.599	2.808	2.592	2.572	2.578	2.583	2.626
Al	1.401	1.442	1.103	1.349	1.401	1.192	1.408	1.428	1.422	1.417	1.374
ΣT	**4.000**	**4.000**	**4.000**	**4.000**	**4.000**	**4.000**	**4.000**	**4.000**	**4.000**	**4.000**	**4.000**
Al	1.470	1.471	1.767	1.419	1.574	1.675	1.520	1.511	1.524	1.507	1.572
Ti	0.009	0.006	0.007	0.008	0.004	0.017	0.007	0.007	0.003	0.011	0.004
Fe(ii)	2.077	2.044	1.696	2.012	2.158	2.050	2.283	2.140	2.139	2.108	2.110
Mn	0.018	0.021	0.012	0.015	0.020	0.010	0.010	0.022	0.014	0.015	0.015
Mg	2.375	2.431	2.075	2.488	2.144	1.926	2.113	2.264	2.256	2.296	2.188
ΣR	**5.949**	**5.973**	**5.556**	**5.943**	**5.900**	**5.679**	**5.933**	**5.943**	**5.936**	**5.937**	**5.889**
Ca	0.001	0.000	0.000	0.003	0.000	0.002	0.002	0.001	0.000	0.004	0.006
Na	0.008	0.007	0.022	0.012	0.017	0.014	0.001	0.010	0.014	0.002	0.004
K	0.005	0.006	0.187	0.010	0.001	0.106	0.002	0.005	0.003	0.004	0.000
F	0.017	0.000	0.030	0.019	0.055	0.055	0.012	0.000	0.000	0.015	0.007
Total	**9.964**	**9.985**	**9.766**	**9.968**	**9.919**	**9.802**	**9.938**	**9.960**	**9.954**	**9.947**	**9.900**
Fe/Fe+Mg	**0.467**	**0.457**	**0.450**	**0.447**	**0.502**	**0.516**	**0.519**	**0.486**	**0.487**	**0.479**	**0.491**

(Table A8 continued)

Chlorite

	WW02C (Transition Unit Metasedimentary Rock)							
Label	**02C-1**	**02C-2**	**02C-3**	**02C-4**	**02C-24**	**02C-25**	**02C-26**	**02C-27**
No	**24**	**25**	**26**	**27**	**36**	**37**	**38**	**39**
wt %								
SiO_2	23.08	22.91	23.35	23.04	22.87	23.31	23.02	23.22
TiO_2	0.11	0.17	0.24	0.17	0.19	0.11	0.19	0.14
Al_2O_3	22.89	22.03	22.40	22.63	21.75	22.46	22.51	22.74
FeO	32.90	32.58	32.66	34.19	32.43	32.72	32.99	32.95
MnO	0.14	0.15	0.11	0.22	0.15	0.16	0.11	0.13
MgO	8.38	8.42	8.22	8.01	8.46	8.82	8.25	8.48
CaO	0.02	0.04	0.05	0.03	0.05	0.01	0.00	0.00
Na_2O	0.03	0.10	0.09	0.20	0.08	0.05	0.04	0.02
K_2O	0.03	0.05	0.10	0.17	0.20	0.06	0.04	0.04
Cr_2O_3	0.04	0.03	0.11	0.02	0.03	0.00	0.02	0.04
F	0.00	0.08	0.11	0.02	0.00	0.13	0.01	0.08
Total	**87.63**	**86.48**	**87.33**	**88.68**	**86.21**	**87.72**	**87.17**	**87.77**
moles	(based on 14 O)							
Si	2.544	2.563	2.584	2.532	2.570	2.565	2.554	2.556
Al	1.456	1.437	1.416	1.468	1.430	1.435	1.446	1.444
ΣT	**4.000**	**4.000**	**4.000**	**4.000**	**4.000**	**4.000**	**4.000**	**4.000**
Al	1.519	1.469	1.505	1.463	1.450	1.477	1.498	1.505
Ti	0.009	0.014	0.020	0.014	0.016	0.009	0.016	0.012
Fe(ii)	3.032	3.048	3.022	3.141	3.047	3.011	3.061	3.032
Mn	0.013	0.014	0.010	0.020	0.014	0.015	0.010	0.012
Mg	1.377	1.405	1.355	1.312	1.417	1.446	1.365	1.391
ΣR	**5.951**	**5.950**	**5.913**	**5.951**	**5.944**	**5.958**	**5.951**	**5.952**
Ca	0.003	0.005	0.006	0.004	0.006	0.001	0.000	0.000
Na	0.006	0.021	0.019	0.043	0.018	0.011	0.008	0.005
K	0.005	0.007	0.014	0.024	0.029	0.009	0.006	0.006
F	0.000	0.029	0.039	0.007	0.000	0.045	0.002	0.026
Total	**9.965**	**9.984**	**9.952**	**10.022**	**9.998**	**9.980**	**9.965**	**9.963**
Fe/Fe+Mg	**0.688**	**0.685**	**0.690**	**0.705**	**0.683**	**0.676**	**0.692**	**0.686**

Table A9

Feldspar

	WW05004 (Burwash Metased.)				WW05030 (Trans. Metased.)				WW05028 (Burw. Metased.)		
Label	**04-1**	**04-2**	**04-3**	**04-4**	**30-1**	**30-2**	**30-3**	**30-4**	**28-1**	**28-2**	**28-3**
No	**1**	**2**	**3**	**4**	**5**	**6**	**7**	**8**	**15**	**16**	**17**
wt %											
SiO_2	64.92	65.41	64.92	65.17	63.95	64.66	63.86	63.97	61.58	62.27	61.91
Al_2O_3	22.36	21.71	22.25	22.00	23.03	22.76	22.90	22.97	23.48	23.84	24.28
Fe_2O_3	0.18	0.17	0.13	0.14	0.04	0.10	0.17	0.06	0.38	0.06	0.12
CaO	3.35	2.69	3.08	3.04	3.73	3.64	3.75	3.78	4.81	5.27	5.52
Na_2O	9.84	9.88	9.92	9.71	9.22	9.29	9.28	9.34	8.33	8.66	8.41
K_2O	0.08	0.08	0.05	0.07	0.06	0.07	0.06	0.05	0.40	0.06	0.07
MgO	0.02	0.01	0.01	0.00	0.01	0.00	0.00	0.00	0.01	0.00	0.01
MnO	0.02	0.03	0.00	0.02	0.00	0.00	0.00	0.00	0.01	0.00	0.00
Total	**100.76**	**99.96**	**100.35**	**100.14**	**100.04**	**100.54**	**100.02**	**100.17**	**99.01**	**100.16**	**100.31**
moles	(based on 8 O)										
Si	2.844	2.879	2.851	2.865	2.817	2.834	2.818	2.816	2.763	2.756	2.738
Al	1.155	1.126	1.152	1.140	1.196	1.176	1.191	1.192	1.242	1.243	1.265
Fe(iii)	0.002	0.002	0.002	0.002	0.001	0.001	0.002	0.001	0.005	0.001	0.002
Ca	0.157	0.127	0.145	0.143	0.176	0.171	0.177	0.178	0.231	0.250	0.261
Na	0.836	0.843	0.844	0.827	0.787	0.789	0.794	0.797	0.725	0.743	0.722
K	0.004	0.004	0.003	0.004	0.003	0.004	0.003	0.003	0.023	0.004	0.004
Total	**4.998**	**4.981**	**4.997**	**4.981**	**4.980**	**4.975**	**4.986**	**4.988**	**4.990**	**4.996**	**4.992**
An	**16**	**13**	**15**	**15**	**18**	**18**	**18**	**18**	**24**	**25**	**26**
Ab	**84**	**87**	**85**	**85**	**81**	**82**	**81**	**81**	**74**	**75**	**73**
Or	**0**	**0**	**0**	**0**	**0**	**0**	**0**	**0**	**2**	**0**	**0**

(Table A9 continued)

Feldspar

	WW02C (Transition Unit Metasedimentary Rock)						WW05068 (Giauque L. Metabasalt)			
Label	**02C-17**	**02C-18**	**02C-19**	**02C-20**	**02C-21**	**02C-22**	**68-1**	**68-2**	**68-3**	**68-4**
No	**9**	**10**	**11**	**12**	**13**	**14**	**18**	**19**	**20**	**21**
wt %										
SiO_2	73.23	59.01	58.07	59.83	58.86	58.68	62.36	68.78	61.49	63.67
Al_2O_3	17.49	26.19	26.20	25.48	25.83	26.39	23.92	19.92	24.48	23.03
Fe_2O_3	0.01	0.09	0.13	0.20	0.09	0.01	0.11	0.11	0.18	0.12
CaO	5.22	7.73	7.97	7.39	7.77	8.03	5.41	3.59	6.20	4.35
Na_2O	4.97	7.08	6.82	7.37	7.00	6.72	8.50	8.10	8.05	8.97
K_2O	0.01	0.04	0.18	0.05	0.08	0.13	0.07	0.08	0.07	0.14
MgO	0.00	0.01	0.00	0.00	0.00	0.00	0.00	0.00	0.00	0.00
MnO	0.01	0.00	0.00	0.00	0.02	0.01	0.02	0.01	0.00	0.00
Total	**100.94**	**100.16**	**99.37**	**100.32**	**99.64**	**99.98**	**100.40**	**100.58**	**100.48**	**100.28**
moles	(based on 8 O)									
Si	3.120	2.630	2.613	2.661	2.637	2.619	2.754	2.981	2.721	2.806
Al	0.878	1.376	1.390	1.335	1.364	1.388	1.245	1.018	1.276	1.196
Fe(iii)	0.000	0.001	0.002	0.003	0.001	0.000	0.001	0.001	0.002	0.002
Ca	0.238	0.369	0.384	0.352	0.373	0.384	0.256	0.167	0.294	0.205
Na	0.411	0.611	0.595	0.636	0.608	0.582	0.728	0.680	0.691	0.767
K	0.001	0.002	0.010	0.003	0.004	0.007	0.004	0.004	0.004	0.008
Total	**4.647**	**4.989**	**4.994**	**4.990**	**4.987**	**4.981**	**4.989**	**4.852**	**4.989**	**4.983**
An	**37**	**38**	**39**	**36**	**38**	**39**	**26**	**20**	**30**	**21**
Ab	**63**	**62**	**60**	**64**	**62**	**60**	**74**	**80**	**70**	**78**
Or	**0**	**0**	**1**	**0**	**0**	**1**	**0**	**1**	**0**	**1**

Table A10

WW14A (Giauque Lake Unit Metabasalt): Feldspar

Label	**14A-2**	**14A-4**	**14A-7**	**14A-10**	**14A-12**
No	**13**	**15**	**18**	**21**	**23**
wt %					
SiO_2	61.87	61.52	63.75	61.97	61.30
Al_2O_3	23.50	23.12	22.61	22.42	22.62
FeO	0.10	0.23	0.39	0.53	1.63
CaO	5.22	5.00	4.10	4.20	4.03
Na_2O	8.50	8.67	9.38	9.09	8.82
K_2O	0.06	0.11	0.04	0.07	0.24
MgO	0.00	0.00	0.00	0.02	0.14
MnO	0.02	0.01	0.09	0.02	0.02
Total	**99.27**	**98.66**	**100.36**	**98.33**	**98.80**
moles	(based on 8 O)				
Si	2.762	2.768	2.816	2.800	2.785
Al	1.237	1.226	1.177	1.193	1.211
Σ	**3.999**	**3.994**	**3.993**	**3.993**	**3.996**
Ca	0.249	0.241	0.194	0.203	0.196
Na	0.736	0.756	0.803	0.796	0.777
K	0.004	0.007	0.002	0.004	0.014
ΣX	**0.989**	**1.004**	**0.999**	**1.003**	**0.987**
Fe(iii)	0.001	0.003	0.005	0.007	0.022
Total	**4.989**	**5.001**	**4.998**	**5.004**	**5.005**
An	**25**	**24**	**19**	**20**	**20**
Ab	**74**	**75**	**80**	**79**	**79**
Or	**0**	**1**	**0**	**0**	**1**

A Geological Map of the Ormsby Member, Yellowknife Greenstone Belt, Slave Province, Northwest Territories, Canada

Plate 1: This map is part of a thesis submitted in partial fulfillment of the requierments for the degree of Master of Science in the Faculty of Graduate Studies

by William H.R. Whitty, GIT

B.Sc. Honours, Carleton University, Ottawa, Canada, 2004

Mineral Deposit Research Unit
Department of Earth and Ocean Sciences
The University of British Columbia
Vancouver, BC, Canada
(December 2007)

Tyhee NWT Corp.
Yellowknife Gold Project
Northwest Territories, Canada

Projection: NAD 83 UTM Zone 12

Scale: 1:2500

100 0 100 200

metres

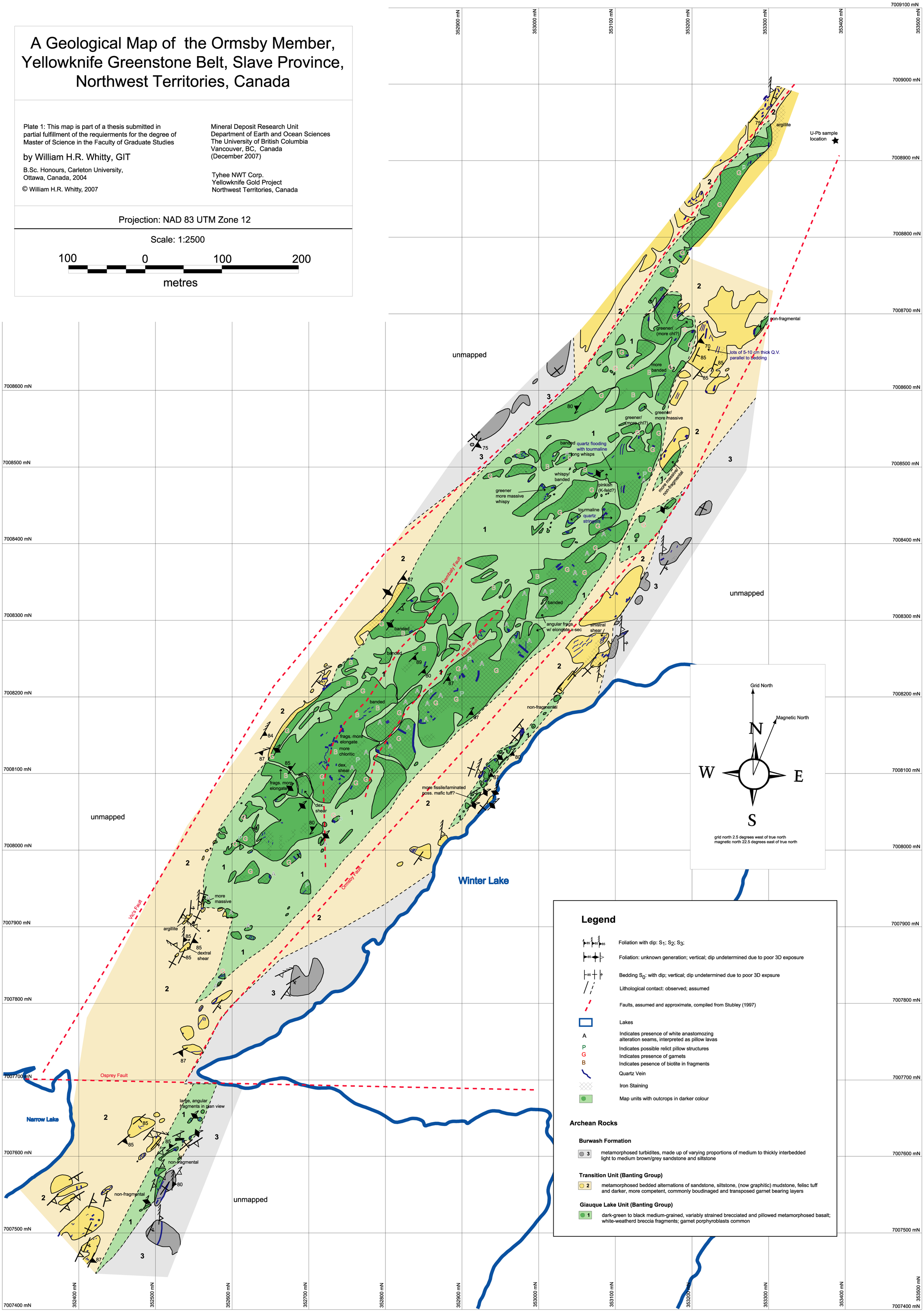

Legend

- Foliation with dip: S_1; S_2; S_3;
- Foliation: unknown generation; vertical; dip undetermined due to poor 3D exposure
- Bedding S_0: with dip; vertical; dip undetermined due to poor 3D expsure
- Lithological contact: observed; assumed
- Faults, assumed and approximate, compiled from Stubley (1997)
- Lakes
- A — Indicates presence of white anastomozing alteration seams, interpreted as pillow lavas
- P — Indicates possible relict pillow structures
- G — Indicates presence of garnets
- B — Indicates pesence of biotite in fragments
- Quartz Vein
- Iron Staining
- Map units with outcrops in darker colour

Archean Rocks

Burwash Formation

3 — metamorphosed turbidites, made up of varying proportions of medium to thickly interbedded light to medium brown/grey sandstone and siltstone

Transition Unit (Banting Group)

2 — metamorphosed bedded alternations of sandstone, siltstone, (now graphitic) mudstone, felisc tuff and darker, more competent, commonly boudinaged and transposed garnet bearing layers

Giauque Lake Unit (Banting Group)

1 — dark-green to black medium-grained, variably strained brecciated and pillowed metamorphosed basalt; white-weatherd breccia fragments; garnet porphyroblasts common